A simple surface radiation budget model for a point in snow covered mountainous terrain.

R. Uijlenhoet

RAPPORT 20

April 1992

Vakgroep Waterhuishouding
Nieuwe Kanaal 11, 6709 PA Wageningen

ISSN 0926-230X

ABSTRACT

Title of Thesis: A SIMPLE SURFACE RADIATION BUDGET MODEL FOR A POINT IN SNOW COVERED MOUNTAINOUS TERRAIN (125 pp.)

Author: Remko Uijlenhoet, 1990

Thesis directed by: Dr. W.P Kustas, United States Department of Agriculture, Agricultural Research Service Hydrology Laboratory, Building 265, Beltsville Agricultural Research Center - East, 10300 Baltimore Avenue, Beltsville, Maryland 20705, United States

Ir. J.N.M. Stricker, Wageningen Agricultural University, Department of Hydrology, Soil Physics and Hydraulics, Nieuwe Kanaal 11, 6709 PA Wageningen, The Netherlands

This investigation deals with the development and operation of a simple radiation budget model at a point on a surface in snow covered mountainous terrain. Net radiation is usually the most important component of the surface energy balance in alpine environments, both with respect to its magnitude and with respect to its temporal and spatial variability. A positive energy balance at the snow surface will cause snowmelt once the snow pack is in thermal equilibrium. A radiation budget model can therefore provide an estimate of the snow surface energy balance and the associated snowmelt.

To allow easy incorporation into operational snowmelt runoff models, snowmelt factors should be simple with respect to the amount of required input parameters and their temporal resolution. Most deterministic snowmelt runoff models employ a degree-day factor for computing the amount of snowmelt from a watershed. It is postulated that the incorporation of a radiation balance algorithm will provide a more physically based snowmelt factor than the presently applied temperature index methods, which may reduce the parameter variability associated with local calibrations and adjustments based on observations of snow properties or hydrological judgments of the model operator.

To maintain a high operational capability under a variety of atmospheric conditions and terrain configurations without the need for extensive measurements, a Radiation Budget Module (RBM) was developed based on broadband radiative transfer parameterizations. Topographic complexity associated with the effects of obstruction, reflection and emission by surfaces surrounding the model point is accounted for by means of isotropic conversion factors. The complex physical processes associated with snowmelt that take place underneath the snow surface are not modeled explicitly.

The independent input variables required to drive RBM are: (1) Fixed geographical parameters which need to be determined only once from topographic maps and/or digital elevation data: Latitude, longitude, altitude, slope, aspect and local horizon of the surface in question; (2) Temporal variables: Day of the year, time of the day and amount of days since the last snow accumulation event occured; (3) Atmospheric/meteorological variables which need to be determined at least on a daily basis from ground truth or remote

sensing measurements: Optical depth of the atmosphere, air pressure, surface temperature, air temperature, vapor pressure and mean fractional cloudcover (and/or duration of sunshine). RBM provides means of estimating the first three atmospheric variables on a daily basis.

Computed twenty minute values of incoming shortwave and net radiation for a whole day were compared with observations taken over a uniform wheat field under clear skies. RBM performed satisfactorily under these ideal topographic and atmospheric conditions. Computed daily averages of incoming shortwave radiation for a complete ablation period were compared with observations taken over an unobstructed horizontal snow covered surface in a Swiss alpine watershed under highly variable atmospheric conditions. Although RBM performed rather accurate on a seasonally averaged basis, the model could not explain the large variability of the measured values: It generally underpredicted high values and overpredicted low values. More realistic cloud treatment procedures than the current daily average corrections will undoubtedly improve RBM's simulation capacity. Computed daily averages of point snowmelt depth for a complete ablation period were compared with observed lysimeter outflows. Three different snowmelt prediction methods were compared: (1) The original degree-day method; (2) A combined temperature index-radiation budget approach, referred to as the restricted degree-day method; (3) The reduced energy budget method which contains the radiation balance and bulk turbulent transfer parameterizations. In addition to a direct comparison, the simulated snowmelt depths and measured lysimeter outflows were used to generate artificial hydrographs for a complete watershed by means of the Rango-Martinec Snowmelt Runoff Model (SRM). Although all three methods performed equally well on a seasonally averaged basis, the original degree-day method could not explain the variability associated with snowmelt and the consequent runoff to the same extent as the other two methods. The restricted degree-day method performed even slightly better than the reduced energy budget method.

Although this investigation deals with the development of a point radiation budget model, it is envisioned that distributed models using digital elevation data should become operational in the near future. The hydrological character of the currently available operational snowmelt runoff models however, should become more distributed in order to take full advantage of the benefits of a snowmelt factor based on the radiation budget.

SAMENVATTING

Titel van Scriptie: A SIMPLE SURFACE RADIATION BUDGET MODEL FOR A POINT IN SNOW COVERED MOUNTAINOUS TERRAIN (125 pp.)

Auteur: Remko Uijlenhoet, 1990

Scriptie begeleid door: Dr. W.P Kustas, United States Department of Agriculture, Agricultural Research Service Hydrology Laboratory, Building 265, Beltsville Agricultural Research Center - East, 10300 Baltimore Avenue, Beltsville, Maryland 20705, Verenigde Staten

Ir. J.N.M. Stricker, Landbouwuniversiteit Wageningen, Vakgroep Hydrologie, Bodemnatuurkunde en Hydraulica, Nieuwe Kanaal 11, 6709 PA Wageningen, Nederland

Dit onderzoek behelst de ontwikkeling en werking van een eenvoudig stralingsbalansmodel voor een punt op een oppervlak in met sneeuw bedekt bergachtig terrein. Netto straling is gewoonlijk de belangrijkste component van de energiebalans aan het aardoppervlak in alpiene milieus, zowel wat betreft grootte als wat betreft temporele en ruimtelijke resolutie. Een positieve energiebalans aan het sneeuwoppervlak zal sneeuwsmelt veroorzaken zodra het sneeuwpakket in thermisch evenwicht is. Een stralingsbalansmodel kan daarom een schatting geven van de energiebalans aan het sneeuwoppervlak en de daarmee samenhangende sneeuwsmelt.

Om een gemakkelijke inpassing in operationele sneeuwsmelt-afvoermodellen mogelijk te maken, dienen sneeuwsmeltfactoren eenvoudig te zijn wat betreft het aantal vereiste invoerparameters en hun temporele resolutie. De meeste deterministische sneeuwsmelt-afvoermodellen gebruiken een graad-dag factor om de hoeveelheid sneeuwsmelt in een stroomgebied te berekenen. Hier wordt gesteld dat de toepassing van een stralingsbalansalgoritme tot een meer fysisch gebaseerde sneeuwsmeltfactor zal leiden dan de huidige temperatuur-index methoden, hetgeen de parametervariabiliteit zal reduceren die samenhangt met locale calibraties en aanpassingen die gebaseerd zijn op waargenomen sneeuweigenschappen of het hydrologisch oordeel van de gebruiker van het model.

Om in hoge mate operationeel te kunnen blijven onder een verscheidenheid van atmosferische omstandigheden en terreinconfiguraties zonder dat uitgebreide metingen nodig zijn, is een stralingsbalansmodule (RBM) ontwikkeld die gebaseerd is op parameterisaties van de voortplanting van kort- en lang-golvige straling in de atmosfeer en aan het aardoppervlak. De topografische complexiteit die samenhangt met de effecten van onderbreking, reflectie en emissie van straling door oppervlakken die het gemodelleerde punt omringen wordt in rekening gebracht door middel van conversiefactoren die gebaseerd zijn op een uniforme stralingsverdeling. De gecompliceerde, door sneeuwsmelt geïnduceerde fysische processen die in het sneeuwpakket zelf plaatsvinden worden niet expliciet gemodelleerd.

De benodigde onafhankelijke invoervariabelen ten behoeve van RBM zijn: (1) Vaste geografische parameters die slechts eenmalig bepaald behoeven te worden

van topografische kaarten en/of digitale terreinmodellen: De breedtegraad, lengtegraad, hoogte, helling, richting en locale horizon van het betreffende oppervlak; (2) Temporele variabelen: De dag van het jaar, de locale tijd en het aantal dagen sinds de laatste sneeuw is gevallen; (3) Atmosferische/ meteorologische variabelen die tenminste op dagbasis bepaald dienen te worden uit waarnemingen aan het aardoppervlak of uit teledetectiegegevens: De optische diepte of transmissiviteit van de atmosfeer, de luchtdruk, de oppervlakte- en luchttemperatuur, de dampspanning en de gemiddelde bewolkingsgraad (en/of zonneschijnduur). RBM biedt de mogelijkheid om de eerste drie atmosferische variabelen op dagbasis te schatten.

Berekende twintig minuten waarden van inkomende kortgolvige- en netto straling voor een hele dag zijn vergeleken met metingen gedaan boven een uniform tarweveld onder een onbewolkte hemel. RBM presteerde naar behoren onder dergelijke ideale topografische en atmosferische omstandigheden. Berekende daggemiddelden van inkomende kortgolvige straling voor een heel sneeuwsmeltseizoen zijn vergeleken met metingen gedaan boven een horizontaal met sneeuw bedekt oppervlak in een Zwitsers alpien stroomgebied onder zeer variabele atmosferische omstandigheden. Alhoewel RBM tamelijk goed presteerde met betrekking tot de seizoengemiddelden, bleek het model niet in staat om de grote variabiliteit in gemeten waarden te verklaren: In het algemeen werden hoge waarden onderschat en lage waarden overschat. Meer realistische procedures ter correctie van bewolking dan de huidige daggemiddelde correctiefactoren zullen de simulatiecapaciteit van RBM ongetwijfeld verbeteren. Berekende daggemiddelden van sneeuwsmelt voor een compleet sneeuwsmeltseizoen zijn vergeleken met gemeten lysimeterafvoeren. Daarbij is een vergelijking gemaakt tussen drie verschillende sneeuwsmelt-voorspellingsmethoden: (1) De originele graad-dag methode; (2) Een gecombineerde temperatuur index-stralingsbalans methode, waaraan gerefereerd wordt als "de beperkte graad-dag methode"; (3) De gereduceerde energiebalans methode die de stralingsbalans en parameterisaties voor de turbulente uitwisseling bevat. Naast een directe vergelijking zijn de gesimuleerde sneeuwsmeltdiepten en gemeten lysimeterafvoeren gebruikt om kunstmatige hydrografen voor een heel stroomgebied af te leiden met behulp van het Rango-Martinec sneeuwsmelt-afvoermodel (SRM). Alhoewel alle drie de methoden even goed presteerden met betrekking tot de seizoengemiddelden, bleek de originele graad-dag methode niet in staat de variabiliteit die samenhangt met sneeuwsmelt en de resulterende afvoer in dezelfde mate te verklaren als beide andere methoden. De beperkte graad-dag methode presteerde zelfs enigszins beter dan de gereduceerde energiebalans methode.

Alhoewel het hier een onderzoek naar de ontwikkeling van een stralingsbalansmodel voor een punt betreft, zullen gedistribueerde modellen die gebruik maken van digitale hoogte gegevens in de nabije toekomst operationeel worden. Het hydrologische karakter van de huidige generatie operationele sneeuwsmelt-afvoermodellen zal echter meer gedistribueerd dienen te worden om ten volle gebruik te kunnen maken van de voordelen die een op de stralingsbalans gebaseerde (gedistribueerde) sneeuwsmeltfactor biedt.

ACKNOWLEDGMENTS

Most of the work for the preparation of this thesis was done at the Hydrology Laboratory of the Agricultural Research Service of the United States Department of Agriculture in Beltsville, Maryland, where the author was a visiting student from April through December, 1989. The author is indebted to the Staff of the Hydrology Laboratory for making his stay a very educative and pleasant one. Special thanks go to Al Rango for making it all possible, Bill Kustas for his fruitful advice and for providing the Maricopa data, Victor van Katwijk for all inspiring discussions, Leoma Kruzic for providing all requested papers, J. Martinec for providing the Weissfluhjoch data and Han Stricker for his patience.

TABLE OF CONTENTS

LIST OF TABLES

LIST OF FIGURES

CHAPTER 1.

INTRODUCTION

Net radiation is normally the most important term in the surface energy balance at a point in snow covered mountainous terrain [Zuzel and Cox, 1975]. Results of previous investigations have shown that net radiation remains the dominant energy source under a wide range of microclimates and terrain configurations [Granger and Male, 1978; Olyphant, 1984; 1986b; Marks, 1988]. Hence, the reliability of snowmelt predictions depends largely on the accuracy of radiation measurements, simulations and forecasts.

The general energy budget equation of a snow cover may be expressed in terms of energy flux densities as follows [e.g., U.S. Army Corps of Engineers, 1956; Male and Gray, 1981; Brutsaert, 1982]:

$$\Delta Q = R_n + Q_h + Q_e + G + A_h \qquad (1)$$

where[1]:

ΔQ = Change in internal energy
R_n = Net radiation
Q_h = Sensible heat flux
Q_e = Latent heat flux
G = Heat flux by soil conduction
A_h = Heat flux by advection

[1] Unit of energy flux density is [Wm^{-2}].

The advection term is mainly associated with rainfall, however it includes the total energy flux associated with water flowing in or out of the system to which (1) is applied. If the energy fluxes toward the snow layer are defined as positive and those away from it as negative, then positive values of ΔQ result in snowmelt once the entire snow cover is isothermal at 0°C [Marks, 1988].

Since the temperature gradients in a melting snow cover and the soil directly beneath it are always small, the heat flux by soil conduction can be neglected for most purposes [Male and Gray, 1981]. The same holds for the energy contribution as a result of advection (due to the release of latent heat by freezing or cooling rain), since precipitation occuring during the snowmelt season tends to have a temperature close to 0°C [Marks et al., 1986]. These theoretical considerations are confirmed by the experimental findings of several investigators [Granger and Male, 1978; Marks, 1988].

The turbulent exchange terms, Q_h and Q_e, may be major components relative to the other terms in (1) just before the actual beginning of the snowmelt season, when the daily radiation balance changes from a net energy loss to a net gain [Marks, 1988]. Moreover, advection of sensible heat (not to be confused with A_h) may have a considerable influence on the melting process

over remaining snow covered areas towards the end of the snowmelt season [Granger and Male, 1978; Olyphant and Isard, 1988]. But for most of the snowmelt season the net turbulent heat transfer is small, since Q_h and Q_e are partly counterbalancing one another due to their opposite signs [Marks, 1988]. During the snowmelt season, the former is namely associated with an energy input, whereas the latter is associated with an energy loss due to evaporation. Therefore net radiation is usually the dominant energy source.

Various investigators have used an empirical temperature index approach for modeling snowmelt [e.g., Martinec, 1960; Pysklywec et al., 1968; Granger and Male, 1978; Kuusisto, 1980; Martinec et al., 1983; Martinec and Rango, 1986; van Katwijk and Rango, 1988; Moussavi et al., 1989]. Such an approach assumes the existance of a linear relationship between the ambient air temperature and the snowmelt resulting from a positive energy balance. Although air temperature may be correlated to the energy budget, it cannot account for its temporal or spatial variability in mountainous terrain, which is mainly associated with the radiation budget [Pysklywec et al., 1968; Zuzel and Cox, 1975]. Conceptual snowmelt models based on an empirical temperature index therefore require local calibrations for the identification of their parameters. Hence, their simulation and forecast reliability will be inferior under extreme conditions. Moreover, the application of a temperature based approach is restricted to lumped or quasi-distributed hydrologic models, but will not comply with the input requirements of forthcoming distributed models. In an effort to improve snowmelt modeling by reducing parameter variability, some invesigators have used a combination of a temperature index and a surface radiation budget [Martinec and de Quervain, 1975; Ambach, 1988; Martinec, 1989]. Generally, a more physically based snowmelt factor has distinct advantages over the empirical degree day factor, particularly when the atmospheric conditions are variable and the topography is rough [Charbonneau et al., 1981].

Because a snowmelt factor based on net radiation accounts for atmospheric and geographic variability, its determination is more complex than merely determining an empirical factor. General problems related to modeling radiation are concerned with the partition of solar radiation into a direct and a diffuse component, the effect of cloud cover on incident solar and thermal radiation, the angular distribution of the diffuse radiation components and the spatial, temporal and spectral dependency of the reflectivity of snow [Dozier, 1980]. Moreover, modeling radiation in mountainous areas brings about specific topographic difficulties due to the effects of obstruction, reflection and emission by surrounding terrain.

This investigation deals with developing a (spectrally and geometrically) simplified approach as a first step towards modeling the radiation budget in complex terrain, in order to limit the required number of input parameters. This will reduce the need for extensive measurements and facilitate the incorporation of basin scale energy budget estimates in operational snowmelt runoff models. It is envisioned that future radiation budget estimates will

be the result of distributed modeling efforts combining digital terrain models and satellite remote sensing scenes in the environment of geographic information systems [Dozier, 1987; Leavesley, 1989]. However, recent investigations have shown that broadband radiation models in combination with simple terrain models can yield acceptable results [Olyphant, 1984; 1986a]. Olyphant [1986b] argues that in mountainous terrain the effects of terrain heterogenity must be nearly as great as the effects of spectral variation in determining variations in the surface radiation budget. Moreover, modeling the complex spatial and spectral properties of radiative transfer through an atmosphere containing cloud layers requires a large amount of detailed information and has rarely been applied in an operational environment [e.g., Lacis and Hansen, 1974; Kimball et al., 1982].

In the next chapter the general theory of radiation modeling and its application to uniform surfaces and complex terrain will be discussed. The third chapter presents an outline of the developed computer simulation model RBM (Radiation Budget Module) and its model assumptions and input requirements. Chapter four deals with the validation and verification (testing) of RBM, and presents its application to various sites and a comparison between a simplified energy budget method and two temperature index methods for the simulation of point snowmelt for a complete ablation period. In the final chapter a summary and conclusions of this investigation will be presented and remarks will be made with respect to future work in this field.

CHAPTER 2.

MODELING RADIATION

2.1. General Theory

The net allwave electromagnetic flux density at a point at the surface-atmosphere interface is defined as the total incident monochromatic radiation (irradiance) less the total exiting monochromatic radiation (upward) integrated over all wavelengths [e.g., Marks et al., 1986]:

$$R_n = \int_{l=0}^{\infty} (I[l] - E[l]) * dl \qquad (2)$$

where:

R_n = Net allwave radiation [Wm^{-2}]
l = Wavelength [μm]
I = Monochromatic irradiance [$Wm^{-2}\mu m^{-1}$]
E = Exiting monochromatic radiation [$Wm^{-2}\mu m^{-1}$]

For the purpose of modeling the surface radiation budget, it is both reasonable and convenient to separate the total electromagnetic spectrum into two distinct spectral regions, i.e. one emitted by the sun and one emitted by the earth and its atmosphere. That is to say, their overlap is negligible and their behaviour in the atmosphere and at the earth's surface differs markedly. According to Wien's displacement law, the product of the absolute temperature of a perfect emitter (black body) and the wavelength of the most intense radiation, is a constant [e.g., Liou, 1980]. Hence, since the effective radiative temperature of the sun (between 5800 and 6000 K [Fritz, 1951]) is much higher than that of the earth (approximately 288 K [Ramanathan et al., 1989]) and the earth-atmosphere system (approximately 250 K [Liou, 1980]), it emits at shorter wavelengths (effectively in the range from 0.3 to 4.0 μm, with an energy peak at 0.47 μm) than does the earth and its atmosphere (effectively in the range from 4.0 to 50 μm, with an energy peak at 10 μm) [Marks et al., 1986].

Not only do the origins of shortwave (solar) and longwave (terrestrial) radiation differ, but also their behaviour in the earth's atmosphere and at its surface: shortwave radiation is attenuated due to absorption and scattering by terrestrial materials, but it is not emitted; longwave radiation on the other hand is absorbed and emitted, without appreciable scattering.

2.1.1. Radiation in the Earth's Atmosphere

The atmosphere consists of a group of nearly permanent gases (nitrogen, oxygen and carbon dioxide, among others), a group of gases with variable concentration (mainly water vapor and ozone) and various liquid and solid particles (water drops, ice crystals and aerosols). They are responsible for the radiative processes (scattering, absorption and emission) in the atmosphere.

The main absorbers of shortwave radiation are water vapor in the troposphere and ozone in the stratosphere, accounting for appoximately 7 and 2 percent attenuation, respectively [Kimball, 1928; List, 1966]. The former absorbs primarily in the near infrared wavelength region, whereas the latter is the main gaseous absorber in the shorter visible and ultraviolet wavelengths [Lacis and Hansen, 1974]. Absorption by miscellaneous gases (oxygen, carbon dioxide and nitrogen compounds) is of minor importance in this spectral region. The most important longwave absorbing (and consequently emitting) constituents are water vapor in the lower atmosphere, and carbon dioxide and ozone in the upper atmosphere [Idso and Jackson, 1969].

It is common in radiation modeling to distinguish between two types of scattering, namely molecular or Rayleigh scattering and aerosol scattering. The former is caused by air molecules that tend to scatter equal amounts of electromagnetic waves (radiation) forward and backward (isotropic scattering); its intensity is inversely proportional to the fourth power of the wavelength. The latter is caused by particles whose sizes are much larger than the wavelength of the incoming solar radiation, partly by dust particles that tend to affect radiation at longer wavelengths than air molecules (Mie scattering), and partly by water droplets that scatter all wavelenghts in equal amounts (non selective scattering) [Liou, 1980]. Aerosol scattering is generally peaked forward [Fritz, 1951; Lo, 1986]. The purpose of using the terms forward and backward instead of downward and upward is that the atmosphere as a whole scatters both the incoming solar radiation and the upcoming surface reflection.

Since the atmosphere is a scattering volume containing many particles, each particle is exposed to and also scatters radiation which has already been scattered by other particles. Multiple scattering is of great importance to radiative transfer in the atmosphere. The result of atmospheric scattering is that part of the total amount of shortwave radiation reaches the surface as direct radiation, and part of it as diffuse radiation. This partition and the hemispherical distribution of the diffuse component are of great importance to the surface radiation budget, the latter especially in mountainous terrain.

Clouds can contain considerable amounts of water, both in the form of water vapor and of liquid droplets, and in some cases also as ice and snow particles [Fritz, 1951]. Therefore, they enhance the mentioned radiative effects of the atmosphere due to increased scatter of shortwave radiation (both downcoming solar radiation and upcoming surface reflection) and increased absorptance and

emittance of longwave radiation. The former generally has an effect of net cooling, whereas the latter has a net warming effect [Ramanathan et al., 1989]. The net result of these opposing feedback mechanisms however, is still very much in doubt among researchers. Since cloud-radiative interaction is a very complex phenomenon both for large scale climate applications and for small scale radiation budget studies, it is common among investigators to either simplify or even completely omit the influence of clouds on the surface radiation budget [e.g., Marks and Dozier, 1979; Dozier, 1980; Bird and Riordan, 1986]. Although omitting cloud effects may be useful for theoretical purposes, it is not acceptable in operational radiation budget models [e.g., Munro and Young, 1982].

2.1.2. Radiation at the Earth's Surface

When the various radiation components eventually reach the earth after their modification by the atmosphere, a complex interaction with its surface and the features upon it takes place. Depending on the spectral and spatial distribution of the incoming radiation and on the intrinsic and geometric properties of its recipients, this process consists of different amounts of scattering (eventually resulting in upwelling reflection), absorption and transmission. The intrinsic properties of the surface (such as chemical and mineral composition, texture (grain size), structure (roughness) and content of moisture and organic matter) determine the radiation-surface interaction on a microscopic scale and consequently influence both the spectral and the spatial characteristics of this process; they are quantified by means of such well known terms as reflectivity, emissivity and albedo. The surface's geometric properties (terrain relief) on the other hand, determine the radiation-surface interaction on a macroscopic scale and consequently mainly influence its spatial characteristics; they are quantified by means of conversion factors (section 2.3.2.).

When a ray of electromagnetic radiation strikes the surface of an object, it may be absorbed, transmitted or reflected. What kind of interaction or combination of interactions (reflection, refraction of diffraction) actually takes place at the surface-atmosphere interface depends on the microstructure of the surface layer, i.e. its roughness and homogeneity observed on a microscopic scale. The amount of (intrinsic) microrelief relative to the scale of observation determines whether the surface appears as a specular (Fresnel) or as a diffuse reflector, and if the latter is the case whether it appears as an isotropical (Lambertian) or as an anisotropical reflector. It follows from Rayleigh's criterion (which distinguishes optically smooth surfaces from optically rough surfaces by relating the dimensions of surface perturbations on a molecular scale to the wavelength of the incident radiation), that most natural surfaces appear to be diffuse reflectors. Specular reflection of direct insolation is therefore often ignored, since it occurs too infrequently

to be of importance in the radiation budget [Dozier, 1980]. The exact distribution of reflected radiation, however, is a complex function of the direction of the incident rays and of the microstructure of the surface layer, which is determined a.o. by its mineral compostion, texture, moisture content and organic matter content. The relationship between the surface reflectance on the one hand and the incident and reflected beam geometry on the other hand is known as the Bidirectional Reflectance-Distribution Function (BRDF) [Horn and Sjoberg, 1979]. The amount of (geometric) macrorelief and the position of the sun determine the source-object-receptor geometry and consequently the occurence of obstruction (shading), reflection and emission by adjacent surfaces. Even for the simplified case where the intrinsic surface would behave like a Lambertian (perfect diffuse) reflector, the surface roughness observed on a macroscopic scale would always cause the entire land surface to reflect the incident radiation nonuniformly as a result of the complex geometric effects at the land surface [Dozier and Frew, 1989].

Particularly in the case of snow, reflection is the dominant component in the shorter (ultraviolet and visible) wavelengths, whereas absorption and transmission are dominant in the longer (infrared) wavelengths [Geiger, 1959; Kondratyev, 1973; Kondratyev et al., 1982; Dozier et al., 1989]. According to Kirchhoff's law, the emissivity of a medium under local thermodynamic equilibrium equals its absorptivity for a given wavelength [e.g., Liou, 1980]. Hence, snow acts as a nearly perfect emitter, as do most terrestrial materials [Geiger, 1959; Kondratyev et al., 1982]. Although the distinctive spectral dependency of the reflectivity of snow and of the optical properties of the substances in the atmosphere will not be taken into account in this study, their interaction affects the spectrally integrated reflectivity (albedo) of snow and thus significantly influences the radiation budget at the surface. For instance, the fact that the reflectivity of snow for near infrared radiation is much smaller than its reflectivity for ultraviolet or visible radiation (roughly 0.2 versus 0.8) [Dozier, 1980] causes (1) attenuation of solar radiation by water vapor in the near infrared wavelength region to result in a markedly higher reduction of the surface radiation budget than the same amount of attenuation by aerosols in the ultraviolet and visible bands, and causes (2) diffuse radiation to consist of shorter wavelengths than direct radiation as a result of multiple reflections between the snow surface and the atmosphere (in particular the cloud bases). Hence, the snow reflectivity for diffuse radiation is generally higher than that for direct radiation, and the snow albedo consequently increases with an increasing cloud cover [Petzold, 1977].

The roughness of a snow surface is mainly a function of its mean grain size, which increases during the snow melt season. Grain growth and contamination bring about a decay of the snow reflectivity for both the direct and the diffuse radiation during the melt season: The snow grain size mainly affects the snow reflectivity in the near infrared wavelength region, whereas absorbing impurities mainly affect snow reflectivity in the visible wavelength

region [Dozier, 1987]. The liquid water content of snow does not appreciably affect its bulk radiative transfer properties [Dozier et al., 1989]. The diffuse reflectivity for direct insolation is also dependent on the angle of incidence as determined by the sun's position [Kondratyev, 1973; Kondratyev et al., 1982]. Reliable parameterizations of this relationship have yet to be developed for most land surface types [Briegleb et al., 1986]. As for snow however, several investigators have presented empirical formulae which allow the determination of the albedo as a function of grain size and solar zenith angle [Petzold, 1977; Marks, 1988; Williams, 1988]. Although the intrinsic reflection of solar radiation from a snow cover is more closely isotropical than scattering by vegetation [Eyton, 1989], it contributes along with the geometric effects in mountainous areas to the complex anisotropic properties of reflection from adjacent terrain [Dozier and Frew, 1989; Shoshany, 1989].

The radiation balance at a point can be written as the sum of net shortwave and net longwave radiation and their respective components [e.g., Garnier and Ohmura, 1970; Marks and Dozier, 1979; Marks et al., 1986]:

$$R_n = K_n + L_n \qquad (3)$$
$$= K\downarrow - K\uparrow + L\downarrow - L\uparrow$$
$$K\downarrow = K_{dir} + K_{dif} + K_{trn}$$
$$K\uparrow = a * K\downarrow$$
$$L\downarrow = L_{sky} + L_{trn}$$
$$L\uparrow = L_{sfc} + (1 - \epsilon) * L\downarrow$$

where[1]:

R_n = Net radiation
K_n = Net shortwave radiation
L_n = Net longwave radiation
$K\downarrow$ = Downward shortwave radiation
$K\uparrow$ = Upward shortwave radiation
$L\downarrow$ = Downward longwave radiation
$L\uparrow$ = Upward longwave radiation
K_{dir} = Direct solar radiation
K_{dif} = Diffuse sky radiation
K_{trn} = Reflection from adjacent terrain
a = Surface albedo [-]
L_{sky} = Emission from atmosphere
L_{trn} = Emission and reflection from adjacent terrain
L_{sfc} = Surface emission
ϵ = Surface emissivity [-]

[1] Unit of radiative flux density is [Wm^{-2}].

This is a more convenient set of equations than expression (2) since it consists of components which are more easily defined in terms of broadband radiative flux densities.

2.2. Uniform Surfaces

2.2.1. Direct Solar Radiation

The instantaneous solar radiative flux density at the top of the atmosphere is transformed in two ways to provide the direct solar radiation incident on a uniform (i.e. horizontal and unobstructed) surface under cloudless conditions: (1) through a modification due to the fact that its direction is rarely perpendicular to the receiving surface, and (2) through an attenuation in the earth's atmosphere, as described in section 2.1.1. The former requires the application of spherical trigonometry, whereas in broadband radiation modeling the latter is accounted for by means of a generalization of the Beer-Bouguer-Lambert law for the exponential extinction of monochromatic radiation traversing a homogeneous absorbing medium. The solar radiation at the top of the atmosphere, corrected for the angle of incidence, is usually referred to as extraterrestrial radiation. The direct insolation on a horizontal surface under cloudless conditions (potential insolation) can be expressed as the product of the extraterrestrial radiation and an attenuation factor accounting for atmospheric absorption and scattering [e.g., Kondratyev, 1973]:

$$K_o = S_o * r^{-2} * \cos[\theta_s] \quad (4)$$

$$K_{diro} = K_o * \exp[-M_a * p * p_o^{-1} * \tau] = K_o * T^{(Ma*p*po-1)} \quad (5)$$

where:

K_o = Extraterrestrial radiation [Wm^{-2}]
K_{diro} = Direct insolation under cloudless conditions [Wm^{-2}]
S_o = Solar constant [Wm^{-2}]
r = Earth's radius vector [-]
θ_s = Solar zenith angle [rad]
M_a = Relative optical airmass or relative path length of atmosphere [-]
p = Air pressure at surface [Pa]
p_o = Standard air pressure at mean sea level [Pa]
τ = Integral atmospheric extinction coefficient or normal optical depth [-]
T = Zenith path transmissivity or transparency of atmosphere [-]

S_o is the flux density of solar radiation perpendicular to the rays at the mean earth-sun distance. A value of 1353 (±21) Wm^{-2} issued by the National Aeronautics and Space Administration (NASA) has been accepted as a standard solar constant, which happens to be exactly the same value as proposed earlier by the Smithsonian Institution [List, 1966; Liou, 1980]. Moreover, it is in good agreement with experimental findings resulting from recent investigations as part of the Earth Radiation Budget Experiment (ERBE): they show 1365 Wm^{-2} to be a reasonable average for the second half of the 1980's [Ramanathan et

al., 1989; Barkstrom et al., 1990].

The radius vector of the earth quantifies the deviation from the mean earth-sun distance. Its value as a function of the day of the year can be found from tables prepared by List [1966], from Fourier series representations as derived by various authors [e.g., Spencer, 1971], or from representations based on the theory of conics [Whiteman and Allwine, 1986] (appendix A.). None of these formula types explicitly takes into account the effects of leap years, precession and fluctuations in the earth's orbital eccentricity and the inclination angle of the axis of the earth's rotation. Blackadar [1984] therefore proposed a more accurate algorithm which gives the radius vector of the earth and the solar declination as a function of the Julian date. However, since the value of r^{-2} never differs more than about 3.5 percent from unity, assuming r to remain constant during the day is only a minor approximation.

From spherical trigonometry it can be seen that the cosine of the solar zenith angle with respect to a horizontal surface is a function of the corresponding date and time and of the latitude of the receiving surface [e.g., List, 1966; Kondratyev, 1973; Liou, 1980]:

$$\cos[\theta_s] = \sin[\Phi] * \sin[\delta] + \cos[\Phi] * \cos[\delta] * \cos[H] \qquad (6)$$

where[1]:

θ_s = Solar zenith angle [rad]
Φ = Latitude of receiving surface [rad]
δ = Solar declination [rad]
H = Hour angle [rad]

[1] Latitudes in the northern hemisphere are taken as positive; those in the southern hemisphere as negative.

The solar declination is the terrestrial latitude of the point where the sun is in the zenith at true solar noon, i.e. when $\theta_s = 0$ and $H = 0$ in (6). As for the approximation of δ as a function of the day of the year, the same sources may be consulted as mentioned in the case of the earth's radius vector. However, the variation of the solar declination over the year is an order of magnitude larger than that of the radius vector: its maximum, which occurs around June 22, is approximately 0.41 rad (23.44°), whereas its minimum, occuring around December 22, is -0.41 rad. Between these so-called (summer and winter) solstices occur the (vernal and autumnal) equinoxes, at which the solar declination becomes 0 (approximately March 21 and September 23) [List, 1966].

The hour angle is the angular distance between the solar longitude and the meridian of the observer. By definition, H is 0 at true solar noon and is $-\pi$ rad or π rad at true midnight. The hour angles of sunrise and sunset on a horizontal surface are found by setting θ_s equal to $\pi/2$ ($\cos[\theta_s] = 0$) in (6) and then solving for H. As a result, (4) can be integrated analytically between sunrise and sunset (with the minor approximations that δ and r are

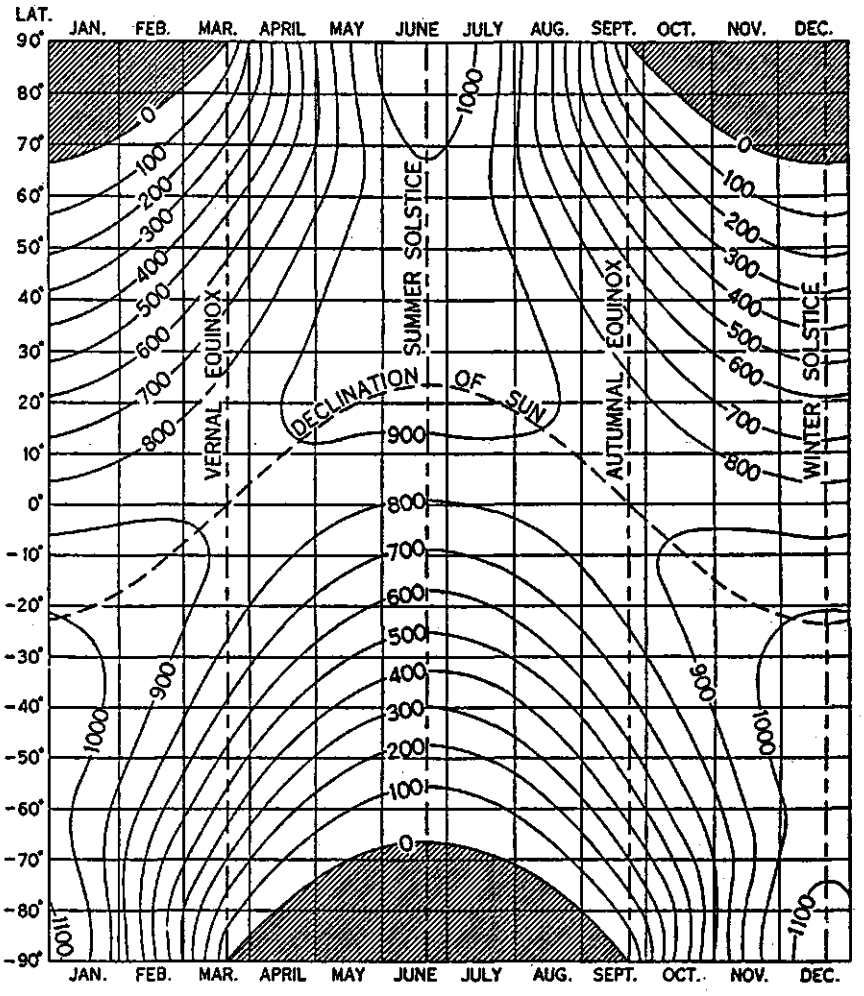

fig. 2.1.1. Total daily solar radiation reaching a horizontal surface at the top of the atmosphere. Solid curves represent lines of equal radiation [calcm^{-2}d^{-1} ≈ 4.184 * 10^{4} Jm^{-2}d^{-1}]; shaded areas represent regions of continuous darkness [List,1966].

constant during the day) to yield the total daily radiation reaching a hypothetical horizontal surface at the top of the atmosphere [List, 1966; Liou, 1980] (appendix C.; figure 2.1.1.). Since (5) cannot be integrated analytically, it has to be evaluated numerically when daily totals are required. Garnier and Ohmura [1968, 1970] and Isard [1983] apply integration steps of 20 minutes ($dH = \pi/36$) with reasonable accuracy, whereas Olyphant [1986b] uses Simpson's rule with integration steps of one hour ($dH = \pi/12$).

True solar time is generally not the same as local standard time (zone time). The first reason for this deviation is that each degree of longitudinal difference from the standard meridian results in a time difference of 4 minutes. The second reason is related to the irregular motion of the earth around the sun, known as the equation of time. The maximum departure from the longitudinally corrected time is about 17 minutes and occurs presently in the beginning of November. The equation of time can be approximated as a function of the day of the year by means of tables [e.g., List, 1966] and Fourier series representations as derived by various authors [e.g., Spencer, 1971; Whiteman and Allwine, 1986] (appendix A.).

The relative optical airmass is the path length traversed by the sun's rays in the atmosphere relative to this length when the sun is in the zenith. For solar zenith angles less than $\pi/3$ rad (60°), M_a may be approximated with an accuracy of 0.25 percent by the secant of θ_s ($\cos^{-1}[\theta_s]$) [Kasten, 1966]. However, for lower solar elevation angles, the curvature of the earth and its atmosphere and atmospheric refraction cannot be neglected. Tables based on Bemporad's computations made in the beginning of this century [e.g., Kondratyev, 1973], have been widely used for this purpose. More recently, Kasten [1966] developed a table for the relative optical airmass based on a new model atmosphere and provided the following approximation formula which generally deviates no more than 0.1 percent from the tabulated values:

$$M_a = (\cos[\theta_s] + 0.1500 * (93.885 - \theta_s * 180 * \pi^{-1})^{-1.253})^{-1} \qquad (7)$$

where:

M_a = Relative optical airmass or path length of atmosphere [-]
θ_s = Solar zenith angle [rad]

Especially in mountainous terrain, the actual air pressure at the surface (p) is generally different from the standard air pressures at sea level (p_0) on which the airmass tables are based (10^5 Pa for Bemporad's and $1.01325 * 10^5$ Pa for Kasten's table, respectively). A common altitude correction for M_a consists therefore of multiplying the tabulated values by the relative air pressure (p/p_0) [List, 1966; Kondratyev, 1973]. If no air pressure measurements are available, a relative air pressure can be approximated by one of the following expressions, based on the hypsometric formula for a dry atmosphere. Equation (8) assumes a constant temperature lapse rate ($T_a * T_0^{-1} = 1-$

$\Gamma * T_o^{-1} * h$) [Marks and Dozier, 1979], whereas (9) assumes a nearly constant exponential temperature decay with altitude ($T_a * T_o^{-1} = \exp[-\Gamma * T_o^{-1} * h]$) [Willet and Sanders, 1959]:

$$p * p_o^{-1} = \exp[-g * (\Gamma * R_d)^{-1} * \ln[1 + \Gamma * h * T_a^{-1}]] \quad (8)$$

$$\approx \exp[-g * h * (R_d * T_o)^{-1}] \quad (9)$$

where:

p = Air pressure at surface [Pa]
p_o = Standard air pressure at mean sea level [Pa]
g = Gravitational acceleration [$\approx 9.81\ ms^{-2}$]
Γ = Temperature lapse rate [$\approx 0.0065\ Km^{-1}$]
R_d = Gas constant for dry air [$\approx 287.04\ Jkg^{-1}K^{-1}$]
h = Surface altitude above mean sea level [m]
T_a = Absolute air temperature at surface [K]
T_o = Mean air temperature at sea level [≈ 288.15 K]

Van Katwijk and Rango [1988] and Leavesley [1989] suggested that the assumption of a constant temperature lapse rate in snow covered mountainous terrain may not be accurate, especially in the vicinity of transition zones between snow covered and snow free areas. However, values close to the standard lapse rate for the troposphere of 0.0065 Km^{-1} [Brutsaert, 1975; Liou, 1980] have been applied in alpine areas yielding reasonable results [Dozier and Outcalt, 1979; Marks and Dozier, 1979; Munro and Young, 1982; Running et al., 1987]. Moreover, (8) is relatively insensitive to departures from the standard lapse rate, whereas (9) does not contain a lapse rate at all.

If accurate solar photometer measurements are not available, the optical depth (τ) or transmissivity (T) of the atmosphere for clear skies may be approximated by integrating standard monochromatic transmission parameterizations of the various constituents of the atmosphere over all solar wavelengths [e.g., Fritz, 1951; Leckner, 1978; Dozier, 1980; Bird and Riordan, 1986]. Rearranging (5) to obtain τ or T as a function of K_{dir}, yields reasonable approximations when daily averages of direct solar radiation are available [Garnier and Ohmura, 1970]. As a first approximation of the atmospheric transmissivity for clear sky conditions at high altitudes, a value of 0.75 (corresponding to an optical depth of about 0.29) seems appropriate [Isard, 1983]. Using the shortwave radiative transfer parameterizations of Lacis and Hansen [1974], Dozier and Outcalt [1979], Munro and Young [1982] or Stuhlmann et al. [1990] to determine K_{dir}, values for τ or T close to these average values can be obtained.

Substituting the equations (4) and (6)-(9) in (5), thereby making use of the approximation formulae for the earth's radius vector, the sun's declination and the equation of time (appendix A.), and of the mentioned typical values for the solar constant and the atmospheric transmissivity, one yields an estimate of the desired potential direct insolation. The required input parameters are the latitude, longitude and altitude of the surface, and

the time and day of the year.

2.2.2. Diffuse Sky Radiation

As mentioned in section 2.1., diffuse sky radiation has two sources, which cannot be measured separately, but need both be taken into account when modeling radiative transfer: (1) radiation that is scattered downward out of the solar beam, and (2) radiation that is reflected upward from the earth's surface and subsequently backscattered by the atmosphere (referred to as multiple reflection or multiple scattering). The latter is especially important over snow covered surfaces, because of the highly reflective nature of snow. Diffuse sky radiation on an unobstructed horizontal surface contributes about 25 percent to the global insolation on an average clear day [e.g., Becker and Boyd, 1957] and offsets roughly half of the reduction of direct insolation during periods of partial cloud cover [Olyphant, 1984]. Over snow covered surfaces these figures are generally even more pronounced.

Different methods have been developed for determining the amount of diffuse sky radiation reaching horizontal surfaces, ranging from more physically based scattering models to more empirically based parameterizations. The latter usually relate the ratio of diffuse and global insolation on an unobstructed horizontal surface ($K_{dif}/K\downarrow$) to the ratio of global and extraterrestrial insolation corrected for the incidence angle ($K\downarrow/K_o$), which is interpreted as a clearness index [Liu and Jordan, 1960; 1961]. These relationships are based on the observation that the fraction of diffuse sky radiation decreases from 1 to about 0.15 as the global transmission increases from 0 to about 0.8. These parameters have been correlated through polynomial regression functions for averaging intervals of one minute [Smietana et al., 1984], an hour [Erbs et al., 1982], a day [Liu and Jordan, 1960; 1961; Erbs et al., 1982] and a month [Liu and Jordan, 1960; Erbs et al., 1982]. The scatter of measurements about these regression lines is significant, particularly for the shorter intervals. Hay and Davies [1978] suggested that a major part of the spatial and temporal variability associated with these relationships might be attributed to the effect of multiple scattering between the earth's surface and the atmosphere. However, Olyphant [1984] compared his measurements to the one hour correlation of Erbs et al. [1982] and concluded that "the relationship is indeed location independent". Moreover, the agreement between this one hour standard correlation and the curves obtained by Stuhlmann et al. [1990], both from radiation measurements and model simulations, is striking. Although these empirical parameterizations allow easy adjustment for the influence of cloudiness on the amounts of direct insolation and diffuse sky radiation (section 2.2.3.), the simplified assumption that the amount of diffuse sky radiation under clear skies is a constant fraction of the global insolation is insufficient for application in radiation models that do not

require radiation measurements as input data.

Lacis and Hansen [1974] developed a monochromatic radiative transfer model and broadband parameterizations for absorption and scattering in the atmosphere and at the earth's surface based on accurate multiple scattering computations in a plane-parallel atmosphere [e.g., Liou, 1980]. However, their parameterization for the incident solar radiation at an unobstructed horizontal surface does not allow the required separation into a direct and a diffuse flux density. Leckner [1978], Dozier [1980] and Bird and Riordan [1986] among others applied exponential decay functions based on the Beer-Bouguer-Lambert law to model absorption and scattering by substances in the atmosphere. Although these models distinguish between direct and diffuse radiation, they cannot easily be generalized to broadband parameterizations.

A simple but physically based algorithm for estimating the amount of scattered sky radiation reaching a uniform surface on a daily basis was originally proposed by Fritz [List, 1966]. He stated (1) that the total amount of radiation scattered from the solar beam may be expressed as the difference between a fictitious radiative flux, subject to atmospheric absorption only, and the direct beam, subject to both absorption and scattering, and (2) that half of the resulting flux is scattered downward towards the earth's surface. The latter is strictly only a correct assumption when the scattering takes place in a pure Rayleigh atmosphere (a clear dry atmosphere without dust particles or water vapor). The actual fraction of the total scattered radiation that reaches a uniform surface under clear sky conditions is increased by aerosol scattering and decreased as a function of the solar zenith angle. According to Blackadar [1985b], this fraction amounts to only about 36 percent on a daily basis. On the other hand, the relative amount of diffuse sky radiation generally increases with increasing solar zenith angle due to increased scattering of the direct beam with increasing path lengths [Fritz, 1951].

Robinson [1966] introduced an empirical correction factor to account for the zenith angle dependency of the fraction of the total scattered radiation reaching the earth's surface [Dozier, 1980]. Temps and Coulson [1977] proposed an additional correction factor to account for the circumsolar or aureole component, i.e. for brightening of the sky in the vicinity of the sun. Applying these factors to Fritz's algorithm and neglecting absorption of solar radiation by miscellaneous gases in the atmosphere leads to the following expression for the instantaneous scattered radiation reaching an unobstructed horizontal surface under clear sky conditions:

$$
\begin{aligned}
K_{scto} &= C_z * C_s \\
&\quad * (K_o * (1 - A_w[M_w * w] - A_o[M_o * (O_3)]) - K_{diro}) \qquad (10)\\
C_z &= 0.5 * \cos^{1/3}[\theta_s] \\
C_s &= 1 + \cos^2[\theta_s] * \sin^3[\theta_s]
\end{aligned}
$$

where:

K_{scto} = Radiation scattered downward from direct beam under cloudless conditions [Wm^{-2}]
C_z = Fraction of scattered radiation reaching surface [-]
C_s = Correction for sky brightening in vicinity of sun [-]
K_o = Extraterrestrial radiation [Wm^{-2}]
A_w = Fraction of radiation absorbed by water vapor or absorptivity of water vapor [-]
M_w = Relative path length for water vapor [-]
w = Zenith path water vapor content of atmosphere or normal path length for water vapor [kgm^{-2}]
A_o = Fraction of radiation absorbed by ozone or absorptivity of ozone [-]
M_o = Relative path length for ozone [-]
(O_3) = Zenith path ozone content of atmosphere [m(NTP)]
K_{diro} = Direct solar radiation under cloudless conditions [Wm^{-2}]
θ_s = Solar zenith angle [rad]

Alternative parameterizations for determining the amount of scattered solar radiation reaching an unobstructed horizontal surface under clear skies are provided by Dozier and Outcalt [1979] and Munro and Young [1982].

Absorption of solar radiation by water vapor is more difficult to parameterize than absorption by ozone, because (1) the absorption spectrum of water vapor is more complicated, (2) the absorption by water vapor occurs in the lower atmosphere where there is both absorption and significant scattering, and (3) the absorption by water vapor depends strongly on temperature and pressure [Lacis and Hansen, 1974; Wang, 1976]. Yet, various authors have derived simple parameterizations, either as a function of the actual (precipitable) water vapor content of the atmosphere or as a function of the effective (temperature and pressure scaled) water vapor amount. Wang [1976] presented an empirical expression that includes the effects of atmospheric inhomogeneity:

$$\log_{10}[A_w] = -1.6754 + 0.5149 * \log_{10}[M_w * w] - 0.0345 * (\log_{10}[M_w * w])^2 \qquad (11)$$

where:

A_w = Absorptivity of water vapor [-]
M_w = Relative path length for water vapor [-]
w = Actual zenith path water vapor content of atmosphere or normal path length for water vapor [kgm^{-2}]

Although this parameterization is based on a tropical model for both the water vapor profile and for the temperature and pressure distributions, it retains its reliability for a subarctic winter atmosphere and for the case of a high (snow) surface albedo. Moreover, it remains a satisfactory approximation for water vapor contents outside the fitting interval of $0.08 <= M_w*w <= 41.5$ kgm^{-2}, which may occur at high solar zenith angles [Wang, 1976].

Various investigators assume the relative path length for water vapor to be equal to the relative optical airmass [Leckner, 1978; Bird and Riordan, 1986]. Although this is a reasonable approximation, Kasten [1966] adjusted the coefficients of his air mass formula to provide an expression for the relative water vapor path length:

$$M_w = (\cos[\theta_s] + 0.05480 * (92.650 - \theta_s * 180 * \pi^{-1})^{-1.452})^{-1} \quad (12)$$

where:

M_w = Relative path length for water vapor [-]
θ_s = Solar zenith angle [rad]

The zenith path precipitable water vapor content of the atmosphere above the surface can be approximated by assuming an exponential decay of the water vapor density with the altitude. Combining this assumption with the equation of state of moist air and integrating over the appropriate altitudes, yields the water vapor amount in the atmosphere as a function of the surface air temperature and vapor pressure (appendix B.):

$$w = 0.622 * e_a * (k_w * R_d * T_a)^{-1} \quad (13)$$
$$\approx 0.622 * e_a * (k_w * R_d * (T_o - \Gamma * h))^{-1} \quad ==>$$
$$w_o = 0.017 * e_o$$

where:

w = Actual zenith path water vapor content of atmosphere or normal path length for water vapor [kgm^{-2}]
e_a = Vapor pressure at surface [Pa]
k_w = Water vapor density decay coefficient [$\approx 4.4 * 10^{-4}$ m^{-1}]
R_d = Gas constant for dry air [≈ 287.04 $Jkg^{-1}K^{-1}$]
T_a = Absolute air temperature at surface [K]
T_o = Mean air temperature at sea level [≈ 288.15 K]
Γ = Temperature lapse rate [≈ 0.0065 Km^{-1}]
h = Surface altitude above mean sea level [m]
w_o = Actual zenith path water vapor content of atmosphere at sea level [kgm^{-2}]
e_o = Vapor pressure at sea level [Pa]

Since the vapor pressure decay with increasing altitude is an order of magnitude larger than the temperature decay (due to its strong temperature dependence), (13) implicitly accounts for the decrease of the amount of precipitable water vapor in the atmosphere above a surface with increasing altitude.

In order to obtain the last expression, the indicated representative values were substituted for k_w and T_o [Brutsaert, 1975]. The resulting approximation for the amount of water vapor in a vertical path through the atmosphere at sea level is consistent with previous results [Kimball, 1928; Monteith, 1961; Leckner, 1978; Munro and Young, 1982; Iqbal, 1983]. The approximate nature of the assumed vertical water vapor density profile does not allow application of (13) for instantaneous values. However, these formulae may be expected to

yield reasonable approximations of daily or weekly averages.

The total absorption of visible and ultraviolet radiation by ozone in the stratosphere can be accurately parameterized because it is primarily the result of exponential attenuation at each wavelength with negligable scattering or temperature and pressure dependence [Wang, 1976]. Lacis and Hansen [1974] derived parameterizations for the visible and ultraviolet bands with an accuracy exceeding that with which the ozone amount in the atmosphere is likely to be known in most cases:

$$A_o = A_o^{vis} + A_o^{uv} \tag{14}$$

$$A_o^{vis} = 2.118 * M_o * (O_3) * (1 + 4.2 * M_o * (O_3) + 3.23 * (M_o * (O_3))^2)^{-1}$$

$$A_o^{uv} = 108.2 * M_o * (O_3) * (1 + 1.386 * 10^4 * M_o * (O_3))^{-0.805} + 6.58 * M_o * (O_3) * (1 + (1.036 * 10^4 * M_o * (O_3))^3)^{-1}$$

where:

A_o = Total absorptivity of ozone [-]
A_o^{vis} = Absorptivity of ozone in visible band [-]
A_o^{uv} = Absorptivity of ozone in ultraviolet band [-]
M_o = Relative path length for ozone [-]
(O_3) = Zenith path ozone content of atmosphere [m(NTP)]

According to Lacis and Hansen [1974], Rodgers [1967] proposed a simple formula for the relative ozone path length, which is in close agreement with Kasten's [1966] expression for the relative optical air mass (7):

$$M_o = 35 * (1224 * \cos^2[\theta_s] + 1)^{-1/2} \tag{15}$$

where:

M_o = Relative path length for ozone [-]
θ_s = Solar zenith angle [rad]

Since the amount of ozone in a vertical path through the atmosphere shows typical spatial and temporal variations between about 0.002 to 0.006 m(NTP), it can be estimated with reasonable accuracy. Briegleb et al. [1986] used a simple trigonometric approximation that is a function of the latitude only ((O_3)=0.0031+0.001*sin[Φ]). Van Heuklon [1979] developed a more accurate empirical formula that describes the seasonal, latitudinal and longitudinal variations in Northern America. However, it neglects the short term variations in the lower atmosphere and the long term trends in the upper atmosphere associated with air pollution:

$$(O_3) = 0.00235 + \sin^2[1.28 * \Phi] * (0.0015 + 0.0004 * \sin[0.0172 * (D - 30)] - 0.0002 * \sin[3 * 1]) \tag{16}$$

where[1]:

(O_3) = Zenith path ozone content of atmosphere [m(NTP)]
Φ = Latitude of surface [rad]
D = Day of year [-]
l = Longitude of surface [rad]

[1] Longitudes west of the meridian at Greenwich are taken as positive; those east of the meridian at Greenwich as negative.

Since the ozone absorption of solar radiation mainly takes place in the upper atmosphere (stratosphere), it is assumed that the altitude dependency of (16) is negligible.

Substituting the equations (4), (5) and (11)-(16) in (10), thereby making use of the approximation formulae for the earth's radius vector, the sun's declination and the equation of time (appendix A.), and of the mentioned typical values for the solar constant and the atmospheric transmissivity, one yields an estimate of the desired scattered sky radiation on an unobstructed horizontal surface under clear sky conditions. The required input parameters are the latitude, longitude and altitude of the surface, the time and day of the year, and the vapor pressure at the surface.

The remaining fraction of the diffuse sky radiation is a result of an infinite converging series of multiple reflections between the earth's surface and the atmosphere [Hay and Davies, 1978; Dozier, 1980; Liou, 1980; Bird and Riordan, 1986]. With the rough approximations of isotropic reflection by the snow covered ground and isotropic backscatter from the atmosphere, this phenomenon can be modeled as follows:

$$K_{bck} = (a_{dir} * K_{dir} + a_{dif} * K_{dif}) * a_{sky}$$
$$= (a_{dir} * K_{dir} + a_{dif} * K_{sct}) * a_{sky} * (1 - a_{dif} * a_{sky})^{-1} \qquad (17)$$
$$\approx (K_{dir} + K_{sct}) * ((a * a_{sky})^{-1} - 1)^{-1}$$

where:

K_{bck} = Backscatter from atmosphere [Wm^{-2}]
a_{dir} = Diffuse surface reflectivity for direct radiation [-]
K_{dir} = Direct insolation [Wm^{-2}]
a_{dif} = Surface reflectivity for diffuse radiation [-]
K_{dif} = Diffuse sky radiation [Wm^{-2}], which can be computed from:

$$K_{dif} = K_{sct} + K_{bck}$$

K_{sct} = Radiation scattered downward from direct beam [Wm^{-2}]
a_{sky} = Fraction of surface reflection backscattered by atmosphere or effective sky albedo [-]
a = Surface albedo [-], which can be computed from:

$$a = (a_{dir} * K_{dir} + a_{dif} * K_{dif}) * (K_{dir} + K_{dif})^{-1} \qquad (18)$$

The above equations imply that the area surrounding the model point is uniformly covered with snow. Since this does not always have to be the case, the application of an estimate of the (significantly lower) areal average surface albedo ($a=a_{trn}$) would probably yield more accurate results (section 3.3.2.).

Parameterizations for the reflectivity of snow for direct and diffuse radiation will be presented in section 2.2.3. The (broadband) surface albedo is generally defined as a weighted average of the spectral surface reflectivities, using all monochromatic irradiances as weights. For the snow reflectivity parameterization used in this investigation, this results in a weighted average of the reflectivities for direct and diffuse radiation, using the direct insolation and the diffuse radiation as weights. The albedo of snow ranges roughly from 0.4 for old (contaminated), wet snow to 0.9 for fresh, dry snow [U.S. Army Corps of Engineers, 1956; List, 1966; Kondratyev, 1973; Kondratyev et al., 1982; Brutsaert, 1982].

The term effective sky albedo in (17) and (18) is used instead of sky albedo to denote the difference between reflection from a flat surface and that from a nonhomogeneous, transparent slab of air. The latter is a combined result of (multiple) backscattering of part of the surface reflection and absorption of part of the backscattered radiation, integrated over the entire spherical solid angle and over all appropriate altitudes and wavelengths. Several investigators assume backscattering to be entirely the result of Rayleigh scattering, since aerosol scattering is generally forward peaked [Lacis and Hansen, 1974; Dozier, 1980].

According to Hay and Davies [1978], the effective sky albedo can be adequately expressed as a weighted average of the effective albedo of an overcast sky and that of a cloudless atmosphere, using the mean fractional cloudcover and its complement as weights:

$$a_{sky} = m_c * a_c + (1 - m_c) * a_o \qquad (19)$$

where:

a_{sky} = Effective sky albedo [-]
m_c = Mean fractional cloud cover [-]
a_c = Effective albedo of overcast sky [$\approx$ 0.5]
a_o = Effective albedo of clear sky [$\approx$ 0.15]

The mean fractional cloudcover can be defined as some kind of projection of the fraction of the part of the sky dome unobstructed by terrestrial objects that is covered with clouds on a point at the earth's surface. It may be estimated from the earth's surface by means of human observations or whole sky photography, or from the sky by means of satellite observations. However, serious discrepancies between estimates may arise from differences in applied projection methods and from the fact that observers tend to overestimate the angular distance between points in the sky closer to the horizon in comparison with points closer to the zenith. The actual effect of this phenomenon depends on the cloud type, since for some types the apparent fractional cloudcover tends to increase towards the horizon, whereas for others it tends to decrease [McGuffie and Henderson-Sellers, 1989]. Although the anisotropy that is characteristic for surface reflection is not taken into account in this study, the projection of the fraction of the sky covered with clouds should actually

be weighted for the angular distribution of the surface reflection that reaches the cloud bases [Unsworth and Monteith, 1975]. Munro and Young [1982] successfully applied an effective mean fractional cloudcover, defined as a weighted average of the actual observed mean fractional cloudcover and 1 minus the relative sunshine duration.

The fraction of the surface reflection that is backscattered by the base of the cloud cover, is commonly approximated by the cloud top albedo as measured by airborne or spaceborne instruments [Müller, 1985]. Although the albedo of the base of a cloud cover is a function of the cloud's water content (as determined by its thickness and density) and of its altitude (as determined in part by the cloud type), fixed mean values are usually applied [Hay and Davies, 1978].

Cloud base and clear sky albedos are markedly higher when the underlying surface is snow covered, since the reflection from snow is shifted towards the shorter visible and ultraviolet wavelengths that are more effectively Rayleigh backscattered and not absorbed by water vapor. Obviously, multiple reflections contribute a considerable amount of diffuse sky radiation to snow covered terrain [Fritz, 1951]. Kondratyev [1973] even reports cloud base albedo's above snow of 0.51 to 0.86 and clear sky albedos of 0.45 to 0.79. From tables prepared by List [1966] and Kondratyev [1973] a cloud base albedo averaged over different types of clouds of about 0.55 can be derived. This figure is in close agreement with the average value of 0.5 to 0.55 mentioned by Fritz [1951] and that of 0.6 used by Hay and Davies [1978] and Munro and Young [1982]. Hay and Davies, however, propose a mean clear sky albedo of 0.25, which is very different from the value of 0.13 that Williams [1988] uses above snow covered terrain, from a value between 0.08 and 0.13 that Fritz [1951] derives and from the value of 0.0685 that Lacis and Hansen [1974] derive as "the albedo of the Rayleigh atmosphere for illumination from below".

With conservative values for the snow albedo (0.7), the effective (single scattering) sky albedo under overcast conditions (0.5), and the effective sky albedo under cloudless conditions (0.15), the use of (17) results in insolation increases from more than 10 to more than 50 percent compared with a situation without multiple reflections. Thus, the atmospheric backscatter on an unobstructed horizontal surface can be estimated by substituting equation (19) in (17), when the direct insolation, the scattered radiation, the mean fractional cloudcover and the surface reflectivities for direct and diffuse radiation are known.

2.2.3. Global and Net Solar Radiation

Since reflection from adjacent terrain does not play a role in the radiation budget at a point of an unobstructed horizontal surface, the total shortwave radiative flux received per unit area (global radiation) is the sum of the direct insolation and the diffuse sky radiation. Combining equation (3)

with (17), yields for the global radiation under clear skies:

$$K\downarrow_o = K_{diro} + K_{scto} + K_{bcko} \approx (K_{diro} + K_{scto}) * (1 - a * a_o)^{-1} \quad (20)$$

where:

$K\downarrow_o$ = Downward shortwave radiation under cloudless conditions [Wm^{-2}]
K_{diro} = Direct solar radiation under cloudless conditions [Wm^{-2}]
K_{scto} = Radiation scattered downward from direct beam under cloudless conditions [Wm^{-2}]
K_{bcko} = Backscatter from atmosphere under cloudless conditions [Wm^{-2}]
a = (Areal average) surface albedo [-]
a_o = Effective albedo of clear sky [-]

In the previous sections of this chapter, simple expressions are presented for computing K_{dir} and K_{sct} for cloudless conditions and K_{bck} for cloudy conditions. As stated before, when a model is to become truly operational it should provide some means to correct for the complex effects of clouds. However, a physically based (e.g., effective sky albedo) approach as commonly used for modeling atmospheric backscatter has not yet been developed for providing cloudcover corrections for direct and scattered solar radiation. Hence, investigators dealing with the influence of (partial) cloudcover on global radiation have developed several empirical correction formulae. Apart from some temperature based corrections [Bristow and Campbell, 1984; Zuzel, 1989, personal communication], they are generally linear relationships between (1) the quotient of the daily average global radiation under cloudy to that under clear skies and (2) either the relative duration of sunshine or the mean fractional cloud cover [Fritz, 1951; Geiger, 1959; List, 1966; Kondratyev, 1973; Brutsaert, 1982]. Although local calibration will probably yield more accurate results, various tables are available from which the coefficients of these relationships can be found as a function of the cloud type, cloud height, and surface latitude.

A nonlinear expression that guarantees a reasonable accuracy has been developed by Berlyand [Kondratyev, 1973]:

$$K\downarrow * K\downarrow_o^{-1} = 1 - (c_1 + c_2 * m_c) * m_c \quad (21)$$

where:

$K\downarrow$ = Downward shortwave radiation [Wm^{-2}]
$K\downarrow_o$ = Downward shortwave radiation under cloudless conditions [Wm^{-2}]
c_1, c_2 = Empirical coefficients [$c_2 \approx 0.38$]
m_c = Mean fractional cloudcover [-]

The coefficient c_1 is reported to have a value of about 0.40 from the equator to 60°N and of about 0.15 for higher latitudes, whereas c_2 has a fixed

value of 0.38. Since the decrease of c_1 with increasing latitude implicitly accounts for the influence of the surface albedo on global radiation, a value of 0.15 will probably yield more satisfactory results in snow covered alpine areas of the lower latitudes than a value of 0.40. Nevertheless, $c_1 \approx 0.40$ is in better agreement with the parameter value that Kimball [1928] used for the linear equivalent of (21), namely $c_1 + c_2 * m_c = 0.71$.

The above expression has serious shortcomings for application in a more detailed snow surface radiation budget model because (1) it does not distinguish between direct and diffuse radiation, (2) it does not explicitly take into account the dependency of the amount of global radiation on the surface albedo and (3) it does not depend on the optical air mass as determined by the sun's position. However, (21) and similar empirical expressions allow easy operational application since they lack the need for a significant number of input parameters associated with detailed calculations by more sophisticated models [e.g., Lacis and Hansen, 1974].

When the global radiation is known as a function of the mean fractional cloudcover from (20) and (21), estimates of the fractions of direct and diffuse radiation can be obtained from empirically determined relationships between the ratio of diffuse to global radiation ($K_{dif}/K\downarrow$) and the ratio of global to extraterrestrial radiation ($K\downarrow/K_o$), as mentioned in section 2.2.2. Olyphant [1984] conducted extensive radiation measurements during different snow melt seasons in an alpine area and concluded that the one hour standard correlation of Erbs et al. [1982] (figure 2.2.3.) "provides a convenient basis for separating the direct and diffuse components of global insolation under a broad range of atmospheric conditions". The striking agreement between this one hour standard correlation and curves obtained by Stuhlmann et al. [1990], both from radiation measurements and model simulations, suggests the same.

Only a part of the global radiation that reaches the snow surface is absorbed. The absorptivity of a surface is generally determined as the complement of its reflectivity in the case of a spectral model, and of its albedo in the case of a broadband model. The albedo of a snow surface decreases during a snow melt season from about 0.9 to about 0.4 as a result of grain growth and contamination. The U.S. Army Corps of Engineers [1956] and Petzold [1977] among others derived typical snow albedo decay functions for ablation seasons. As mentioned before, snow reflectivity is not only a function of the amount of days since the last snowfall occured, but also of wavelength and solar zenith angle. Examples of spectral snow reflectivity models are the monochromatic model of Dozier [1980] that is based upon actual measurements and the two band model of Marks [1988]. Williams [1988] used a physically based broadband parameterization for the snow albedo that seems suitable for the simplified approach of the present study. This scheme accounts implicitly for some of the distinct spectral properties of snow reflection because it distinguishes between the reflectivities for direct insolation and diffuse radiation:

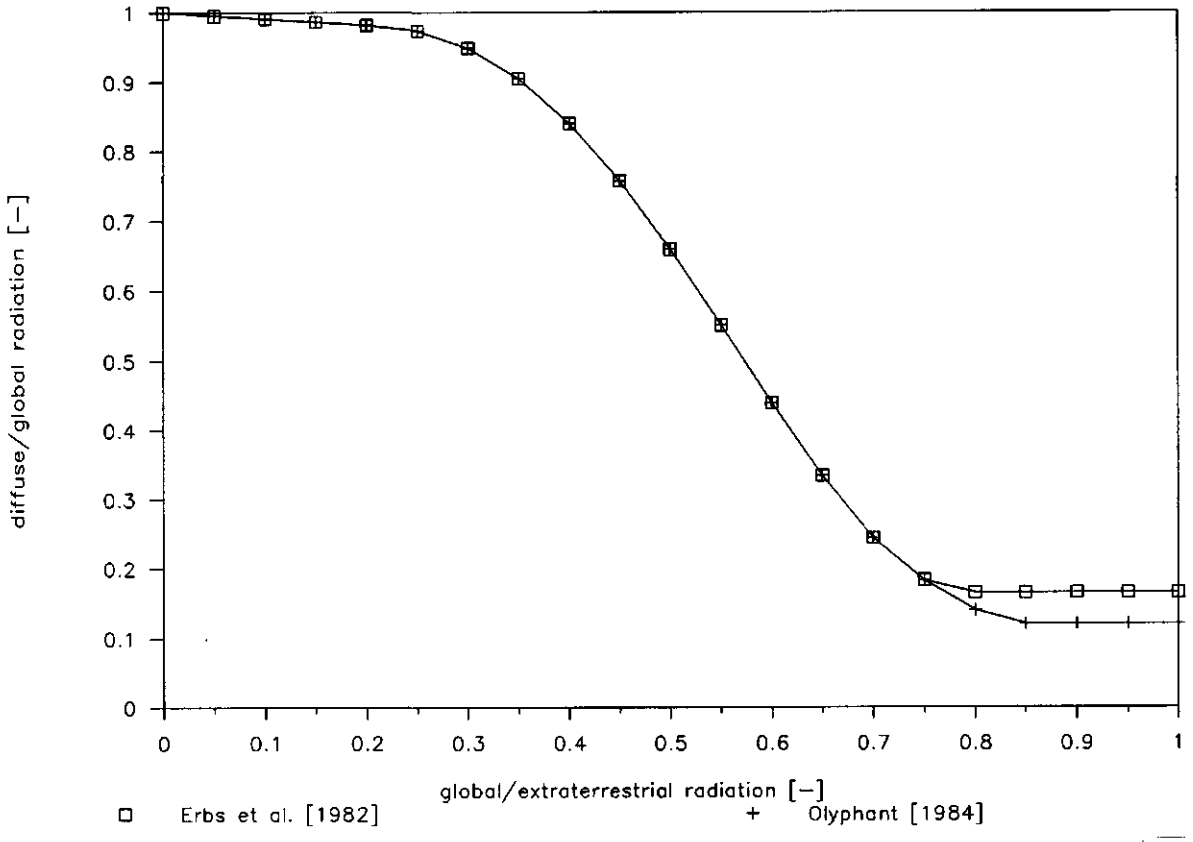

fig. 2.2.3. One hour standard correlation between the ratio of diffuse to global radiation ($K_{dif}/K\downarrow$) and the ratio of global to extraterrestrial radiation ($K\downarrow/K_o$) [Erbs et al., 1982]:

$$K_{dif}/K\downarrow = 1 - 0.09 * K\downarrow/K_o \text{ for } K\downarrow/K_o \leq 0.22$$

$$K_{dif}/K\downarrow = 0.9511 - 0.1604 * K\downarrow/K_o + 4.388 * (K\downarrow/K_o)^2 - 16.638 * (K\downarrow/K_o)^3 + 12.336 * (K\downarrow/K_o)^4 \text{ for } 0.22 < K\downarrow/K_o \leq 0.80$$

$$K_{dif}/K\downarrow = 0.165 \text{ for } K\downarrow/K_o > 0.80$$

Olyphant [1984] found $K_{dif}/K\downarrow = 0.12$ for $K\downarrow/K_o > 0.80$ to be more appropriate for high altitude environments.

$$a_{dir} = a_{diro} - (0.083 + 7.27 * r^{1/2}) * \cos^{1/2}\theta_s \quad (22)$$

$$a_{dif} = a_{difo} - 6.64 * r^{1/2} \quad (23)$$

$$r = (r_o^3 + 2.52 * 10^{-10} * D_s)^{1/3} \quad (24)$$

where[1]:

a_{dir} = Diffuse surface reflectivity for direct radiation [-]
a_{diro} = Diffuse surface reflectivity for direct radiation at sunrise or sunset [$\approx$ 0.965]
r = Mean grain size [m]
θ_s = Solar zenith angle [rad]
a_{dif} = Surface reflectivity for diffuse radiation [-]
a_{difo} = Surface reflectivity for diffuse radiation of fresh, dry snow [$\approx$ 0.96]
r_o = Mean grain size before melting occurs [$\approx 1 - 4*10^{-4}$m]
D_s = Number of days since last snowfall [-]

[1] Although "reflectivity" normally refers to the spectral (monochromatic) scattering properties of a medium, it is used here to denote the difference between the scattering properties of a surface for broadband (i.e. direct plus diffuse) radiation ("albedo") and those for direct and diffuse radiation separately.

The formulation of (24) implicitly assumes (1) that the surface of a melting snow pack is wet during the entire day, and (2) that each new snow accumulation consists of dry uncontaminated snow with the same mean grain size. The fraction of the day that the snow surface has been wet is actually not a constant, but is determined by the positive feedback between the mean grain size of the snow surface and the amount of solar radiation it absorbes (and consequently by the complex feedback mechanisms with the other terms of the energy budget) [Dozier et al., 1989]. However, (22) and (23) are not very sensitive to changes in the empirical factor in (24) that accounts for the daily number of hours that the snow has been wet. Marks [1988] provides an alternative grain growth function which is not based on the physics of grain growth either, but which can generate reflectivities that closely fit observed decays because its asymptotic functional form allows to specify the expected grain growth maximum (and consequently the expected albedo minimum). For the model presented above the reflectivity decays with the square root of the mean grain size and with the cosine of the solar zenith angle however, which is consistent with Marks' two band model. Lastly, the broadband albedo (a) of a snow surface can be evaluated as a weighted average of (22) and (23), using the direct insolation (K_{dir}) and the total diffuse radiation ($K_{sct} + K_{bck}$) as weights (equation (18)).

The net shortwave radiation on an unobstructed horizontal surface can be defined as the product of global radiation and the complement of the snow surface albedo, i.e. the surface absorptivity:

$$K_n = (1 - a_{dir}) * K_{dir} + (1 - a_{dif}) * K_{dif} \quad (25)$$
$$= (1 - a) * K\downarrow$$

where:

K_n = Net shortwave radiation [Wm^{-2}]
a_{dir} = Diffuse surface reflectivity for direct radiation [-]
K_{dir} = Direct solar radiation [Wm^{-2}]
a_{dif} = Surface reflectivity for diffuse radiation [-]
K_{dif} = Diffuse sky radiation [Wm^{-2}]
a = Surface albedo [-]
K↓ = Downward shortwave radiation [Wm^{-2}]

The procedure for determining the components of the shortwave radiation budget at an unobstructed horizontal surface as a function of the ambient atmospheric conditions can be summarized as follows:

(1) Computation of the potential direct and scattered insolation on an unobstructed horizontal surface from (5) and (10), as described in sections 2.2.1. and 2.2.2.
(2) Computation of the diffuse surface reflectivity for direct insolation and the surface reflectivity for diffuse radiation from (22)-(24).
(3) Substitution of the computed values in (17) with $a_{sky} = a_o$ to obtain the atmospheric backscatter under cloudless conditions.
(4) Substitution of the computed values in (20) to obtain the global radiation under cloudless conditions; continue to step (5) if the mean fractional cloudcover is greater than zero, else skip to step (11).
(5) Multiplication by the cloudcover correction factor from (21) to obtain the global radiation as a function of the ambient atmospheric conditions.
(6) Substitution of the ratio of global and extraterrestrial radiation (from (4)) in the one hour standard correlation of Erbs et al. [1982] (figure 2.2.3), and multiplication of the result by the global radiation to obtain the diffuse sky radiation.
(7) Subtraction of the diffuse sky from the global radiation to obtain the direct insolation.
(8) Computation of the effective sky albedo as a function of the ambient atmospheric conditions from (19).
(9) Substitution of the obtained values in (17) to obtain the atmospheric backscatter.
(10) Subtraction of the obtained value from the diffuse sky radiation to obtain the scattered insolation.
(11) Direct substitution of the obtained values in (25), or computation of the (broadband) surface albedo from (18) and substitution of the resulting albedo and the obtained global radiation in (25), to yield the net shortwave radiation on an unobstructed horizontal surface as a function of the ambient atmospheric conditions.

2.2.4. Longwave Radiation

Longwave radiation in the terrestrial environment originates mainly from two sources, namely as emission from the atmosphere and from the earth's surface. Although the sun also contributes to the amount of longwave radiation, this source is generally neglected because it represents less than one percent of the solar energy received at the top of the atmosphere and is reduced to a negligible amount at the earth's surface due to atmospheric absorption. It is therefore reasonable to treat the terrestrial (thermal or longwave) radiative flux separately from the solar (shortwave) flux [Marks and Dozier, 1979; Liou, 1980]. Since no appreciable scattering takes place at wavelengths longer than 4 μm, radiation in this wavelength region is mainly associated with emission and absorption. This makes thermal radiative processes much easier to model than shortwave radiative transfer. Moreover, thermal infrared radiation does not have the marked diurnal, seasonal or latitudinal zenith angle dependence that characterizes shortwave radiation [Liou, 1980].

The three major components affecting thermal radiation in the atmosphere are water vapor in the lower atmosphere (troposphere), and carbon dioxide and ozone in the upper atmosphere (stratosphere). Most of the longwave radiation originates within the lower hundreds of meters of the atmosphere [Brunt, 1932; Swinbank, 1963; Unsworth and Monteith, 1975]. The atmosphere therefore acts as an optically active gas, absorbing and emitting radiation as the atoms and molecules undergo transitions (quantum jumps) between fixed energy states, which results in line and band spectra (selective radiation). The earth's surface on the other hand essentially behaves as a black body in the thermal wavelength region, generating continuous absorption and emission spectra (continuous radiation) [Geiger, 1959; Liou, 1980]. This implies that the surface reflectivity is nearly zero for radiation with wavelenghts above 4 μm. For snow this is already the case for wavelenghts as low as 2.5 μm [Marks and Dozier, 1979].

Planck's law expresses the emitted monochromatic intensity of a black body as a function of the wavelength of the emitted radiation and the temperature of the emitting body [e.g., Liou, 1980]. Integrating this expression over all wavelengths and over the entire spherical solid angle (assuming an isotropic radiation field) yields Stefan-Boltzmann's law, which states that the radiative flux density emitted by a black body is proportional to the fourth power of its absolute temperature [e.g., Liou, 1980]. For convenience, the radiative flux density emitted by a real body can be related to that of a black body of the same temperature by means of a proportionality factor known as the emissivity of the body. This can be interpreted as the ratio of the actual to the potential thermal radiation. The emission of a point at the earth's surface is therefore defined as follows:

$$L_{sfc} = \epsilon * \sigma * T_s^4 \qquad (26)$$

where:

L_{sfc} = Surface emission [Wm^{-2}]
ϵ = Surface emissivity [≈ 0.98]
σ = Stefan-Boltzmann's constant [$\approx 5.6697 * 10^{-8}$ $Wm^{-2}K^{-4}$]
T_s = Absolute surface temperature [≈ 273 K]

The average emissivity of the earth's surface can be assumed to be 0.95, whereas for snow an even higher value of about 0.98 seems appropriate [Kondratyev et al., 1982]. This value is very insensitive to changes in snow cover properties resulting from grain growth or contamination during the snow melt season [Marks, 1988]. Snowmelt is a result of a net energy input at the snow surface once the entire snow pack is isothermal at 0°C. Therefore the snow surface temperature will approximately be constant at 273 K throughout the snowmelt season resulting in a mean surface emission of a little more than 300 Wm^{-2}.

Because the atmosphere behaves as a band or selective radiator, it is not feasible to describe its emission analytically. Numerous investigators over the past 75 years have therefore sought to establish (semi-)empirical relationships between the actual emission of a cloudless atmosphere and that of a black body at screen level air temperature. Although some of them related atmospheric emission directly to air temperature [Swinbank, 1963; Unsworth and Monteith, 1975], most of them presented expressions for the effective emissivity of such an atmosphere as a function of screen level values of either air temperature or vapor pressure or both, which will be presented here.

Both Ångström and Brunt [1932] developed equations that contained vapor pressure alone and required the determination of empirical coefficients from local observations. Ångström's formula took the form of a linear relationship between the effective atmospheric emissivity and an exponential function of the vapor pressure at screen level. Brunt, on the other hand, established a relationship with the square root of the vapor pressure, based on the analogy he assumed between radiative transfer and heat conduction. Theoretical evidence for this relationship was found by Monteith [1961] (as cited by Idso and Jackson [1969]) and Unsworth and Monteith [1975]. One disadvantage of these empirical relationships is the wide variation of the "constants" with locality, which Brunt ascribed largely to differences in experimental procedure instead of to differences in vertical air temperature and vapor pressure profiles.

Swinbank [1963] argued that "the correlation between emissivity and vapor pressure (in both Ångström's and Brunt's equations, R.U.) arises, not from any significant influence of variation of vapor pressure on atmospheric emission, but from a correlation between temperature and humidity", and furthermore that the wide variations in the empirical coefficients with locality are "due to

differences in the temperature-humidity regime from place to place, and not to any basic difference in the nature of the incoming radiation". He related the atmospheric emissivity directly to the square of the air temperature at screen level, without making use of empirical coefficients (i.e. he related the atmospheric emission to the sixth power of the air temperature).

Idso and Jackson [1969], questioned the value of the power of the temperature in Swinbanks relationship. They showed that powers varying from 1 to 10 all yielded very high correlations with Swinbank's original radiation data and argued that "there appears to be no theoretical justification for the power of the air temperature being greater than 4 for any air temperature obtainable on earth". According to Idso and Jackson, the atmospheric emissivity is symmetrical about a minimum at 273K and tends exponentially toward unity both for increasing and for decreasing temperatures, because ice and snow behave as nearly perfect emitters.

In an effort to reconcile some of the earlier discrepancies and to account for emission and absorption of longwave radiation in the atmosphere due to water vapor and carbon dioxide, Brutsaert [1975] took a more physically based approach that was completely different from the previously discussed empirical parameterizations. By substistuting exponential decay functions for temperature, pressure and water vapor density (as close approximations of their mean vertical profiles), he was able to integrate the equation for infrared radiative transfer in a plane stratified and nonscattering atmosphere in local thermodynamic equilibrium to yield the effective atmospheric emissivity as a function of both screen level vapor pressure and air temperature. The result was a relationship which is not very sensitive to changes in air temperature. The advantages of this formula over empirical expressions are (1) that it does not require empirical parameters to be determined from radiation experiments, and (2) that it allows easy adjustment for local conditions, both with respect to changes in surface elevation (appendix B.) and with respect to changes in humidity or temperature stratification.

A comparison experiment of Aase and Idso [1978] showed that both Idso and Jackson's empirical and Brutsaert's analytical formula adequately predicted longwave radiation from the atmosphere for screen level air temperatures above 0°C. Under freezing conditions however, the former was generally found to overestimate and the latter was found to underestimate the atmospheric emissivity. In response to this problem, Satterlund [1979] derived an exponential formula (again containing both vapor pressure and air temperature) that improved the agreement with measurements under freezing conditions.

Although Idso [1981] stated like Swinbank that "the relative successes of all prior equations have been due to general correlations between vapor pressure and air temperature", he took a different approach and developed a new physically based set of equations for the effective atmospheric emissivity of the entire spectrum and of two wavelength bands as functions of both air temperature and vapor pressure instead of air temperature alone. Idso showed

that "the true effect of increasing temperature (keeping vapor pressure constant, R.U.) is to decrease the effective emissivity of a cloudless atmosphere". He argued that "it is only because screen level vapor pressure generally increases with screen level air temperature that on a gross scale the Idso-Jackson (and Swinbank's and Satterlund's, R.U.) equation appears to give qualitatively correct results". Idso's equations are based on the postulation that the variable concentration of water dimers (pairs of water molecules linked together by weak hydrogen bonds) in the free atmosphere is the main source of variations in the effective emissivity associated with water vapor [Liou, 1980]. His equation for the entire spectrum yields accurate results over a wide range of screen level air temperatures, including freezing conditions.

Although Satterlund's and Idso's equations generally yield more reliable results for freezing conditions, Brutsaert's equation seems preferable not only from a theoretical point of view (i.e., it is not in contradiction with Idso's [1981] conceptual model) but also because the form of his derivation allows adjusting for the decreasing amount of water vapor in the atmosphere with increasing surface altitude. Moreover, during the melting season screen level air temperatures tend not to fall far below zero, thus generally avoiding the temperature region that causes this equation to deviate slightly from observations:

$$\epsilon_{skyo} = 0.642 * (e_a * T_a^{-1})^{1/7} \qquad (27)$$

where:

ϵ_{skyo} = Effective atmospheric emissivity under cloudless conditions [-]
e_a = Vapor pressure at surface [Pa]
T_a = Absolute air temperature at surface [K]

It can be shown that when Brutsaert's derivation is generalized to yield the effective atmospheric emissivity at any altitude in the atmosphere as a function of vapor pressure and air temperature at that altitude, the functional form of his equation remains exactly the same (appendix B.). Brutsaert's equation in its original form already implicitly accounts for the effect of an increasing surface altitude, because it contains the ratio of vapor pressure and air temperature at screen level above the surface. This ratio decreases with increasing surface altitude, since vapor pressure, as a result of its significant temperature dependence, decreases much faster than air temperature itself (equation (13) and subsequent remarks). A linear pressure correction in combination with an extrapolation of vapor pressure and air temperature towards mean sea level (assuming a constant temperature lapse rate and a constant relative humidity), as proposed by Marks and Dozier [1979] and Marks [1988], seems therefore inappropriate (appendix B.).

As a result of Kirchhoff's law, the fraction of the incident longwave radiation that is absorbed by a surface equals its emissivity. Therefore, the

net longwave radiation at an unobstructed horizontal surface can be written as follows:

$$L_n = \epsilon * L_{sky} - L_{sfc} \qquad (28)$$
$$= \epsilon * \sigma * (\epsilon_{sky} * T_a^4 - T_s^4)$$

where:

L_n = Net longwave radiation [Wm^{-2}]
ϵ = Surface emissivity [≈ 0.98]
L_{sky} = Atmospheric emission [Wm^{-2}]
L_{sfc} = Surface emission [Wm^{-2}]
σ = Stefan-Boltzmann's constant [$\approx 5.6697 * 10^{-8}$ $Wm^{-2}K^{-4}$]
ϵ_{sky} = Effective atmospheric emissivity [-]
T_a = Absolute air temperature at surface [K]
T_s = Absolute surface temperature [≈ 273 K]

Under cloudy skies the atmospheric emission increases, mainly as a result of the increased water vapor content. An appropriate adjustment for this effect would be to increase the effective atmospheric emissivity. Yet, various authors apply correction factors to the net longwave radiation under clear skies instead. These factors often take the form of a reduction of the longwave radiation budget proportional to the mean fractional cloud cover [Geiger, 1959; Unsworth and Monteith, 1975; Brutsaert, 1982]. This approach assumes the net longwave radiation under clear skies to be negative which may be true in most cases, but may actually be invalid in snow covered mountainous terrain. This is caused by snow surface temperatures that tend to be appreciably lower than air temperatures during snowmelt seasons (equation (28)). Therefore, an adjustment to the effective atmospheric emissivity seems more suitable under these conditions.

Such an adjustment basically can take three forms: (1) a linear relationship between the effective atmospheric emissivity under cloudy conditions and the mean fractional cloudcover, based upon weighing the emissivities for clear and overcast skies over the unobscured and obscured portions of the whole sky dome, respectively [Unsworth and Monteith, 1975]; (2) a quadratic empirical relationship that seems to be in better agreement with observations [Geiger, 1959; Brutsaert, 1982]; (3) a more physically based relationship as developed by Kimball et al. [1982] that takes into account the cloud amount and altitude for up to four cloud layers. The latter is based upon the emissivity equations developed by Idso [1981], and on the assumption that the cloud contribution to the atmospheric longwave radiation has to be transmitted to the earth's surface through the "atmospheric window". Although this method has yielded promising results, its relative complexity does not allow application to simplified operational approaches.

Therefore, the atmospheric emissivity under clear skies is adjusted for the effect of cloudcover through a nonlinear function of the mean fractional cloudcover:

$$\epsilon_{sky} * \epsilon_{skyo}^{-1} = 1 + c_3 * m_c^2 \quad (29)$$

where:

ϵ_{sky} = Effective atmospheric emissivity [-]
ϵ_{skyo} = Effective atmospheric emissivity under cloudless conditions [-]
c_3 = Empirical coefficient [≈ 0.22]
m_c = Mean fractional cloudcover [-]

Although the coefficient c_3 is actually dependent on cloud type, Brutsaert [1982] suggested that 0.22 should be a reasonable average. This is in good agreement with the experimental findings of Kimball et al. [1982] and with Sellers' [1965] remark that cloud layers generally do not increase atmospheric emission by more than 25 percent [Kimball et al., 1982]. If the atmosphere is assumed to behave like a perfect emitter for overcast skies (i.e. if ϵ_{sky} is assumed to become close to unity when m_c equals unity), then a value of 0.22 for c_3 restricts ϵ_{skyo} to a maximum of about 0.82. Under typical atmospheric conditions however, the effective clear sky emissivity (as can be seen from Brutsaert's formula, equation (27)) seldom becomes larger than this maximum.

After application of this correction to (27), (28) can be used to determine the net longwave radiation at an unobstructed horizontal surface as a function of the atmospheric conditions. The required input parameters are the surface temperature, the air temperature and vapor pressure at the surface and the mean fractional cloudcover.

2.3. Complex Terrain

2.3.1. Problems Encountered

The difficulties concerned with modeling the radiation budget in mountainous terrain are mainly associated with an additional topographic modification of incident electromagnetic radiation as compared to a uniform surface. The radiation-terrain interaction at a uniform surface is fully determined by its intrinsic reflective properties, whereas the radiation budget at a surface in complex terrain also is significantly influenced by obstruction, reflection and emission of radiation by adjacent surfaces. These effects are especially important in alpine watersheds where most of the larger snow covered areas have slopes of 10° to 30° [Olyphant, 1986a]. Similar obstacles as those in topoclimatology are encountered in building and urban climatology, bioclimatology and solar energy studies [Becker and Boyd, 1957; Arnfield, 1982]. Although most attention in this section will be paid to the effects of terrain geometry, altitude differences play an important role in radiation modeling because incoming solar radiation can vary by 25 percent over an elevation change of order 3000 meters [Dozier, 1980].

As far as modeling methodology for a point in complex terrain is concerned,

basically three types of incident radiation can be distinguished [Dozier and Frew, 1989]: (1) direct insolation, subject to a modification due to its projection at the surface and to possible obstruction by neighboring surfaces and objects superimposed on them (e.g., forest canopy); (2) diffuse radiation from the sky (both scattered solar and emitted thermal radiation), subject to a reduction as compared to a point at a uniform surface due to the partial obstruction of the sky hemisphere; (3) diffuse radiation from adjacent surfaces (both reflected solar and emitted thermal radiation), proportional to the viewed fraction of the hemisphere that is covered by surrounding terrain. As already mentioned, specular reflection of direct insolation is usually ignored. Although it might be of importance at particular combinations of solar position and slope exposure, its occurence is too infrequent to be of any significance in the radiation budget [Dozier, 1980; Proy et al., 1989].

The topography induced effect concerning direct insolation in mountainous areas is twofold: (1) a possible reduction of the day length due to shadowing, resulting both in large temporal and spatial variabilities; (2) a modification of the direct beam as a function of slope exposure, resulting mainly in large spatial variability. Dozier [1980] stated that "at all times of year horizons reduce the effective day length by intercepting direct beam radiation at low sun angles", and Whiteman et al. [1989] found that shadowing "is critical to the daily radiation totals".

Because multiple reflections are a major contribution to global radiation in snow covered terrain (section 2.2.2.), partial obstruction of diffuse sky radiation will cause a significant reduction of global radiation in complex terrain. Garnier and Ohmura [1970] argued that the interception of reflected radiation from adjacent surfaces plays a minor role in the energy budget of surfaces with albedo's less than 0.30. However, Kondratyev and Manolova [1960] found that the diurnal variation of the sum of scattered sky radiation and intercepted surface reflection on slopes with albedo's of about 0.20 was nearly independent of the inclination angle. They attributed their observation to "the tendency for compensation of the decrease of scattered radiation inflow (with increase in slope inclination angle) by the increase in the reflected radiation inflow". In snow covered terrain the latter will have even greater importance due to the high albedo of snow [Becker and Boyd, 1957; Shoshany, 1989]. Moreover, Olyphant [1986a] concluded that "surrounding rockwalls enhance the radiation balance of cirque glaciers and snowfields by reducing the net longwave loss 37-63 percent below that of an unobstructed horizontal surface".

2.3.2. Conversion Factor Approach

Since being proposed by Liu and Jordan [1961], it has been common practice to relate the components of the radiation budget in complex terrain to their corresponding values at uniform surfaces (as presented in section 2.2.) by

means of conversion factors. Applying the geometrical ray optics approach to describe the illumination of a terrain object and the shadow it casts, the conversion factor for direct radiation (or beam shading function) can be derived analytically. It is merely of function of the angle of incidence relative to the surface and of a binary coefficient that determines whether or not the surface is shadowed by itself or by surrounding slopes. The geometrical ray optics approach is based on the common assumption that the incident beam of light may be thought of as consisting of separate localized rays pursuing their own strait-line paths [Liou, 1980]. For diffuse radiation from the sky and from surrounding terrain however, an analytical solution can only be derived if the radiance (i.e. the broadband radiative flux density per sterradian of the spherical solid angle) distribution over the viewed fraction of the hemisphere is known.

Various authors have proposed semi-empirical radiance distribution functions for background (i.e. excluding the circumsolar or aureole component) scattered solar radiation [Moon and Spencer, 1942; Steven and Unsworth, 1979; 1980], for atmospheric emission [Unsworth and Monteith, 1975] and for net longwave radiation [Geiger, 1959; Kondratyev and Manolova, 1960]. Since background solar or thermal radiance in most cases do not possess any significant azimuthal dependence, they are usually given merely as functions of the zenith angle. A radiance distribution can be conveniently expressed as a so-called anisotropy factor [Dozier and Frew, 1989], defined as the ratio of the equivalent flux density from a particular solid angle to the flux density reaching a uniform horizontal surface from the entire hemisphere. It follows from this definition that the radiance from a direction characterized by an anisotropy factor equaling unity equals the average radiance reaching a uniform horizontal surface. The conversion factor that can be derived by integrating the surface projection of such an anisotropy factor over the viewed fraction of the sky hemisphere is usually referred to as the sky view factor. It is expressed as a dimensionless number that falls generally (though not necessarily) between zero and one.

Under the assumptions that the radiance distribution is isotropical and that the local topography can be described by a simple terrain model, integration yields convenient trigonometric conversion factors (appendix E.) [e.g., Hay and Davies, 1978]. The validity of such isotropic approximations however, has been questioned by various authors: Kondratyev and Manolova [1960] argued that although the isotropic approximation proves to be satisfactory for overcast sky conditions and for high solar elevation angles, it usually gives unsatisfactory results for calculating the scattered radiation fluxes on slopes. Steven and Unsworth [1980] state that "although the isotropic assumption (for diffuse solar radiation, R.U.) is mathematically convenient, it is supported neither by theory nor by observation", and they show that even for overcast skies it can result in a significant overestimation of the irradiance of sloping surfaces. On the other hand, they mentioned that both Fritz [1955] and Goudriaan [1977] gave a theoretical

foundation for the fact that the hemispherical uniformity (isotropy) of diffuse sky radiance under overcast skies increases with surface albedo, resulting in a rather weak zenith angle dependence above snow covered terrain! In any case, the suggestion by Becker and Boyd [1957] that the ratios (of solar radiation incident upon tilted surfaces to that incident on horizontal surfaces) would tend toward unity with increased cloudiness completely overlooks the characteristic phenomenon of terrain obstruction of part of the sky hemisphere in complex terrain. Olyphant [1986a] compared isotropic and anisotropic models for the longwave irradiance in a mountainous area and found that the isotropic assumption does not yield satisfactory results for longwave irradiance.

Other investigators have attempted to account for anisotropy without performing the computationally intensive spatial integration of radiance distribution functions (e.g., Temps and Coulson [1977]). Temps and Coulson took a more empirical approach in modeling the anisotropic properties of scattered solar radiation under clear skies by multiplying the isotropic view factor by correction factors to account for brightening of the sky in the vicinity of the sun and the horizon (section 2.2.2.). On the other hand, Klucher [1979] observed that the isotropic approximation yields satisfactory results under overcast sky conditions but underestimates the insolation at higher intensities, whereas the modified model of Temps and Coulson provides an improvement under clear sky conditions but overestimates the insolation under partly cloudy and overcast conditions. He therefore introduced a "modulating function" containing the ratio of diffuse to global insolation at a uniform surface ($K_{dif}/K\downarrow$) to account for the effect of cloudiness. Hay and Davies [1978] used a similar approach by using the ratio of direct to extraterrestrial radiation at a uniform surface (K_{dir}/K_o) for this purpose. Both models were found to be superior to the isotropic model, although the model of Hay and Davies showed a smaller difference in seasonal performance than Klucher's model [Ma and Iqbal, 1983].

The conversion factor that can be derived by integrating the surface projection of the distribution of the intercepted reflection or emission over the viewed fraction of the hemisphere covered by surrounding terrain is usually referred to as the terrain configuration factor. As a result of the complex geometric effects between a point in mountainous terrain and each point in the surrounding terrain with which it is mutually visible, the isotropic assumption is unrealistic even if the surrounding terrain is a Lambertian reflector or a perfect emitter [Dozier and Frew, 1989]. Moreover, radiation received from obscured portions of the sky hemisphere strictly speaking also depends upon transmission and emission by the slab of air between source and receptor [Olyphant, 1986a; Shoshany, 1989]. Temps and Coulson [1977] also derived an empirical correction factor for application to the isotropic terrain configuration factor. Since it was based on reflectance measurements for grass turf however, it does not seem to be suitable for snow covered terrain. Hence, if no measurements of surface reflection or emission

are available an isotropic terrain configuration factor remains the only option.

Since the interception of reflection and emission from surrounding terrain do not have a corresponding value at a uniform surface, they are usually related to the reflected or emitted radiation from a uniform surface. For the diffusely reflected direct insolation however, this is a rather crude approximation since the average reflection from surrounding terrain can be markedly different from the reflection from a uniform surface [Dozier, 1980]. Furthermore, the effects of multiple reflections between facing slopes are generally neglected, although an investigation carried out by Shoshany [1989] suggests that those might be significant for highly reflective (snow) surfaces facing each other at a relatively steep angle. Proy et al. [1989] state that interception of reflection from surrounding terrain can be neglected for directly illuminated sites, but should be taken into account for shadowed sites. Nonetheless, it is postulated that the average reflection from surrounding terrain can be adequately approximated by the reflection from a uniform surface since (1) it is not a major term in the radiation budget and (2) terrain induced effects tend to cancel out when integrated over space [Kondratyev and Manolova, 1960; Shoshany, 1989].

Taking into account the considerations stated above, the shortwave (solar) and longwave (thermal) components of the radiation balance at a point in snow covered mountainous terrain can be conveniently expressed as functions of their equivalents at a uniform snow surface:

$$K_n = (1 - a_{dir}) * V_{dir} * K_{dir} + (1 - a_{dif}) * (V_{sct} * (C_s' * C_s^{-1} * K_{sct} + K_{bck}) + V_{trn} * a_{trn} * K\downarrow) \quad (30)$$

$$L_n = \epsilon * (V_{sky} * L_{sky} + V_{trn} * \epsilon_{trn} * \sigma * T_{trn}^4) - L_{sfc} \quad (31)$$

where[1]:

K_n = Net shortwave radiation
a_{dir} = Diffuse surface reflectivity for direct radiation [-]
V_{dir} = Conversion factor for direct radiation or beam shading function [-]
K_{dir} = Direct solar radiation
a_{dif} = Surface reflectivity for diffuse radiation [-]
V_{sct} = Conversion factor for background solar sky radiation or sky view factor [-]
C_s' = Correction for sky brightening in vicinity of sun in complex terrain [-]
C_s = Correction for sky brightening in vicinity of sun at unobstructed horizontal surface [-]
K_{sct} = Radiation scattered downward from direct beam
K_{bck} = Backscatter from atmosphere
V_{trn} = Conversion factor for diffuse radiation from surrounding terrain or terrain configuration factor [-]
a_{trn} = Average albedo of adjacent terrain [≈ 0.25]
$K\downarrow$ = Downward shortwave radiation
L_n = Net longwave radiation
ϵ = Surface emissivity [≈ 0.98]
V_{sky} = Conversion factor for atmospheric emission or sky view factor [-]

L_{sky} = Emission from atmosphere
ϵ_{trn} = Average emissivity of adjacent terrain [≈ 0.95]
σ = Stefan-Boltzmann's constant [≈ 5.6697 * 10^{-8} $Wm^{-2}K^{-4}$]
T_{trn} = Average surface temperature of adjacent terrain [K]
L_{sfc} = Surface emission

[1] Unit of radiative flux density is [Wm^{-2}].

All radiative flux densities in equation (30) and (31) are already determined in sections 2.2.3 and 2.2.4. (for substitution in equations (25) and (28), respectively). The determination of the conversion factors and of the additional correction factor (C_s'/C_s) accounting for sky brightening in the vicinity of the sun will be discussed in the next section.

This additional correction for sky brightening in the vicinity of the sun is necessary because the radiance distribution functions for scattered solar radiation mentioned earlier and consequently the sky view factors based upon them only account for background radiation (both resulting from scattering of the direct beam and from atmospheric backscatter) but not for the circumsolar or aureole component (merely resulting from scattering of the direct beam) that is present when the direct beam is not obstructed by a local horizon or a cloudcover. This correction takes the form of a ratio because Temps and Coulson [1977] proposed different factors for unobstructed horizontal surfaces (uniform terrain) and obstructed inclined surfaces (complex terrain). Hence, for applications in complex terrain, the former, which has been used in equation (10), should be eliminated and substituted by the latter.

The average surface properties of the terrain surrounding the point at which the radiation budget is modeled (i.e. albedo, emissivity and surface temperature) depend largely on the question of whether it is snow covered or not. In case the adjacent surfaces are completely snow covered, the same values can be applied as determined for the model point itself. In case of bare rock or vegetation however, the surface albedo will be significantly lower (about 0.25-0.30 for rockwalls), the surface emissivity will be somewhat lower (about 0.95), and the daily average surface temperature will be presented more adequately by the daily average air temperature than by the freezing temperature of water [Marks and Dozier, 1979; Olyphant, 1984; 1986a,b]. Such reasonable approximations are accurate enough in most cases, because terrain configuration factors are usually small when compared to sky view factors, even in mountainous terrain.

Although the current investigation deals with determining the radiation budget at a point, simulation of radiation induced snow melt rates for a whole watershed requires spatial integration of point values. Various investigators have used digital elevation data as input for solar [Dozier, 1980; Isard, 1983; Olyphant, 1984; 1986b] and for thermal radiation models [Marks and Dozier, 1979]. Problems related to the efficiency of spatial integration algorithms [Dozier and Frew, 1989] and to the spatial extrapolation of input data [Marks and Dozier, 1979; Running et al., 1987] are not within the scope

of this investigation. Nonetheless, they will be of importance in future implementations of the present model.

2.3.3. Conversion Factor Determination

As mentioned in section 2.3.2., the conversion factor for direct radiation incident on a point in complex terrain (beam shading function) is a function of: (1) a binary shading coefficient that determines whether the observed point is in the shadow or not, and (2) the ratio of the cosine of the incidence angle at the inclined surface which contains the observed point to that at an imaginary horizontal surface at the same location:

$$V_{dir} = \Gamma * \cos[\theta_s'] * \cos[\theta_s]^{-1} \qquad (32)$$

if $\theta_s \geq H[\Phi_s]$ then $\Gamma = 0$, else $\Gamma = 1$

where[1,2]:

V_{dir} = Beam shading function [-]
Γ = Binary shading coefficient [-]
θ_s' = Incidence angle of direct radiation [rad]
θ_s = Solar zenith angle [rad]
H = Zenith angle of local horizon [rad]
Φ_s = Solar azimuth angle [rad]

[1] The incidence angle is defined as the angle between a unit coordinate vector normal to the surface and pointing away from the ground and a unit coordinate vector pointing toward the center of the solar disk.
[2] Azimuths are measured from north through east.

The cosine of the solar zenith angle (i.e. the incidence angle at a horizontal surface) is given by equation (6) as a function of surface latitude, solar declination and hour angle. The cosine of the incidence angle at an inclined surface can be given either (1) directly as a function of the solar zenith and azimuth angles and of the surface geometry as determined by its inclination (slope) and azimuth angles (aspect), or (2) indirectly as a function of latitude, declination, hour angle, slope and aspect. The latter can be derived from the former (equation (36) with $\theta=\theta_s$ and $\Phi=\Phi_s$) when expressions for the solar zenith and azimuth angles are substituted [e.g., List, 1966; Kondratyev, 1973; Whiteman and Allwine, 1986], which is shown in appendix C. Garnier and Ohmura [1968; 1970] took a slightly different approach and used a coordinate transformation following the principles of spherical trigonometry to derive the same convenient formula.

Local horizon functions can be sampled accurately from digital terrain models, although traditional brute force techniques result in a huge computational burden. Dozier and Frew [1989] developed a rapid algorithm for the calculation of terrain parameters from digital elevation data and found that 16 directions around the circle (equivalent with an angular increment of

$\pi/8$ radians or 22.5°) are usually enough to describe the horizon angle adequately. Given the hypothetical case that only self-shading occurs, the inclined surface is described by an infinitely long uniform slope, and the local horizon is merely a function of the inclination and azimuth angles of the surface itself (equation (41)). The criterion for switching the binary shading coefficient from zero to one now reduces to: if ($\cos[\theta_s'] \leq 0$ or $\cos[\theta_s] \leq 0$) then $\Gamma=0$, else $\Gamma=1$. This geometrical simplification is the basis for the well-known simple trigonometric conversion factors for isotropically distributed diffuse radiation from the sky and radiation from adjacent terrain.

Because the additional correction factor used in equation (30) to account for brightening of the sky in the vicinity of the sun is treated geometrically as part of the direct solar beam, it is discussed here before the actual conversion factor for background scattered solar radiation. To account for the possible obstruction of the direct beam by a local horizon or a cloudcover, the binary shading coefficient from equation (32) and Klucher's [1979] modulating function (based on variables whose determination has been discussed extensively in section 2.2.3.) are applied, respectively. As for the rest, Temps and Coulson's [1977] correction factor retains basically its original form (as given in equation (10)) in complex terrain:

$$C_s' * C_s^{-1} = (1 + \Gamma * F * \cos^2[\theta_s'] * \sin^3[\theta_s]) * (1 + F * \cos^2[\theta_s] * \sin^3[\theta_s])^{-1} \quad (33)$$

$$F = 1 - (K_{dif} * K\downarrow^{-1})^2$$

where:

- C_s' = Correction for sky brightening in vicinity of sun in complex terrain [-]
- C_s = Correction for sky brightening in vicinity of sun at unobstructed horizontal surface [-]
- Γ = Binary shading coefficient [-]
- F = Modulating function for cloudcover [-]
- θ_s' = Incidence angle of direct radiation [rad]
- θ_s = Solar zenith angle [rad]
- K_{dif} = Diffuse sky radiation reaching unobstructed horizontal surface [Wm^{-2}]
- $K\downarrow$ = Downward shortwave radiation reaching unobstructed horizontal surface [Wm^{-2}]

The conversion factor for diffuse radiation from the sky (both for background scattered solar and emitted thermal radiation) incident on a point in complex terrain (sky view factor) is by definition the ratio of the hemispherically integrated sky radiance at the inclined surface which contains the observed point to that at an imaginary horizontal surface at the same location. In terms of the previously mentioned anisotropy factor, being the ratio of the equivalent flux density from a particular direction to the diffuse radiation reaching a horizontal surface [Dozier and Frew, 1989], the

sky view factor can be expressed as follows in the polar coordinates of a viewer-oriented (global) coordinate system [Kondratyev and Manolova, 1960; Arnfield, 1982]:

$$V_{dif} = \pi^{-1} * \int_0^{2\pi} \int_0^{H[\Phi]} \Omega_{dif}[\theta,\Phi] * \sin[\theta] * \cos[\theta'] * d\theta * d\Phi \qquad (34)$$

$$\Omega_{dif}[\theta,\Phi] = \pi * R[\theta,\Phi] * R_{dif}^{-1} \qquad (35)$$

$$\cos[\theta'] = \cos[S] * \cos[\theta] + \sin[S] * \sin[\theta] * \cos[\Phi - A] \qquad (36)$$

where:

V_{dif} = Sky view factor [-]
H = Zenith angle of local horizon [rad]
Ω_{dif} = Anisotropy factor for diffuse radiance from the sky [-]
θ = Zenith angle [rad]
θ' = Incidence angle of diffuse radiance from the sky [rad]
Φ = Azimuth angle [rad]
R = Diffuse radiance from the sky [$Wm^{-2}sr^{-1}$]
R_{dif} = Diffuse radiation from the sky reaching unobstructed horizontal surface [Wm^{-2}]
S = Surface inclination angle or slope [rad] (= Zenith angle of surface normal)
A = Surface azimuth angle or aspect [rad] (= Azimuth angle of surface normal)

The previously mentioned semi-empirical distribution functions for background scattered solar radiation and atmospheric emission usually take the form of radiance distributions as functions of the zenith angle only ($R[\theta]$) instead of anisotropy factors as functions of both zenith and azimuth angles ($\Omega[\theta,\Phi]$), i.e. azimuthal dependence is ignored and the convenient anisotropy factor approach is not applied. However, $R[\theta]$ can easily be converted to $\Omega[\theta]$ by means of equation (35), because R_{dif} is merely the hemispherical integration of $R[\theta]$ at an unobstructed horizontal surface, which can be seen from equation (34) by setting $V_{dif}=1$ when $H[\Phi]=\pi/2$ and $\theta'=\theta$:

$$R_{dif} = \int_0^{2\pi} \int_0^{\pi/2} R[\theta] * \sin[\theta] * \cos[\theta] * d\theta * d\Phi$$

$$= 2\pi * \int_0^{1} R[\mu] * \mu * d\mu \; ; \; \mu = \cos[\theta] \qquad (37)$$

where:

R_{dif} = Diffuse radiation from the sky [Wm^{-2}]
R = Diffuse radiance from the sky [$Wm^{-2}sr^{-1}$]
θ = Zenith angle [rad]
Φ = Azimuth angle [rad]
μ = Cosine of zenith angle [-]

It can be seen from this equation that the term $\pi*R[\theta,\Phi]$ in equation (35) is the equivalent flux density from a hemisphere radiating isotropically like the solid angle denoted by the coordinates (θ,Φ). By definition (equation (35)), this equivalent flux density is equal to the actual flux density when the anisotropy factor equals unity.

In appendix D. the following anisotropy factors are derived on the basis of widely used radiance distribution functions for background scattered solar radiation and atmospheric emission for varying atmospheric conditions (figure 2.3.3.):

$$\Omega_k[\mu] = (1 + b_k * \mu) * (1 + b_k * 2/3)^{-1} \quad (38)$$

$$\Omega_l[\mu] = 1 - b_l * \epsilon_{sky}^{-1} * (0.5 - \ln[M_w]) \quad (39)$$

where:

Ω_k = Anisotropy factor for background solar sky radiance [-]
μ = Cosine of zenith angle [-]
b_k = Empirical coefficient [$\approx$ -0.87 for clear skies; $\approx$ 1.23 for overcast skies]
Ω_l = Anisotropy factor for atmospheric emittance [-]
b_l = Empirical coefficient [$\approx$ 0.09]
ϵ_{sky} = Effective atmospheric emissivity [-]
M_w = Relative path length for water vapor [-]

It is noted that the values given above for the empirical coefficients b_k and b_l were derived on the basis of extensive measurements presented by Steven and Unsworth [1979; 1980] and Unsworth and Monteith [1975], respectively. With b_k=2, this yields the well known "Standard Overcast Sky" (SOC) proposed by Moon and Spencer [1942].

It is shown in appendix D. that b_l can be determined solely as a function of ϵ_{sky} if it is assumed that the equivalent emissivity tends to unity as μ approaches zero (zenith angle θ approaches $\pi/2$), as was reasoned both by Brunt [1932] and by Unsworth and Monteith [1975]. Within the range of effective sky emissivities that occur (i.e. that result from equations (27) and (29)), this approach yields values close to 0.09. Hence, the value proposed by Unsworth and Monteith can be reconciled with theoretical considerations.

Unsworth and Monteith [1975] showed the anisotropy factor for atmospheric emittance to be valid for both clear and overcast skies. Olyphant [1986b] proposed a weighted average estimate of the anisotropy factor for background solar sky radiance under partly cloudy skies, using the shortwave

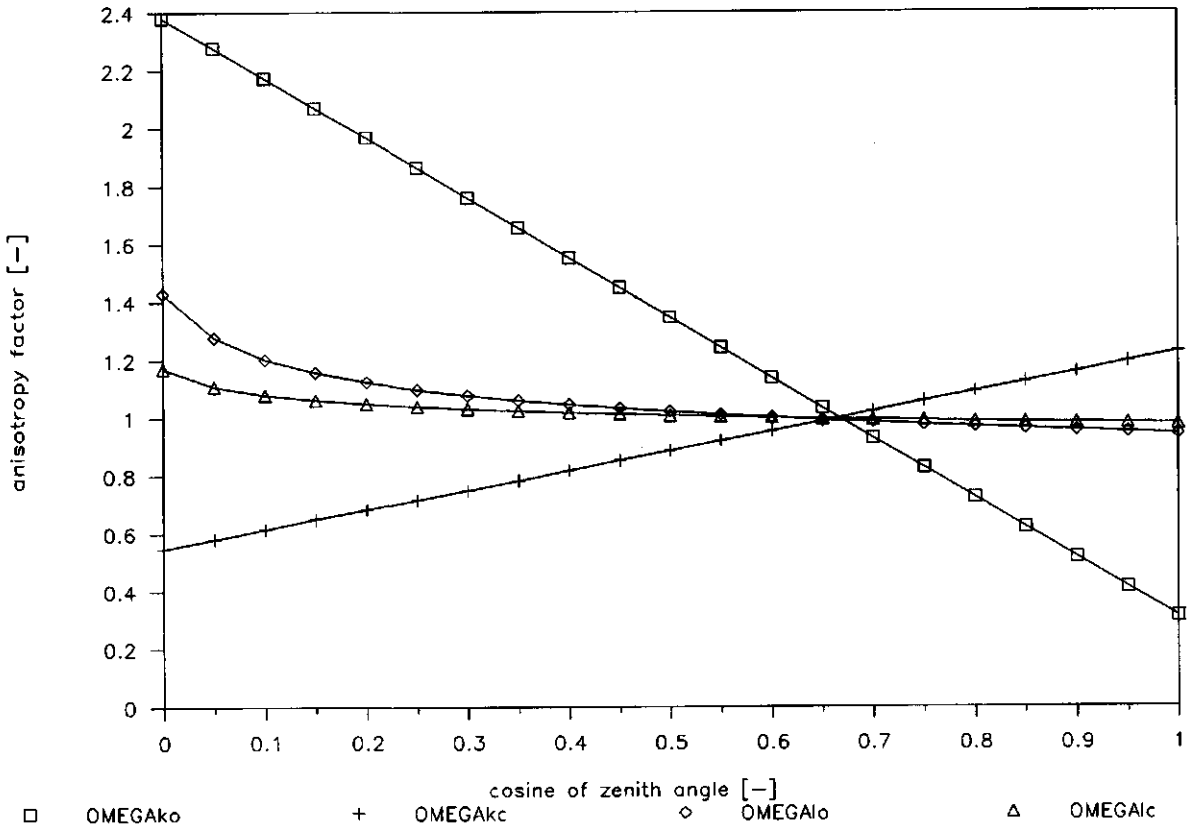

fig. 2.3.3. Anisotropy factors for background solar sky radiance (Ω_k) and atmospheric emittance (Ω_l) as functions of the cosine of the zenith angle (μ) for clear (o) and overcast (c) skies.

transmissivity of the atmosphere ($K\downarrow/K_0$) and its complement as weights, respectively. Since this was meant as an indicator of the percentage cloudiness, direct application of the mean fractional cloudcover (m_c) like in equation (19) seems more obvious. Note that b_k equal to -0.87 in equation (38) accounts for the horizon brightening effect under clear skies (fig. 2.3.3.).

Since the functional form of the horizon function and some of these anisotropy factors prevents us from integrating equation (34) analytically, numerical integration methods remain the only alternative. Arnfield [1982] carried out an error analysis to determine the optimal value (in the tradeoff between computing expense and accuracy) of the angular increment used in the numerical integration over zenith and azimuth angle. He recommended angles of at most $\pi/36$ and $\pi/18$ radians to achieve deviations of no more than 5 and 10 percent respectively from the "exact" solution, which was evaluated with an angular increment of $\pi/180$ radians (1°) using Simpson's numerical integration rule.

When the anisotropy factor in equation (34) is set equal to one, the isotropic approximation of the sky view factor is determined. Dozier and Frew [1989] showed that in that case (34) can be converted to a more convenient expression that merely requires numerical integration over all azimuth directions. An even greater reduction in computational effort can be achieved when the horizon function is described by some integrable expression that is completely determined by the geometrical properties of the surface in question, i.e. slope and aspect. Local topography is than modeled by an infinitely long uniform slope facing an infinitely long horizontal surface. The zenith angle of the local horizon is consequently determined in upslope direction ($\cos[\Phi-A]\leq 0$) by the zenith angle of a ray that is parallel to the slope, and in downslope direction ($\cos[\Phi-A]\geq 0$) by an angle of $\pi/2$ radians. Setting θ equal to H and θ' equal to $\pi/2$ in equation (36) yields the following local horizon function for this simple terrain model:

$$\text{if } \cos[\Phi - A] \geq 0 \text{ then } H[\Phi] = \pi/2,$$
$$\text{else } H[\Phi] = \arctan[-(\tan[S] * \cos[\Phi - A])^{-1}] \qquad (40)$$

where:

Φ = Azimuth angle [rad]
A = Surface azimuth angle [rad]
H = Zenith angle of local horizon [rad]
S = Surface inclination angle [rad]

This simplification allows analytical integration of (34), resulting in the well known isotropic trigonometric sky view factor approximation [e.g., Hay and Davies, 1978]. Steven and Unsworth [1979; 1980] even present an analytical solution for the anisotropic case where the background solar sky radiance distribution is described by equation (38). An extension of the isotropic model to an infinitely long V-shaped valley, i.e. two infinitely long uniform

slopes facing each other leads to the following exact solution of equation (34) (appendix E.):

$$V_{dif} = \cos^2[(S + S') / 2] = (1 + \cos[S + S']) / 2 \qquad (41)$$

where:

V_{dif} = Sky view factor [-]
S = Surface inclination angle [rad]
S' = Inclination angle of facing slope or inclination angle of horizon in direction of facing ridge top [rad]

Obviously, this equation must also be valid at the valley floor of a V-shaped valley composed of two facing slopes of finite dimensions. Setting S' equal to zero yields the solution of (34) for the isotropic case (Ω=1) when the local horizon function is defined according to (40). Olyphant [1984, 1986a] used the square of the sine of the average zenith angle of the local horizon as a sky view factor approximation.

In a preliminary numerical integration study, an intercomparison was made between the sky view factors for a symmetrical infinitely long V-shaped valley computed according to the anisotropic formula (34), the isotropic formula (41) and Olyphant's formula ($V_{dif} = \sin^2[H_m]$). Equation (34) (with the anisotropy factors defined according to (38) and (39)) was integrated numerically over the appropriate zenith and azimuth angles with angular increments of pi/18 radians using Simpson's 1/3 rule. The (Microsoft Quick)BASIC computer program that was constructed for this purpose ("FACTORS" in appendix E.) has been validated in 3 ways [Feldman and Rugg, 1988]: (1) When used for simulating a horizontal surface, the integrated view factors never deviated more than 0.02 percent from unity; (2) When the anisotropy factors were set equal to one, the integrated view factors never departed more than 0.01 percent from their isotropic equivalents; (3) When simulating an infinitely long uniform slope facing an infinitely long uniform surface, the integrated view factors for background solar sky radiance never deviated more than 0.01 percent from the analytical solution that Steven and Unsworth derived for this case. It was found that the isotropic formula is an accurate approximation for the view factor for atmospheric emittance for facing slopes of up to 60° (the maximum error amounted about 3 percent). As an approximation for the view factor for background solar sky radiance however, it performed slightly less accurate, resulting in an overestimation for clear skies of 14 (43) percent and an underestimation for overcast skies of 4 (9) percent for facing slopes of 30° (60°). Olyphant's formula always drastically overpredicted the sky view factor, but will probably yield better results in real mountainous terrain. When the local horizon function defined in FACTORS is delineated from a topographic map or digital terrain model, this computer program can serve as a subroutine in a radiation budget model for mountainous terrain (chapter 3.).

The conversion factor for the intercepted diffuse radiation from adjacent surfaces (both for reflected solar and emitted thermal radiation) incident on

a point in complex terrain (terrain configuration factor) is by definition the ratio of the hemispherically integrated diffuse terrain radiance at the inclined surface which contains the observed point to the radiation reflected or emitted by an imaginary horizontal surface at the same location. The general functional form defining the terrain configuration factor is the same as that of equation (34) (defining the sky view factor), except that the surface projection of the terrain anisotropy factor is integrated over all zenith angles from the local horizon downward to where a ray is parallel to the slope in question (as given by the arctangent expression in (40) without the mentioned azimuthal restriction) instead of over all zenith angles from the zenith downward to the local horizon [Dozier and Frew, 1989]. Hence, an additional component of diffuse irradiance will be contributed to an inclined surface in complex terrain from the lower hemisphere by adjacent surfaces in the downslope direction [Arnfield, 1982]. This effect partially compensates the obstruction of the upper hemisphere by the same surrounding surfaces and by the receiving surface itself, as quantified by the sky view factor. As stated in section 2.3.2., the isotropic approximation remains the only option for the terrain configuration factor if no measurements of surface reflection or emission are available. The same (geometric) simplifications as discussed for the isotropic sky view factor approximation can be applied to the isotropic terrain configuration factor approximation, resulting in the following expression valid for an infinitely long V-shaped valley:

$$V_{trn} = \sin^2[(S + S') / 2] = (1 + \sin[S + S']) / 2 \qquad (42)$$

where:

V_{trn} = Terrain configuration factor [-]
S = Surface inclination angle [rad]
S' = Inclination angle of facing slope or inclination angle of horizon in direction of facing ridge top [rad]

It can be seen from the equations (41) and (42) and from investigations by Olyphant [1984, 1986a], who used the square of the cosine of the average zenith angle of the local horizon as isotropic approximation of the terrain configuration factor, that the sum of these isotropic approximations of V_{dif} and V_{trn} equals unity. Dozier and Frew [1989] state that this sum equals $\cos^2[S/2]$, suggesting that the terrain configuration factor for an infinitely long slope equals zero. The above analysis clearly shows that this is incorrect.

Finally, it is noted that from a computational point of view the two basic differences between the conversion factor for direct solar radiation (beam shading function) on the one hand and the conversion factors for diffuse radiation from the sky (sky view factor) and for intercepted diffuse radiation from surrounding terrain (terrain configuration factor) on the other hand are: (1) that the former represents an instantaneous value whereas the latter represent daily averages (for anisotropical radiation fields) or even constant

values only depending on terrain geometry (in case the radiation fields are assumed to be isotropic), and (2) that the former does not require spatial integration because the solar disk is assumed to be a point source superimposed on a nonradiating background (as far as direct solar radiation is concerned). Thus its radiation field could be described by an appropriate anisotropy factor expressed in terms of the Dirac δ function [Horn and Sjoberg, 1979].

CHAPTER 3.

RADIATION BUDGET MODULE - RBM

3.1. Model Assumptions

The simplified approach toward modeling the radiation budget at a point in snow covered mountainous terrain as presented in the preceeding chapter has been the basis for the development of the computer simulation program RBM (Radiation Budget Module), which is implemented in the (MicroSoft Quick)BASIC programming language [Feldman and Rugg, 1988]. From its source code listing as presented in appendix E. it can be seen that RBM is a structured computer program designed according to the method of procedural abstraction (functional decomposition). That is, the main objective of the program was decomposed into several subfunctions, most of which are implemented as separate subroutines [van Vliet, 1988]. The resulting model structure generally follows that of the radiation budget algorithm as presented in the preceeding chapter.

RBM was actually designed as a module within the framework of the larger modular computer simulation program EBM (Energy Budget Model). The latter not only models the diurnal variation of the radiation balance, but also contains parameterizations for some of the other components of the energy budget as described in equation (1) (i.e. the turbulent exchange terms) and compares the capability of the energy budget method with two methods based on the empirical temperature index approach in simulating daily snowmelt and runoff for a complete melt season. These last functions however are not directly within the scope of this research project, and will therefore be discussed in a later stage (section 4.3.).

Generally, the assumptions of a model should always be given explicitly to avoid ambiguities and to allow a judgement of the model on its merits. Although the basic assumptions of the present modeling approach have been mentioned throughout the text, they will be summarized here for reasons of clearness and completeness:

3.1.1. Assumptions Concerning the Earth's Atmosphere

- The overlap between the region of the electromagnetic spectrum consisting of radiation emitted by the sun (shortwave) and the region consisting of radiation emitted by the earth-atmosphere system (longwave) is negligible and may therefore be treated separately.
- Scattering of electromagnetic radiation only affects the shortwave region of the spectrum, i.e. the longwave region is merely associated with emission and absorption.

- Water vapor and ozone are the only constituents of the atmosphere that absorb shortwave electromagnetic radiation, i.e. absorption of shortwave radiation by permanent or miscellaneous gases (nitrogen, oxygen and carbon dioxide) and by aerosols is negligible.
- Water vapor and carbon dioxide are the only constituents of the atmosphere that absorb and emit longwave electromagnetic radiation.
- In a clear atmosphere at high altitudes (i.e. in mountainous terrain) direct solar radiation is attenuated exponentially with a constant extinction coefficient (optical depth).
- The average vertical temperature profile of the atmosphere is a constant decay with altitude equal to the standard lapse rate.
- The average vertical air pressure and water vapor pressure and density profiles of the atmosphere are exponential decays with altitude.
- There exists a space and time invariant functional relationship between the ratio of diffuse to global solar radiation and the ratio of global to extraterrestrial solar radiation.
- The azimuthal dependency of diffuse (both background scattered solar and emitted thermal) radiance from the sky is negligible.
- The atmosphere acts as an isotropically backscattering medium.

3.1.2. Assumptions Concerning the Earth's Surface

- Net radiation is the dominant component in the surface energy budget at a point in snow covered mountainous terrain.
- The surface of a melting snowpack is wet during the entire day.
- Each new snow accumulation consists of dry uncontaminated snow with the same mean grain size.
- The earth's surface acts as a perfect diffuse (isotropical or Lambertian) reflector, i.e. the occurence of specular (Fresnel) reflection of direct insolation and of anisotropical diffuse reflection resulting from macroscopic geometric effects (terrain relief) are ignored.
- The effects of transmission and emission by the slab of air between neighbouring surfaces in complex terrain on the one hand and the effect of multiple scattering between such surfaces on the other hand cancel out when integrated over space. The average reflection and emission from surfaces surrounding the model point in complex terrain are therefore equal to the reflection and emission from a uniform horizontal surface with the same surface properties (i.e. albedo, emissivity and temperature).
- The possible effects of diffraction and refraction of electromagnetic radiation at the earth's surface are negligible.
- The direct beam of electromagnetic radiation reaching the earth's surface consists of parallel rays, i.e. the earth-sun distance is infinitely large.

- The apparent position of the sun as it is observed at the earth's surface equals the true position of the sun relative to the centre of the earth, i.e. the apparent reduction of the solar zenith angle close to sunrise and sunset as caused both by refraction of electromagnetic radiation in the atmosphere and by parallax is negligible [Blackadar, 1984].

3.2. Required Input

The input parameters and variables required for the simulation of each term of the radiation budget at a point in snow covered mountainous terrain are given in table 3.2. The first six (namely the latitude (Φ), longitude (l), altitude (h), slope (S), aspect (A) and horizon (H) of the surface in question) are fixed geographical parameters that need to be determined only once, whereas the day of the year (D, or date), the number of days since the last snowfall event occured (D_s) and the time of the day (t) are variables that are measured easily and accurately. This leaves six unknown variables that have to be determined on a daily basis (wich is usually sufficient for the simulation of the daily radiation budget throughout a snowmelt season) or with a higher temporal resolution (needed if a more accurate simulation of the diurnal radiation budget variation is desired). Three of these meteorological variables (namely the optical depth (τ) or transmissivity (T) of the atmosphere, the air pressure at screen level (p) and the surface temperature (T_s)) can be estimated with reasonable accuracy as pointed out in the preceeding chapter. The remaining variables serving as input for RBM are the temperature (T_a) and vapor pressure (e_a) of the air at screen level and the mean fractional cloudcover (m_c) (and/or relative sunshine duration).

As a result, the radiation budget simulation module in its present form requires only three variables to be determined on a regular basis for its execution, given the values for the constants and parameters mentioned along with the equations in the preceeding chapter. Hence, it complies with one of the most important objectives of the current research project, namely the development of a physically based radiation budget model requiring only a limited number of input data in order to remain operational relative to the Snowmelt Runoff Model (SRM). However, additional input in the form of measurements of net radiation and other variables may be required for verification purposes (section 4.1.). Moreover, if the meteorological variables (air pressure, temperature and vapor pressure) are not determined at screen level, the altitudes of the measuring devices relative to the modeling point need to be determined in order to be able to extrapolate the measurements using standard vertical profiles.

		INPUT PARAMETERS														
		Φ	l	h	S	A	H	D	D_s	t	r/T	p	T_s	T_a	e_a	m_c
RADIATION TERMS	Kdir	+	+	±	+	+	+	+	-	+	±	±	-	±	-	+
	Ksct	+	+	±	+	+	+	+	-	+	±	±	-	±	+	+
	Kbck	+	+	±	+	+	+	+	+	+	±	±	-	±	+	+
	Kn	+	+	±	+	+	+	+	+	+	±	±	-	±	+	+
	Lsfc	-	-	-	-	-	-	-	-	-	-	-	±	-	-	-
	Lsky	-	-	-	+	+	+	-	-	-	-	-	-	+	+	+
	Ln	-	-	-	+	+	+	-	-	-	-	-	±	+	+	+
	Rn	+	+	±	+	+	+	+	+	+	±	±	±	+	+	+

Table 3.2. Input required for the simulation of each term of the radiation budget at a point in snow covered mountainous terrain, where + = necessary, ± = useful and - = not necessary (see text for notation of symbols).

CHAPTER 4.

SIMULATING RADIATION AND SNOWMELT

4.1. Model Testing

Thorough testing of a computer simulation model can consist of three phases, namely a validation, a verification and possibly a calibration phase. Validation is defined as a means of static analysis that consists of an internal consistency check resulting in a proof of the correctness of the model, which may be accomplished by means of structured testing of the individual refinement steps of the model. In practice this phase reduces to the check on the syntax and semantics of the program with respect to the programming language that is performed automatically by the installed compiler and manually by the author. Verification is defined as a means of dynamic analysis that consists of an accuracy check by means of a comparison of model results with standard references and an assessment of the model performance with respect to the resulting differences [van Vliet, 1988]. Examples of standard references are observations on the modeled system, analytical solutions of numerical equations used in the model and results obtained by other investigators. Calibration is the optimization of model parameters using some criterion to minimize the differences between the results of model simulations and measurements of the modeled system. The Radiation Budget Module has an option for calibrating the optical depth (or transmissivity) of the atmosphere using radiation measurements. The optimized values however, should always be checked to avoid the use of physically unrealistic values.

Apart from the internal consistency checks that were performed throughout the construction of the computer simulation program RBM, the actual model testing was basically an extensive verification procedure. This consisted of comparisons between simulations and measurements of global and net radiation for a whole day at a site near Phoenix, Arizona (section 4.2.) and of global radiation and snowmelt for a complete melt season at a site near Davos, Switzerland (section 4.3.4.).

4.2. Simulating Radiation

The data used for the verification of the Radiation Budget Module (RBM) were collected at Maricopa Agricultural Research Center (MAC farm, 33.1°N and 112.0°W), which is about 60km south of Phoenix, Arizona. The applied data set consists of one minute averages of downward shortwave radiation (global radiation, K↓), net radiation (R_n), air temperature (T_a), surface temperature (T_s) and vapor pressure (e_a). They were collected over a horizontal wheat field

with an elevation (h) of merely 358m under ideal atmospheric conditions (m_c=0) at April 10, 1989 between midnight and 16:17h (Local Standard Time, LST) [The University of Arizona, 1989]. Although measurements of soil temperatures were available, the canopy temperature was used as an estimate of the surface temperature in the computation of the thermal emission from the wheat field. Apart from a few unit conversions, small corrections were applied to the original data of global and net radiation and canopy temperature to account for instrumental errors [Kustas, 1989, personal communication]. The corrected values of global and net radiation range from minima of 0 and -58 Wm^{-2} during the night to maxima of 981 and 668 Wm^{-2} just after local noon (figures 4.2.1. and 4.2.2.). The minimum air and surface temperatures amount 11.5°C and 7.2°C and occur just before local sunrise, whereas their respective maxima of 35.0°C and 30.5°C lag 2 to 3 hours behind the global radiation maximum. The vapor pressure of the air lastly ranges from 368 to 1544 Pa, with the lower values occuring during nighttime and the higher values during daytime.

In order to make an accurate comparison with simulation results possible, RBM converts local standard time to true solar time using the method presented in section 2.2.1 and solar ephemeris formulae as presented in appendix A. For the Maricopa wheat field, this resulted in a total time subtraction of 30 minutes, composed of about 28 minutes to account for the longitude difference with the standard meridian, about 1.5 minutes for the equation of time and 0.5 minutes for the fact that the one minute averages were collected during the preceeding minute. A first verification of the model is provided by the fact that the amounts of global radiation that were registrated by the radiometer at the times which RBM computed for the occurence of the apparent sunrise (corrected for atmospheric refraction) and solar noon, only deviated by 3 and 6 Wm^{-2} from the minimum (zero) and maximum (about 1 kWm^{-2}) registrations, respectively. Those values are well within the sensitivity and accuracy of the applied instrumentation: The latter is commonly found to be around 5 percent [Garnier and Ohmura, 1970; Morris, 1989; Stuhlmann et al., 1990].

The two most important unknowns are the transmissivity (T) or optical depth (τ) of the atmosphere and the albedo of the surface (a). For the ideal atmospheric conditions at the MAC test site, values of 0.75 and 0.29 should suffice for T and τ, respectively. As for the albedo of the wheat field, List [1966] and Kondratyev et al. [1982] report daily average values of 0.07 and 0.05-0.1 during early spring, respectively. Particularly for clear skies however, the diurnal variation of the vegetation albedo shows a strong dependence on the solar elevation. Kondratyev et al. [1982] provide a parameterization for this phenomenon for grass covered surfaces that accounts for the attenuating effect of cloud cover by means of the ratio of diffuse to global radiation. Briegleb et al. [1986] give a simpler expression, which is merely a function of the solar zenith angle and one empirical parameter. This parameterization seems to be applicable to various land surface types without

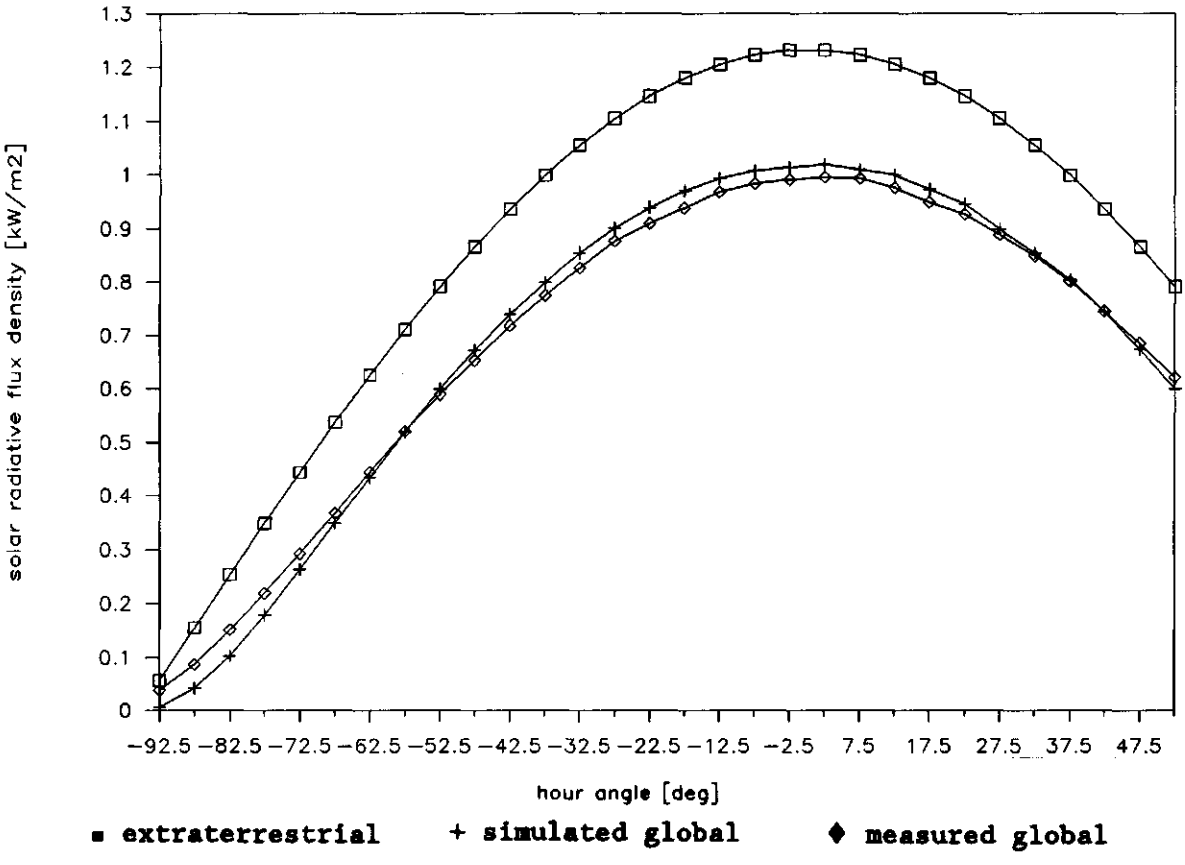

fig. 4.2.1. Simulated extraterrestrial and global radiation and measured global radiation as a function of the hour angle at the MAC wheat field for April 10, 1989 (MBE = 0.6%; RMSE = 3.5%).

exhibiting much scatter in its parameter.

As for the actual verification of the simulated radiation budget at the surface of the wheat field, RBM grouped the total of 947 one minute averages of all input variables into 47 consecutive bins of 20 minutes (disregarding the last 7 measurements) and computed their respective averages. The same time step was applied for the simulation of the various components of the radiation budget. Global and net radiation were computed for all moments representing the center of a measurement bin and were compared with the averages of their measured counterparts. Consecutively, RBM computed two statistics to assess the simulation performance, namely the mean bias error (MBE) and the root mean square error (RMSE). The MBE is defined as the mean difference between the computed and the measured values, which is a measure for overestimation or underestimation on a daily basis. The RMSE on the other hand is defined as the square root of the mean of the squared differences between the simulated and the measured values, which provides more specific information with respect to the model accuracy [Ma and Iqbal, 1983]. It is common practice to express these statistics as a percentage of the measured mean for the time period concerned.

To check the capability of RBM with respect to simulating the thermal (longwave) radiation budget at the surface of the wheat field, the statistical analysis was restricted initially to the 17 time steps between local midnight and sunrise, when the radiation budget is determined completely by its longwave components. This yielded a MBE and a RMSE of -2.6 and 6.0 percent respectively, when the surface emissivity was assumed to be 0.95 and the clear sky effective atmospheric emissivity was computed according to Satterlund [1979]. The model results showed little sensitivity to small changes in the former, but were rather sensitive to changes in the latter. Application of Brutsaert's [1975] formula for the atmospheric emissivity instead of Satterlund's resulted in an average overprediction of the nighttime net longwave radiation loss of about 60 percent (MBE). This can partly be attributed to measurement errors [Kustas, personal communication] and partly to conditions of temperature inversion, for which Brutsaert's formula is not intended. However, the other available formula's (appendix B.) generally yielded deviations of less then 15 percent and moreover, the MBE resulting from Brutsaert's formula decreased to an underprediction of the net radiation of merely 10 percent when applied to all 47 time steps instead of only to the first 17. With respect to all time steps, Satterlund's formula resulted in a MBE and a RMSE of 1.7 and 5.1 percent, respectively.

The capability of RBM in simulating the solar (shortwave) radiation incident at the wheat field was checked through a statistical analysis of the 30 time steps after local surise. When the zenith path transmissivity of the atmosphere was assumed to be 0.75, the effective (clear) sky albedo 0.1 and the surface albedo with the sun in the zenith also 0.1, RBM yielded a MBE and a RMSE of 0.6 and 3.5 percent, respectively. The dependency of the surface albedo on the solar zenith angle was parameterized according to Kondratyev et

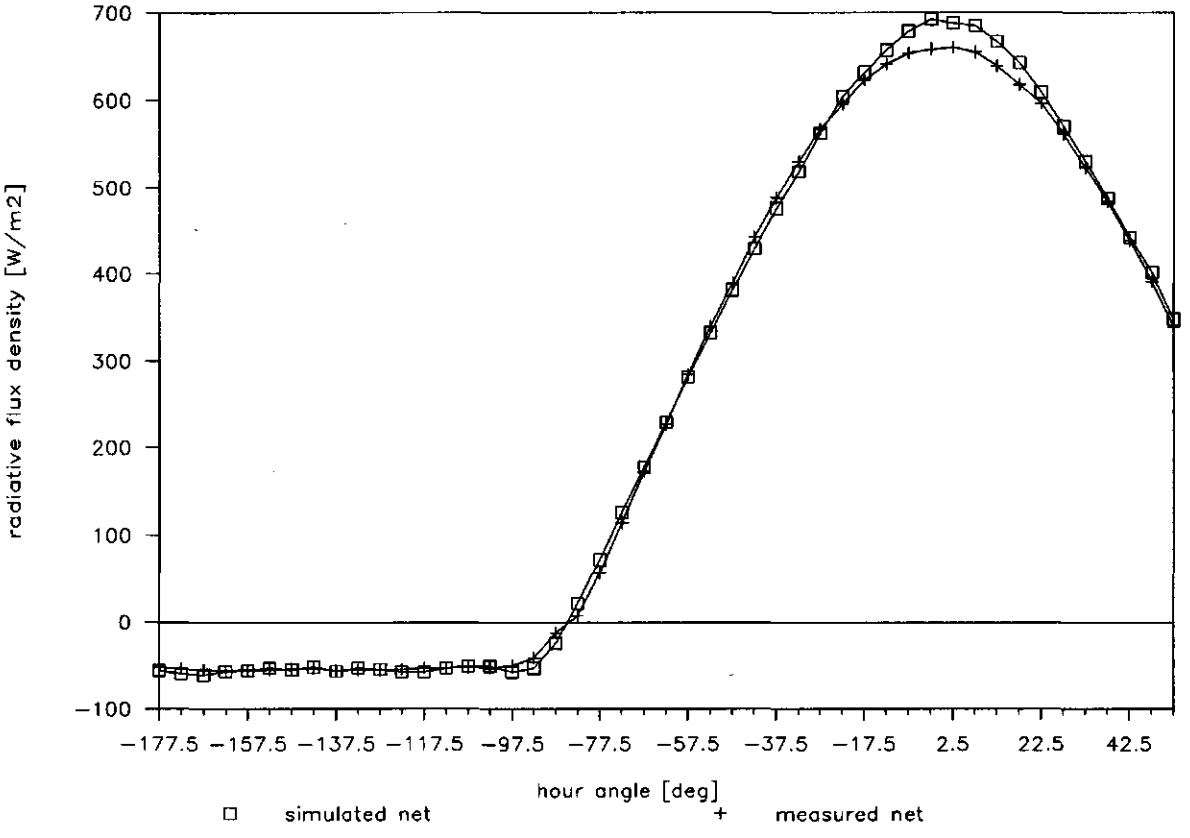

fig. 4.2.2. Simulated and measured net radiation as a function of the hour angle at the MAC wheat field for April 10, 1989 (MBE = 1.7%; RMSE = 5.1%).

al. [1982] (see the appropriate subroutine in the RBM source code as listed in appendix E.).

Unless the surface is snow covered, net shortwave radiation is generally more important in the daily average surface radiation budget than net longwave radiation. For this particular test case, the simulated daily average radiation budget amounted +163 Wm^{-2}, composed of +222 Wm^{-2} for shortwave radiative input and -59 Wm^{-2} for longwave radiative loss. The daily average extraterrestrial radiation, integrated numerically using Simpson's 1/3 rule and a temporal increment of 20 minutes, was found to be 413 Wm^{-2}, and deviates by less than 0.03 percent from the value that results from analytical integration (appendix C.). The ratio of daily global to daily extraterrestrial radiation amounted 0.766, which would result in a diffuse fraction of the global radiation of 0.175 according to the daily standard correlation of Erbs et al. [1982]. RBM yielded a value of 0.148, i.e. about 15 percent lower.

Because the data collected at this particular test site lack the topographic and atmospheric complexity for which RBM is actually designed, additional verifications are required to provide a more exhaustive test of the main module and its subroutines. This holds in particular for the subroutine designed to determine the various conversion factors (FACTORS in appendix E.), which was discussed briefly in section 2.3.3. However, as can be gathered from the statistics assessing the simulation performance and from the figures 4.2.1. and 4.2.2., RBM yields encouraging results when applied to a uniform horizontal surface under clear skies. Its application to a site under less ideal atmospheric conditions will be presented in the next section.

4.3. Simulating Snowmelt

The radiation budget algorithm presented in chapter 2., which has been the basis of RBM, is actually developed to provide a first estimate of the surface energy balance in snow covered mountainous terrain. The latter can provide snowmelt factors that are more physically based than the present temperature index (degree-day) method, which will reduce both the parameter variability associated with local calibrations and the need for extensive measurements. Moreover, a simplified energy balance model of the snowmelt at a point with a limited number of required input parameters will allow easy incorporation in operational snowmelt runoff models like the Snowmelt Runoff Model (SRM). The considerations that provided the basis for the development of more physically based snowmelt factors are discussed below in a short review of the presently available methods for point snowmelt prediction.

4.3.1. The Degree-Day Method

The simplest and still most widely used method both for the short term prediction of snowmelt at a point [e.g., Martinec, 1960; Pysklywec et al., 1968; Granger and Male, 1978; Kuusisto, 1980] and as the basis for snowmelt runoff modeling on a watershed scale [e.g., Martinec et al., 1983; Martinec and Rango, 1986; van Katwijk and Rango, 1988; Moussavi et al., 1989] is the so-called degree-day method. This temperature index approach relates the total daily decrease of the water content of a snow cover directly to the daily mean air temperature above a certain base temperature (usually taken as the freezing temperature of water) by means of the more or less empirical degree-day factor [e.g., Leavesley, 1989]:

$$M = a * T_d \tag{43}$$

$$\text{if } T_a > T_b \text{ then } T_d = T_a - T_b$$

$$\text{else } T_d = 0$$

where:

M = Snowmelt rate (water equivalent) [md^{-1}]
a = Degree-day factor [$mK^{-1}d^{-1}$]
T_d = Degree-day temperature [K]
T_a = Absolute air temperature at surface [K]
T_b = Base temperature [$\approx$ 273.15 K]

The above expression for the degree-day temperature is in fact an approximation, since the instantaneous air temperature might rise above the base temperature (around noon) when the daily mean air temperature is still lower than the base temperature. This can be accounted for when the daily minimum and maximum air temperatures are known and a certain linear [van Katwijk and Rango, 1988] or sinusoidal [Running et al., 1987; Reicosky et al., 1989] temperature variation throughout the day is assumed. However, this will require extra input parameters which will reduce the operational capacity of the model. Moreover, this phenomenon is not likely to occur very often during the snowmelt season and may therefore be disregarded.

A disadvantage of equation (43) is the high spatial and temporal variability of the degree-day factor, which is associated with the fact that it is actually a bulk melt factor, implicitly accounting for all terms of the energy budget that affect the mass balance of the snow pack. Hence, it accounts in some way for the hydrothermal condition of the snow pack itself (affecting both its hydraulic storage and transmissivity characteristics and its optical properties), and for microclimatic conditions as determined by vegetative ground cover and terrain structure. In order to take this variability into account without depending to much on the hydrological judgment of the operator, the degree-day factor is sometimes linearly related to physical parameters that can easily be determined, such as snow density [Martinec, 1960; Kuusisto, 1980], average daily air temperature range

[Moussavi et al., 1989], or mean wind speed [Martinec, 1960]. Because snow density increases during the snowmelt season, a linear relation with the degree-day factor is found to represent several factors affecting snowmelt (e.g. increasing liquid water content and decreasing albedo) rather well. The daily air temperature range has been related to the daily total atmospheric transmittance of solar radiation [Bristow and Campbell, 1984], which is an important term in the snow surface energy budget. Conclusively, although exceptional conditions may require different values for the degree-day factor, they generally lie in the range from $3.5*10^{-3}$ to $6.0*10^{-3}$ $mK^{-1}d^{-1}$ and increase gradually during the snowmelt season as the snow pack ripens [Martinec et al., 1983; Martinec and Rango, 1986].

A statistical analysis carried out by Zuzel and Cox [1975] showed that if only one meteorological variable is available for daily snowmelt prediction, daily average air temperature is the best predictor. It is probably for this reason that the degree-day method has yielded acceptable results over the past decades. However, significant deviations from predicted values particularly occur at days with heavy rainfall or high wind speeds [Martinec, 1960; Pysklywec et al., 1968; Kuusisto, 1980]. This finding is not surprising since heavy rain strongly influences both the mass and the energy balance of a snow pack, the latter because cooling or freezing rain releases latent heat. Strong winds not only directly affect the energy and mass balances because they increase turbulent transfer (sensible and latent heat exchange), but also indirectly since they can cause blowing snow that can be sublimated and redistributed [Morris, 1989]. The latter phenomenon however, also causes problems when predicting snowmelt with more physically based methods.

4.3.2. A Combined Approach: Temperature Index and Radiation Budget

Net radiation is not only the most important term in the surface energy balance at a point in snow covered mountainous terrain because of its magnitude, but also because it explains most of the variation in snowmelt [Zuzel and Cox, 1975; Granger and Male, 1978]. However, Olyphant [1984] found that "there is no simple proportionality between net radiation and glacier ablation", which he partly contributed to the probable importance of other energy sources, especially the sensible heat flux. Hence, a combination of a surface radiation budget (as discussed extensively in chapter 2.) and a temperature index (the so-called restricted degree-day factor) as proposed by several investigators [Martinec and de Quervain, 1975; Ambach, 1988; Martinec, 1989] offers a promising perspective:

$$\begin{aligned} &\text{if } R_n > 0 \text{ then } M = a_T * T_d + a_Q * R_n \\ &\qquad\qquad \text{else } M = a_T * T_d \end{aligned} \tag{44}$$

$$\text{if } T_a > T_b \text{ then } T_d = T_a - T_b$$
$$\text{else } T_d = 0$$
$$a_Q = 86400 * (SQ_T * rho_w * L_f)^{-1} \approx 2.7 * 10^{-4}\ md^{-1}(Wm^{-2})^{-1} \quad (45)$$

where[1]:

- M = Snowmelt rate (water equivalent) $[md^{-1}]$
- a_T = Restricted degree-day factor $[mK^{-1}d^{-1}]$
- T_d = Degree-day temperature [K]
- a_Q = Conversion factor for energy flux density to snowmelt depth $[md^{-1}(Wm^{-2})^{-1}]$
- R_n = Net radiation $[Wm^{-2}]$
- T_a = Absolute air temperature at surface [K]
- T_b = Base temperature [≈ 273.15 K]
- SQ_T = Thermal snow quality [≈ 0.96]
- rho_w = Density of water [≈ 1000 kgm^{-3}]
- L_f = Latent heat of fusion [≈ $3.337*10^5$ Jkg^{-1}]

[1] The factor 86400 accounts for the conversion of s^{-1} to d^{-1}.

Male and Gray [1981] suggested that an average value of 0.96 for the thermal snow quality should account reasonably well for the contamination of the snow pack. Applying this value to (45), it can be seen that each watt per square meter of daily average energy input results in a daily snowmelt depth of about 0.27 millimeter water equivalent.

The restricted degree-day factor in (44) implicitly accounts for the remaining terms of the energy budget at the snow surface as described by (1), i.e. mainly for the turbulent exchange at the interface between the snow surface and the atmospheric boundary layer. Martinec and de Quervain [1975] and Martinec [1989] neglect the transfer of water vapor and the associated latent heat flux and assume the restricted degree-day factor to be entirely related to the sensible heat flux. This is in contradiction with observations published by Granger and Male [1978] and Marks [1988], which show that the latent heat loss (required to produce the measured evaporation) partly or almost entirely offsets the sensible heat input during the snowmelt season. Moreover, Marks et al. [1986] state that even at a high elevation site in the Sierra Nevada where "radiative transfer is by far the largest and most important form of energy exchange over a snow cover during melt", measurements over several years indicate that commonly 25 percent of the mass of the snow cover is lost to evaporation/sublimation during the spring snowmelt. However, an extensive survey carried out by Morris [1989] shows that the latent heat loss of a melting snow cover is usually around 10 percent of the net radiation, whereas the sensible heat input is often around 40 percent of it. The latter is confirmed by Olyphant and Isard [1988] who simulated turbulent transfer over alpine snow fields and concluded that snowmelt by radiant energy will dominate early in the season, while turbulent energy processes will dominate snowmelt late in the season. This conclusion primarily stems from the increasing influence of advected sensible heat as the snow fields decrease in

area. The relative importance of the latent heat loss of a melting snow pack in particular and of the turbulent heat exchange in general obviously is a function of the ambient weather conditions. For instance, Martinec [1989] found that the net outgoing longwave radiation at night promotes refreezing of meltwater and hence appears to be a significant factor in alpine conditions. However, Granger and Male [1978] concluded for a melting prairie snow pack that the positive fluxes of latent and sensible heat that occur at night actually counteract nighttime radiative loss and thus limit refreezing of the snow pack. Although there is some disagreement among investigators about the relative importance of the latent heat loss of a melting snow pack, they generally agree on the fact that it cannot be neglected. Preliminary results of Martinec [1989], who found that the values assessed for the restricted degree-day factor generally lie in the range from $2.0*10^{-3}$ to $2.5*10^{-3}$ $mK^{-1}d^{-1}$ and exhibit much less variability throughout the ablation period than the values for the original degree-day factor, suggest that (44) is a more physically based melt factor. Lower values were generally assessed on days with little wind (reducing the input of sensible heat) and a low air humidity (increasing the evaporation and the associated loss of latent heat).

It follows from (44) that snowmelt might occur as a result of a positive radiation budget at the snow surface, while the degree day temperature still equals zero. In the beginning of the ablation period, this amount of melt water will generally not result in immediate runoff, but will rather be used to saturate the snow pack. Martinec [1989, personal communication] therefore proposed the application of a certain threshold temperature (taken slightly lower than 0°C), below which possible snowmelt resulting from net radiation is not taken into account. During most of the ablation period however, such a correction will not be necessary, since the snow pack is isothermal at 0°C, its liquid water content is nearly constant and the degree day temperature is no longer zero.

Ambach [1988] took a slightly different approach than the parameterization described by equation (44), deriving an expression for a temperature index related to the sensible heat flux only. However, the application of this "heat transfer coefficient", which is a function of mean air pressure and wind speed, is basically equivalent with a bulk turbulent transfer approach for sensible heat, which will be discussed in section 4.3.3 (equation (47)).

4.3.3. The Reduced Energy Budget

The previously mentioned statistical analysis of Zuzel and Cox [1975], also indicated that daily snowmelt prediction could be significantly improved by using net radiation, vapor pressure and wind in predictive equations rather than just an air temperature variable alone. An even more physically based method for the prediction of point snowmelt than the combined temperature-net

radiation approach presented in the preceeding section would therefore consist of parameterizing all terms of the energy balance at the snow surface and consequently determining their respective melt water equivalents by means of (45). However, heat conduction to the soil beneath the snow pack and heat advection to the snow pack due to precipitation events are of little importance to the energy budget during the snowmelt season because the temperatures of soil, snow pack and rain tend to be close to 0°C. Hence, a melt factor was developed based on the reduced energy budget at the snow surface, consisting of the radiation budget and the turbulent exchange terms (sensible and latent heat flux):

$$\begin{aligned} \Delta Q &= R_n + Q_h + Q_e \\ &= R_n + Q_h - L_e * E \qquad (46) \\ \text{if } \Delta Q > 0 \text{ then } M &= a_Q * \Delta Q \\ \text{else } M &= 0 \end{aligned}$$

where:

ΔQ = Energy available for snowmelt [Wm^{-2}]
R_n = Net Radiation [Wm^{-2}]
Q_h = Sensible heat flux [Wm^{-2}]
Q_e = Latent heat flux [Wm^{-2}]
L_e = Latent heat of vaporization [$\approx 2.501*10^6$ Jkg^{-1}]
E = Evaporation [$kgm^{-2}s^{-1}$]
M = Snowmelt rate [md^{-1}]
a_Q = Conversion factor for energy flux density to snowmelt depth [$md^{-1}(Wm^{-2})^{-1}$]

This equation holds for equilibrium conditions, when the snow pack is isothermal at 0°C and its liquid water content is constant. This is normally the case during almost the entire ablation period (section 4.3.4).

The determination of the radiation budget at a point in snow covered mountainous terrain is discussed extensively in chapter 2. Hence, some attention will be paid here to the parameterization of the turbulent exchange at the interface between the surface of a melting snow pack and the atmospheric boundary layer. One of the main objectives of this research effort was to develop and test more physically based snowmelt prediction methods that require only a limited number of input data, both with respect to the number of parameters and to their temporal resolution. Hence, sophisticated methods for the closure of the vertical eddy transfer equations based on the Monin-Obukhov similarity theory [Brutsaert, 1982] are avoided, although they have been shown to yield promising results in snow surface energy balance models [Marks, 1988]. Moreover, even more advanced methods are generally based on the assumption of horizontal uniformity, thus neglecting advection of sensible heat and local (katabatic) pressure gradients, although such phenomena may be important in mountainous terrain [Olyphant and Isard, 1988; Morris, 1989].

For the simulation of the turbulent exchange at the surface of a melting snow pack, the convenient energy budget method is generally not directly

applicable, because the energy flux density (R_n-ΔQ) available for turbulent exchange (L_e*E-Q_h) is not known a priori. Only if the mass budget of the melting snow pack is also taken into account (by means of measurements of lysimeter outflow and precipitation), ΔQ can be estimated from the ratio of the net snowmelt rate (M) and a_Q. This allows expressing Q_h and E in terms of (R_n-ΔQ) and the Bowen ratio (Q_h/Q_e), which is a function of the mean vertical profiles of temperature and water vapor, as can be seen from equations (47) and (48). In this manner, the energy (plus mass) budget method can be used to verify estimates of the turbulent transfer terms directly obtained from the mean vertical scalar profiles.

For the current research effort, the simplified Thornthwaite-Holzman bulk transfer approach towards parameterizing the turbulent transfer of momentum, sensible heat and water vapor was applied, in combination with an atmospheric stability criterion based on the bulk Richardson number [Brutsaert, 1982; Morris, 1989] (fluxes are defined as positive towards the surface):

$$Q_h = F_h * C_n * rho_a * c_p * u * (\theta_a - \theta_s) \quad (47)$$

$$Q_e = F_e * C_n * rho_a * L_e * u * (q_a - q_s) \quad (48)$$

$$Ri_B = g * z * u^{-2} * ((\theta_a - \theta_s) * T_a^{-1} + 0.61 * (q_a - q_s))$$

$$\text{if } Ri_B < 0 \text{ then } F_h = (1 - 58 * Ri_B)^{0.25}$$

$$\text{else } F_h = (1 + 7 * Ri_B)^{-0.1}$$

$$F_e = 0.5 * F_h$$

$$C_n = k^2 * \ln^{-2}[z * z_o^{-1}]$$

$$rho_a = p * (R * T_a)^{-1};\ R = R_d * (1 + 0.61 * q_a)$$

$$c_p = c_{pd} * (1 + 0.84 * q_a)$$

$$\theta = T * (p_o * p^{-1})^K\ ;\ K = R * c_p^{-1}$$

$$q = 0.622 * e_a * (p - 0.378 * e_a)^{-1}$$

where[1,2]:

- Q_h = Sensible heat flux [Wm^{-2}]
- F_h = Ratio of eddy diffusivities for sensible heat and momentum; Correction for departures from neutral stability [-]
- C_n = Bulk transfer coefficient for neutral stability [-]
- rho_a = Air density [kgm^{-3}]
- $c_p(c_{pd})$ = Specific heat of (dry) air [≈ 1005 $Jkg^{-1}K^{-1}$]
- u = Mean wind speed [ms^{-1}]
- θ = Potential temperature [K]
- Q_e = Latent heat flux [Wm^{-2}]
- F_e = Ratio of eddy diffusivities for latent heat and momentum; Correction for departures from neutral stability [-]
- L_e = Latent heat of vaporization [≈ $2.501*10^6$ Jkg^{-1}]
- q = Specific humidity [-]
- Ri_B = Bulk Richardson number [-]
- g = Gravitational acceleration [≈ 9.81 ms^{-2}]
- z = Height of wind, temperature and humidity measurements [≈ 2 m]
- T = Absolute temperature [K]
- k = von Kármán's constant [≈ 0.4]

z_o = roughness lengths for momentum and for the scalars (sensible heat and water vapor) [$\approx 5*10^{-4}$ m]
p = Air pressure [Pa]
$R(R_d)$ = Gas constant of (dry) air [≈ 287.04 $Jkg^{-1}K^{-1}$]
p_o = Standard pressure [10^5 Pa]
K = Ratio of gas constant and specific heat of air [≈ 0.286]
e = Vapor pressure [Pa]

[1] The indices a and s refer to air and surface, respectively.
[2] The effect of water vapor in the expressions for Ri_B, rho_a, θ and q can be neglected for practical purposes, thus $R=R_d$ and $c_p=c_{pd}$.

Although the formulation of the stability parameters (F_h, F_e) in terms of the bulk Richardson number and the formulation of the bulk transfer coefficient according to Thornthwaite and Holzman are based on some simplifying assumptions (e.g. one measurement height (z) for wind, temperature and humidity, and one roughness length (z_o) for momentum, sensible heat and water vapor), similar schemes have been used with success in energy budget models for the prediction of snowmelt in different environments [Granger and Male, 1978; Dozier and Outcalt, 1979; Williams, 1988].

Since Ri_B will generally be positive during the snowmelt season, which is associated with stable atmospheric conditions, F_h will not show much departure from unity most of the time as a result of its functional form. Although taking F_e as half of F_h is significantly different from the generally accepted equality or near equality [Brutsaert, 1982], Granger and Male [1978] showed that this value represents both unstable and stable (nearly neutral) conditions over a melting snow pack adequately.

During the snowmelt season, the air temperature at the snow surface will always be close to the temperature of the melting snow pack, i.e. approximately the freezing temperature of water ($T_s \approx 273.15$ K), and the air layer just above the snow surface will generally be saturated. Hence, the vapor pressure at the snow surface is assumed to be the saturated value that corresponds to the snow surface temperature ($e_s \approx 610.78$ Pa) [Charbonneau et al., 1981; Olyphant and Isard, 1988]. Parameterizations for the saturated vapor pressure over water and ice as functions of the ambient temperature have been presented by various authors [Idso and Jackson, 1969; Aase and Idso, 1978; Brutsaert, 1982; Kimball and Idso, 1982; Williams, 1988].

4.3.4. Comparison of Snowmelt Prediction Methods: Verification of the Energy Budget Model - EBM

For the purpose of comparing the capabilities of the three above presented methods in simulating daily snowmelt at a point in alpine terrain, a (Microsoft Quick)BASIC computer simulation program EBM (Energy Budget Model) was developed based on the radiation budget simulation algorithm of RBM and additional subroutines based on the parameterizations presented in the

preceeding sections [Feldman and Rugg, 1988].

In a verification procedure, the performance of EBM was assessed using outflow measurents from a snow lysimeter at the test site of the Swiss Federal Institute for Snow and Avalanche Research at Weissfluhjoch/Davos, Switzerland (46.8°N, 9.8°E). The applied lysimeter, which has a surface area of $5m^2$, is situated in a horizontal snow field at an altitude of 2540m above mean sea level. Its outflow is intercepted by a steel vessel and recorded continuously using a tipping bucket gauge. Due to resistances in the unsaturated and saturated snow layers and in the pipe leading from the vessel to the gauge, the transformation of a snowmelt depth resulting from a positive energy budget at the snow surface into a outflow hydrograph from the entire snowpack in the lysimeter exhibits a certain time lag and attenuation. However, it was found that, apart from daily fluctuations associated with day time variations in snowmelt and nightly refreezing, the liquid water content of the snow pack did not increase any more after the day on which the lysimeter outflow started. Consequently, on a daily basis snowmelt depth (water equivalent) approximately equals lysimeter outflow [Martinec, 1989].

The data set that was used for the verification of the Energy Budget Model (EBM) was collected during the 1985 ablation season and consists of daily averages of air pressure (p), air temperature (T_a), relative humidity (RH), wind speed (u), fractional cloudcover (m_c), sunshine duration (n), global radiation (K↓), precipitation occuring as rain (P_r), precipitation occuring as snow (P_s) and lysimeter outflow (Q_l) [Federal Institute for Snow and Avalanche Research, 1989]. The entire 1985 snowmelt season lasted from May 9 (start of the decrease in snowpack level) to July 15 (last day with lysimeter outflow). During the first week however, no lysimeter outflow occured because the entire snowmelt depth was used to increase the liquid water content of the snow pack gradually. Hence, equilibrium conditions only occured on the 58 days between May 16 (start of lysimeter outflow) and July 12, which therefore were taken into consideration for verification purposes.

Unfortunately, only the data pertaining to the mass (i.e. water) balance of the snow lysimeter (which was used for the verification of EBM) were collected on the spot: Q_l was measured with the described gauge and lysimeter and P_r was measured by a heated pluviograph. The data pertaining to the energy balance (which is the theoretical framework of EBM) were collected elsewhere: p was measured at an altitude of 2667m and T_a, RH, u, m_c and K↓ at 2693m above mean sea level (at the automatic meteorological station of the Swiss Meteorological Office), i.e. 127m and 153m above the snow field which contains the lysimeter, respectively. Although p and T_a could have been estimated from their respective measurement altitudes and their mean values at sea level using standard vertical profiles (e.g., equations (B4) and (B5)), use was made of their measurements, which were extrapolated downward to the snow field using the same profiles. RH was assumed to be constant over this altitude difference [Marks and Dozier, 1979], which allowed easy computation of the

vapor pressure at the lysimeter and is basically the same as assuming an exponential vertical vapor pressure profile [Brutsaert, 1975]. Although u will most likely be overestimated when applied directly to the lysimeter because it was measured at a mountain summit, there seems no alternative due to a lack of more appropriate data. No correction was made to m_c either, which is supported by the findings of Olyphant [1984], who stated that "the effects of increasing cloud cover (to global insolation, R.U.) are independent of elevation". Finally, K↓ will also be overestimated when applied directly to the lysimeter, because (1) it was measured at a higher elevation at which a lower amount of solar radiation has been absorbed, and (2) it was measured at a ridge top where the effects of obstruction by surrounding terrain are negligible. However, no correction was made to K↓, because it is only needed for verification purposes and moreover, the effects of obstruction by neighboring surfaces to the amount of solar radiation received by the snow lysimeter were neglected in EBM due to a lack of appropriate topographic data.

Apart from a direct comparison between the simulated snowmelt depths and the measured lysimeter outflows during the 1985 snowmelt season at the Weissfluhjoch test site, a brief sensitivity analysis was carried out through the intercomparison of generated artificial hydrographs for a complete watershed. The point snowmelt depths simulated according to the three methods discussed previously and the outflows measured at the snow lysimeter were transformed into their respective runoffs that would occur from the nearby Dischma basin provided that the inputs were representative for the whole basin. Although this extension of point inputs to area inputs obviously has little physical meaning, it will provide some insight into the sensitivity of the applied snowmelt-runoff transformation model to its input data. The simplest form of the Snowmelt Runoff Model (SRM), in case the basin is not subdivided into different elevation zones, was used for this purpose [Martinec et al., 1983]:

$$Q_{n+1} = c_n * (M_n * S_n + P_n) * A * (1 - k_{n+1}) + Q_n * k_{n+1} \quad (49)$$

$$k_{n+1} = x * Q_n^{-y} \quad (50)$$

where[1,2]:

Q = Daily discharge [m^3d^{-1}]
c = Runoff coefficient [≈ 0.9]
M = Snowmelt rate [md^{-1}]
S = Ratio of snow covered area to basin area [-]
P = Precipitation contributing to runoff [md^{-1}]
A = Basin area [≈ $4.33 * 10^7$ m^2]
k = Recession coefficient [-]
x = Recession factor [≈ 0.85]
y = Recession exponent [≈ 0.086]

[1] The subscript n denotes the sequence of days during the discharge computation period.
[2] The parameter values given above are typical values for the alpine Dischma basin in Switzerland, which are not applicable to other basins.

A detailed description of the determination of the parameter values in the above expression exceeds the scope of this document, but the reader is referred to a paper on this subject by Martinec and Rango [1986]. Although their publication shows that runoff coefficients for snowmelt and precipitation can differ markedly from each other, one value is applied for the current purpose because the contribution of rainfall will be small as compared to that of snowmelt and moreover, the contribution of snowfall to the water balance of the basin is ignored completely. The relative snow covered area of the basin is assumed to decrease linearly from 1 to 0 during the snowmelt season, although analyses of data obtained from aircraft photography and satellite imagery show that areal snow cover depletion generally follows an S-curve [Rango and van Katwijk, 1990]. It can easily be seen from (49) that during periods of true recession $k_{n+1}=Q_{n+1}/Q_n$. In SRM, this recession coefficient is not assumed to be a constant as usual (leading to an exponential recession), but rather to be a function of the discharge on the day before according to (50).

	p [10^2Pa]	T_a [K]	e_a [Pa]	u [ms^{-1}]	m_c [-]	$K\downarrow$ [Wm^{-2}]	P_r [$10^{-3}md^{-1}$]	Q_l
min.	739	270	326	0.5	0.13	57	0	0.5
max.	757	285	818	6.9	1.00	458	38.9	59.8
avg.	749	276	605	3.0	0.76	270	2.4	17.0
dev.	4	3	104	1.5	0.29	87	6.6	14.9

Table 4.3.4.1. Minima, maxima, averages and standard deviations of some of the daily average input variables for EBM collected at the Weissfluhjoch test site during the 1985 ablation period (see text for notation).

The minima, maxima, averages, standard deviations and coefficients of variation (i.e. the ratios of the standard deviations and the averages) of some of the corrected input variables are listed in table 4.3.4.1. Some interesting facts that can be gathered from these statistics are: (1) The average vapor pressure of the air (e_a=605 Pa) is only slightly lower than the saturated vapor pressure over melting snow (e_s=611 Pa), indicating that the latent heat loss of the snow pack resulting from evaporation is probably small; (2) The large variability in the magnitude of the mean fractional cloudcover (m_c) as compared to the ideal atmospheric conditions at the MAC test site will provide a thorough test for the radiation budget algorithm; (3) The range in the values of the daily average global radiation ($K\downarrow$) is of the same order of magnitude, with extremes of 57 and 458 Wm^{-2} that correspond with atmospheric global transmission ($K\downarrow/K_o$) values of less than 12 and more than 95 percent, respectively; (4) The total lysimeter outflow (ΣQ_l) during the 58 equilibrium days of the 1985 snowmelt season at the test site at Weissfluhjoch amounted 0.986m, of which 0.136m can be contributed to discharge resulting

from rainfall (ΣP_r) and the remaining 0.850m consequently to actual snowmelt (ΣM), when evaporation losses are neglected.

To assess the simulation performance of the three previously described point snowmelt prediction methods, EBM computes three additional statistics apart from the mean bias error and the root mean square error that were discussed in section 4.2., namely the coefficient of determination (CD) or Nash-Sutcliffe parameter and the slope and the intercept (and the associated residual standard deviation) resulting from a linear regression analysis between the simulated and measured values. The former is a direct measure of the proportion of the variance of the measured values explained by the model [Nash and Sutcliffe, 1970], whereas the latter provide a measure for the model's average overestimation or underestimation as a function of the magnitude of the measured values. The Nash-Sutcliffe parameter is defined as one minus the ratio of (1) the sum of the squared differences between the measured and the simulated values and (2) the sum of the squared differences between the measured values and their average.

For the simulation of global and net radiation, EBM makes use of the radiation algorithm implemented in RBM. Instantaneous values of global radiation were generated on the basis of a clear sky zenith path atmospheric transmissivity of 0.75, clear and overcast sky albedo's of 0.1 and 0.5, respectively, and surface reflectivities for direct and diffuse radiation according to the parameterization presented in section 2.2.3. The obtained values were integrated numerically from sunrise to sunset using Simpson's 1/3 rule with a temporal increment of one hour. Although the resulting daily averages of global radiation represented the measured values rather well on a seasonal average basis, as is indicated by a MBE of -1.2 percent, they could not explain the large variability of the measured values, as is indicated by a RMSE of 23 percent and a CD of 47 percent. Moreover, a linear regression analysis of the simulated versus the measured values yielded the poor statistics of 0.46 for the slope, 143 Wm^{-2} for the intercept and 42 Wm^{-2} for the residual standard deviation. As can be seen from figure 4.3.4.1., the simulated values seem to follow the general trends in the measured values, but underpredict high values and overpredict low values. This observation is confirmed by the fact that the standard deviation of the simulated values is 58 Wm^{-2}, which is almost 30 Wm^{-2} less than the standard deviation of the measured values (table 4.3.4.1.). The measured global radiation on days when the mean fractional cloudcover equaled unity range from 57 to 365 Wm^{-2}, i.e. more than a factor 6. These figures illustrate the problems associated with modeling the variability of global radiation due to cloudcover effects on a daily average basis without taking into account the diurnal variations or the cloud type.

The simulated daily average surface albedo decreases from about 0.85 for each new accumulation of fresh dry snow with a mean grain size of $2*10^{-4}$m to 0.59 for saturated and contaminated snow at the end of the ablation period

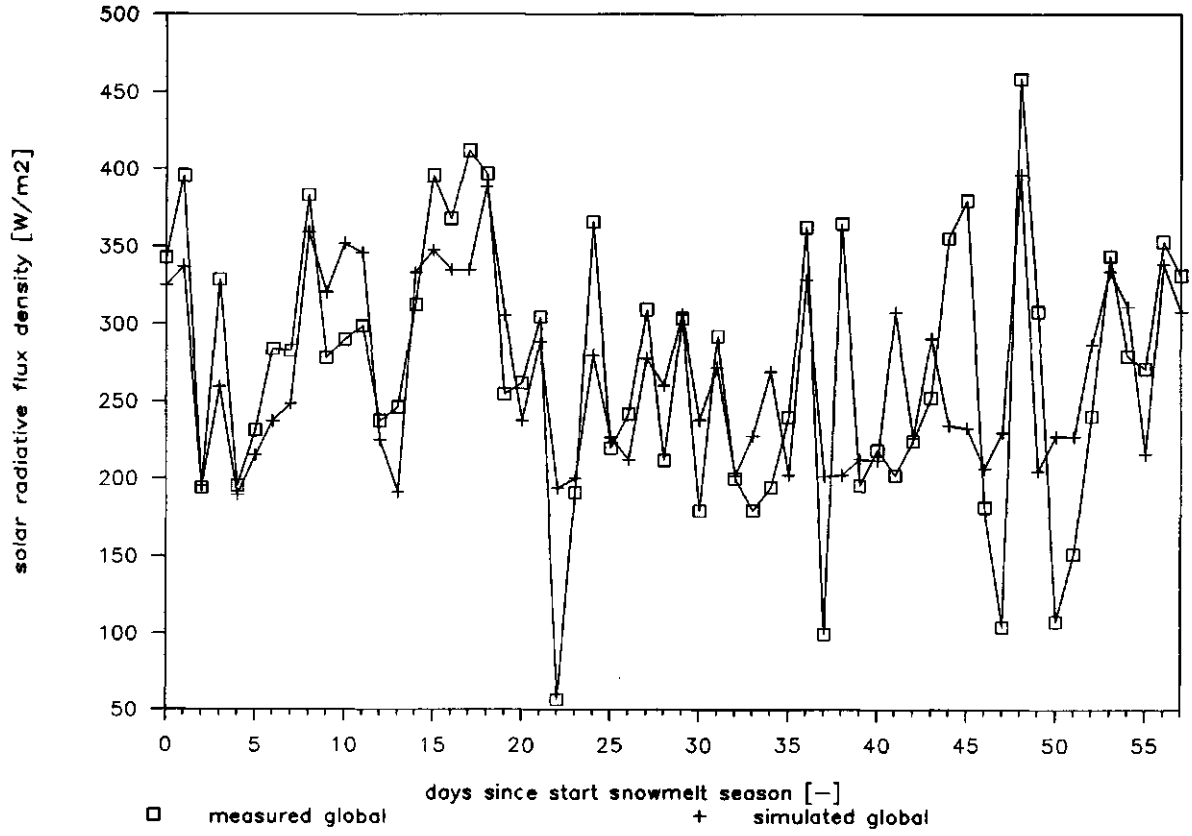

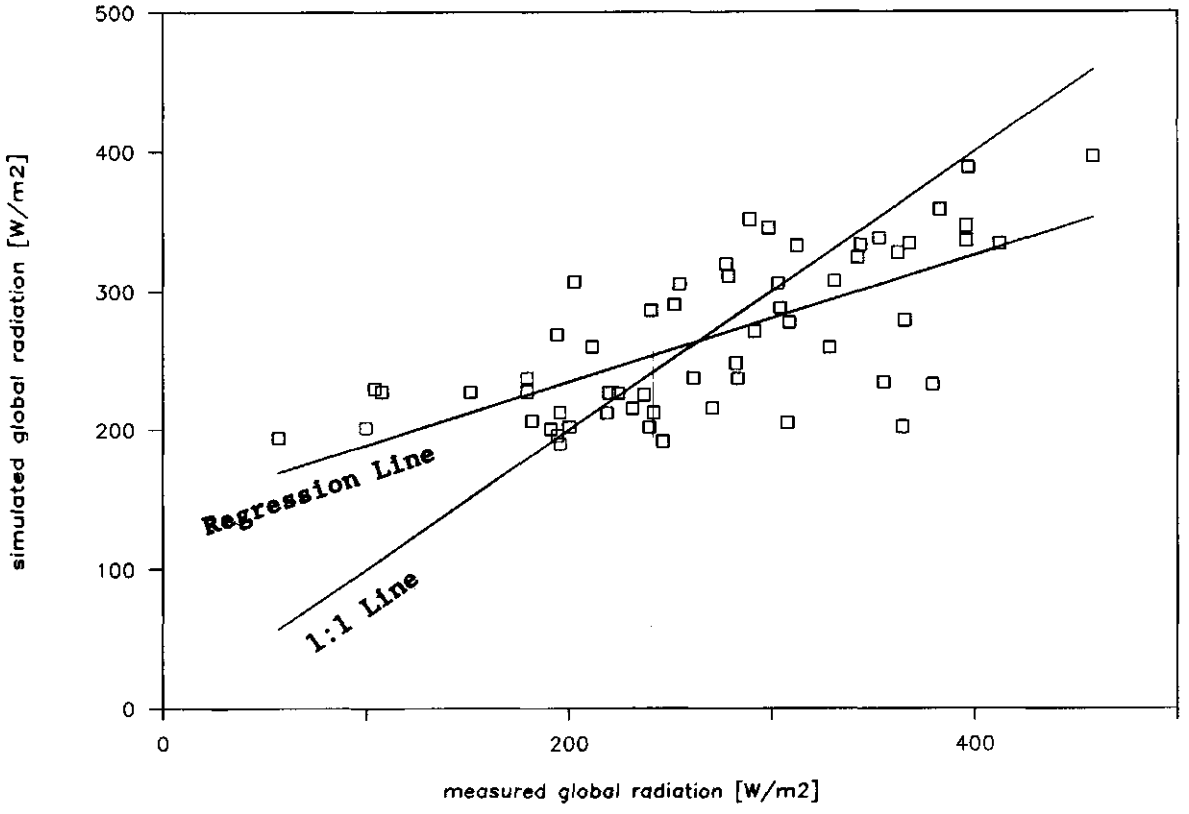

fig. 4.3.4.1. Time series and scatter plot of simulated and measured daily average global radiation throughout the 1985 snowmelt season at the Weissfluhjoch test site (MBE = -1.2%; RMSE = 23%; CD = 47%).

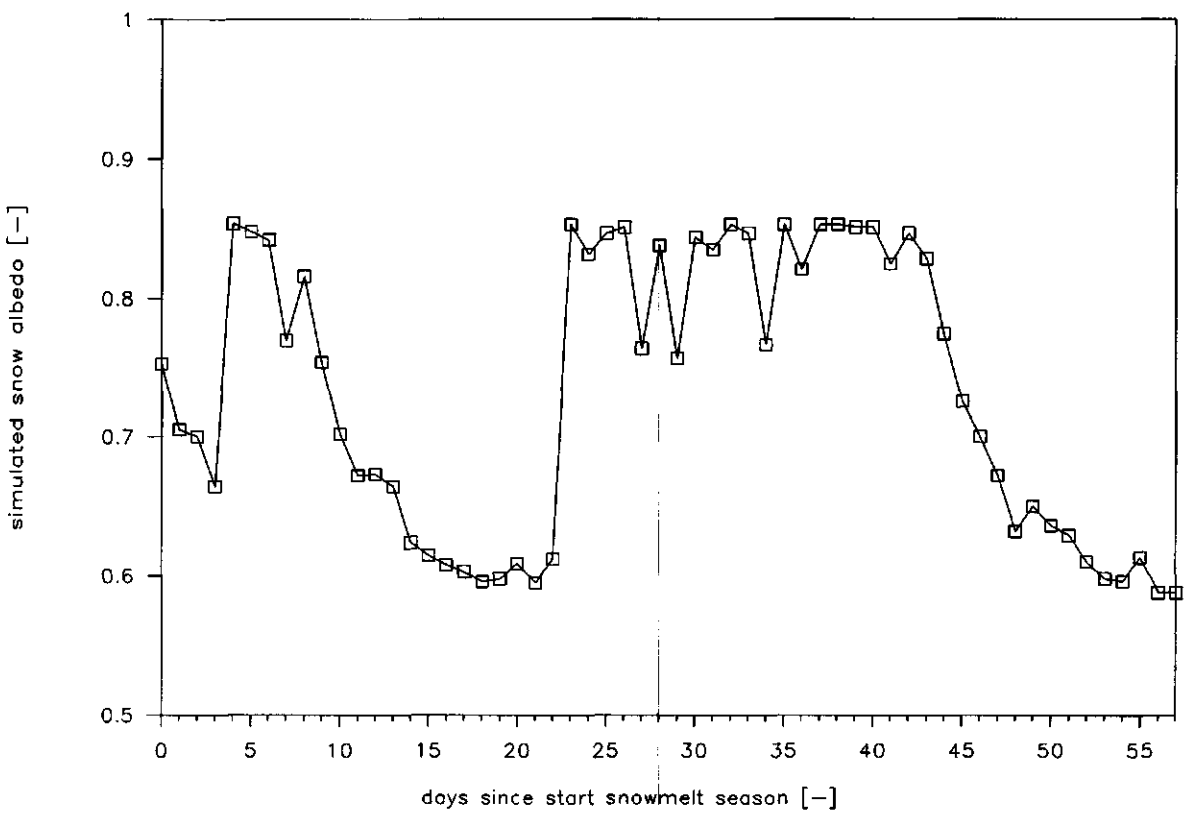

fig. 4.3.4.2. Simulated daily average broadband snow surface albedo throughout the 1985 snowmelt season at the Weissfluhjoch test site.

(figure 4.3.4.2.). Because the shortwave radiation budget is proportional to the complement of the surface albedo, it is quite sensitive to variations in the albedo decay during the snowmelt season. For the same reason however, net solar radiation does not play the same dominant role in the broadband radiation budget at snow covered surfaces as it does with respect to surfaces with lower albedo's. This increases the sensitivity of the surface radiation budget to net longwave radiation, whose variability is mainly associated with the applied formula type for the determination of the effective atmospheric emissivity. When the emissivity of the snow surface was assumed to be 0.98 and the clear sky atmospheric emissivity was computed according to Brutsaert [1975; 1982] then a seasonal average net radiation of +26 Wm^{-2} was obtained, composed of +74 Wm^{-2} for the shortwave radiative input and -48 Wm^{-2} for the longwave radiative loss. The minimum and maximum daily average net radiation were found to be -32 and +95 Wm^{-2}, respectively. The sum of the total measured precipitation and the total simulated snowmelt occuring as a result of a positive radiation budget at the snow surface accounts for 67 percent of the lysimeter outflow during the entire ablation period, i.e. the MBE equals -33 percent. Since the average energy flux density that is associated with cooling of precipitation received by the snow pack is less than 0.5 Wm^{-2} (with a total melt water equivalent of only $7*10^{-3}m$), it is reasonable to conclude that the remaining 33 percent of the cumulative lysimeter outflow are the result of net turbulent heat input at the interface between the snow surface and the atmospheric boundary layer. The proportion of the variance of the measured lysimeter outflows explained by the sum of the measured precipitation and the simulated radiative melt (CD) amounts 69 percent. The RMSE was found to be 48 percent and the slope, intercept and residual standard deviation of the performed linear regression analysis amount 0.77, $-1.7*10^{-3}$ md^{-1} and $4.9*10^{-3}$ md^{-1}, respectively. These statistics confirm the findings of several authors who argue that although net radiation explains most of the variation in snowmelt, there is no simple proportionality between the two [Zuzel and Cox, 1975; Olyphant, 1984].

The seasonal averages of the simulated flux densities associated with the input of sensible heat and the loss of latent heat amount 13 and -0.8 Wm^{-2}, respectively. The latter is the result of a net loss of $13*10^{-3}m$ of water equivalent from the lysimeter due to evaporation of melt water, which is negligible in the mass balance of the snow lysimeter in this particular case. According to the atmospheric stability criterion presented in section 4.3.3., stable (near neutral) conditions prevailed throughout the snowmelt season (43 of the total of 58 days taken into account). The correction factor to account for departures from neutral conditions never departed much from unity. The average restricted degree-day factor assessed to fit the simulated daily average turbulent transfer throughout the snowmelt season amounts $1.8*10^{-3}$ $m*K^{-1}d^{-1}$, which is close to the value of $2.0*10^{-3}$ $mK^{-1}d^{-1}$ that Martinec [1989] assessed for the same ablation period using measurements of global radiation

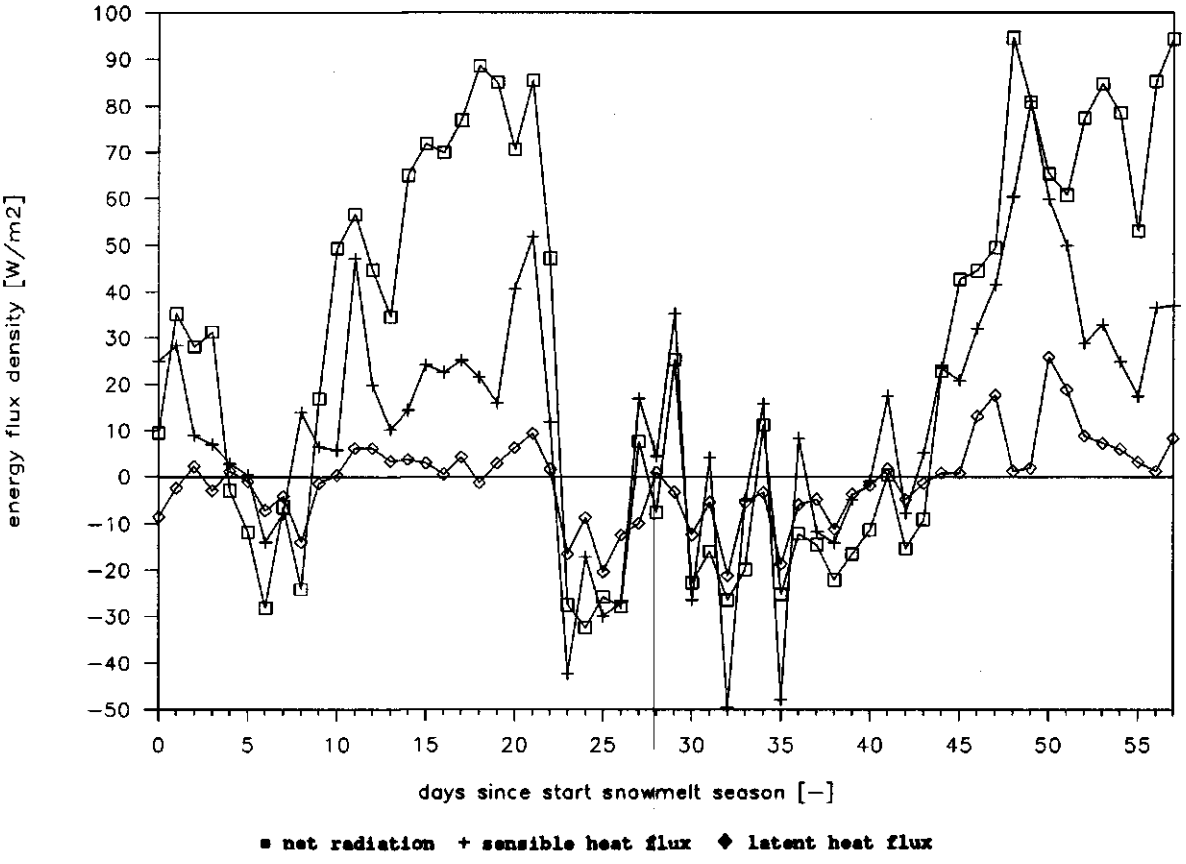

fig. 4.3.4.3. Simulated daily average net radiation, sensible heat flux and latent heat flux throughout the 1985 snowmelt season at the Weissfluhjoch test site.

instead of simulations. Figure 4.3.4.3. shows the seasonal variation of the three terms of the reduced energy budget.

Finally, the simulation capabilities of the three presented methods for the prediction of point snowmelt were compared in a statistical analysis of the melt and flow rates they generated during the 1985 ablation period. Measured precipitation was added to the simulated snowmelt depths. A constant snow restricted degree-day factor of $2.0*10^{-3}$ $mK^{-1}d^{-1}$ was used throughout the snowmelt season, whereas the original degree-day factor was gradually increased from 0.48 $mK^{-1}d^{-1}$ in May to 0.50 $mK^{-1}d^{-1}$ in June and 0.52 $mK^{-1}d^{-1}$ in July [Martinec, 1989]. The resulting statistics are summarized in table 4.3.4.2. and the generated cumulative snowmelt depths for the lysimeter and the artificial discharges for the Dischma basin are visualized in figures 4.3.4.4. and 4.3.4.5.

Water Equivalent	MBE [%]	RMSE [%]	CD [%]	Slope [-]	Intercept $[10^{-3}md^{-1}]$	Res.St.Dev.
Melt-a	-2.2	55	59	0.88	1.7	9.4
Melt-aT	1.6	42	77	1.01	0.1	7.2
Melt-ΔQ	-0.35	45	73	1.12	-2.1	7.7
Flow-a	-1.6	35	82	0.72	1.9	1.9
Flow-aT	4.0	25	91	0.97	0.5	1.8
Flow-ΔQ	-3.8	25	91	0.94	0.2	1.7

Table 4.3.4.2. Summary statistics for the simulation of the daily lysimeter outflow (Melt) and the artificial daily discharge for the Dischma basin (Flow) according to the original degree-day method (-a), the restricted degree-day method ($-a_T$) and the reduced energy budget method ($-\Delta Q$) from input variables collected at the test site at Weissfluhjoch during the 1985 ablation period.

The discharges that result from (49) are converted to equivalent water depths for convenience. It can be seen from table 4.3.4.2. that the snowmelt-runoff transformation of equation (49) decreases the RMSE for all three methods by almost 20 percent, that it increases the proportion of the variance of the measured water equivalents that is explained by the simulated values by more than 15 percent and that it decreases the standard deviation of the residues of the performed linear regressions by more than a factor 4. Although all three methods perform equally well on a seasonal average basis as is indicated by their similar MBE's, the original degree-day method cannot account for the variability associated with snowmelt and runoff to the same extent as the two other methods. This is probably due to the fact that the former requires only air temperature as an input variable, whereas the latter require both air temperature and net radiation as input variables. In this particular case, the restricted degree-day method performs even slightly better than the reduced energy budget method, although the latter requires two additional input variables, namely mean wind speed and vapor pressure. This

indicates that when daily averages are used as input variables, net radiation and air temperature account for a larger part of the variability associated with snowmelt than any other input variable.

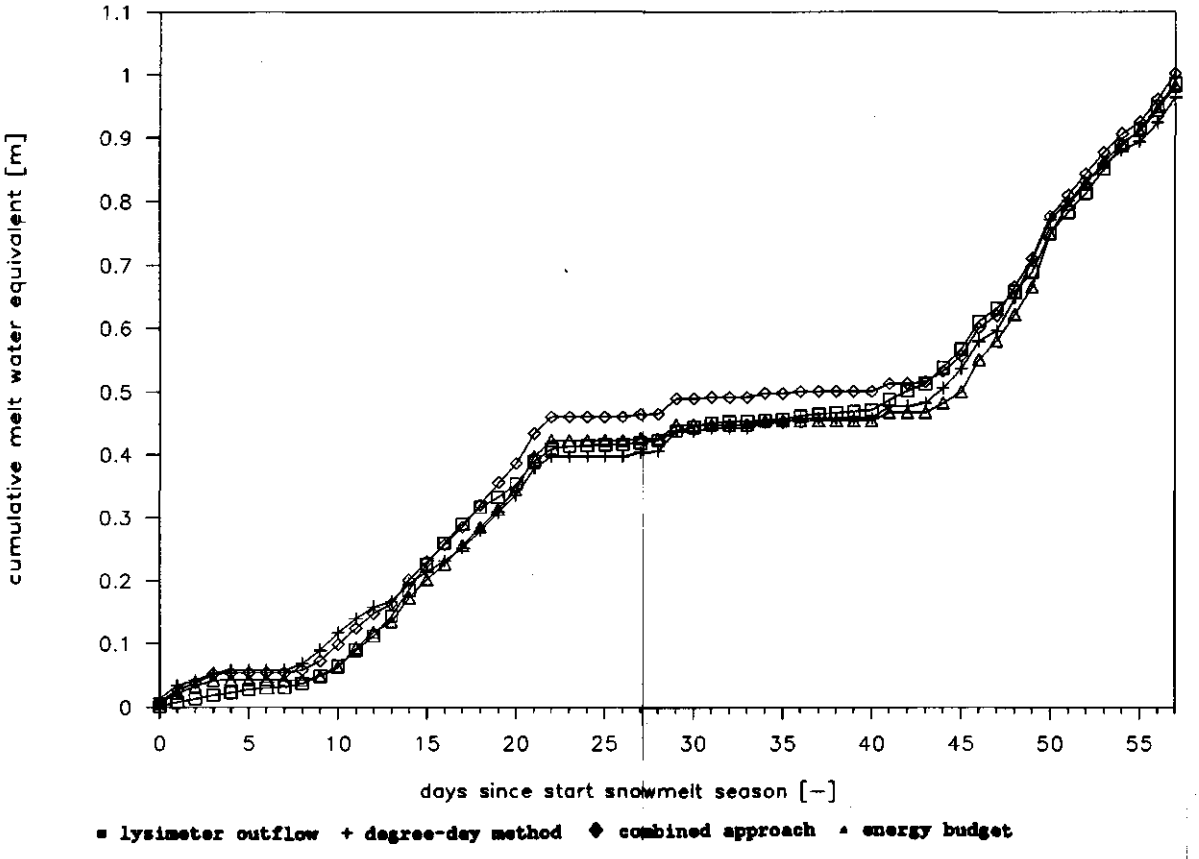

fig. 4.3.4.4. Cumulative measured lysimeter outflows and simulated snowmelt depths according to the original degree-day method (MBE = -2.2%; RMSE = 55%; CD = 59%), the restricted degree-day method (MBE = 1.6%; RMSE = 42%; CD = 77%) and the reduced energy budget method (MBE = -0.35%; RMSE = 45%; CD = 73%) throughout the 1985 snowmelt season at the Weissfluhjoch test site.

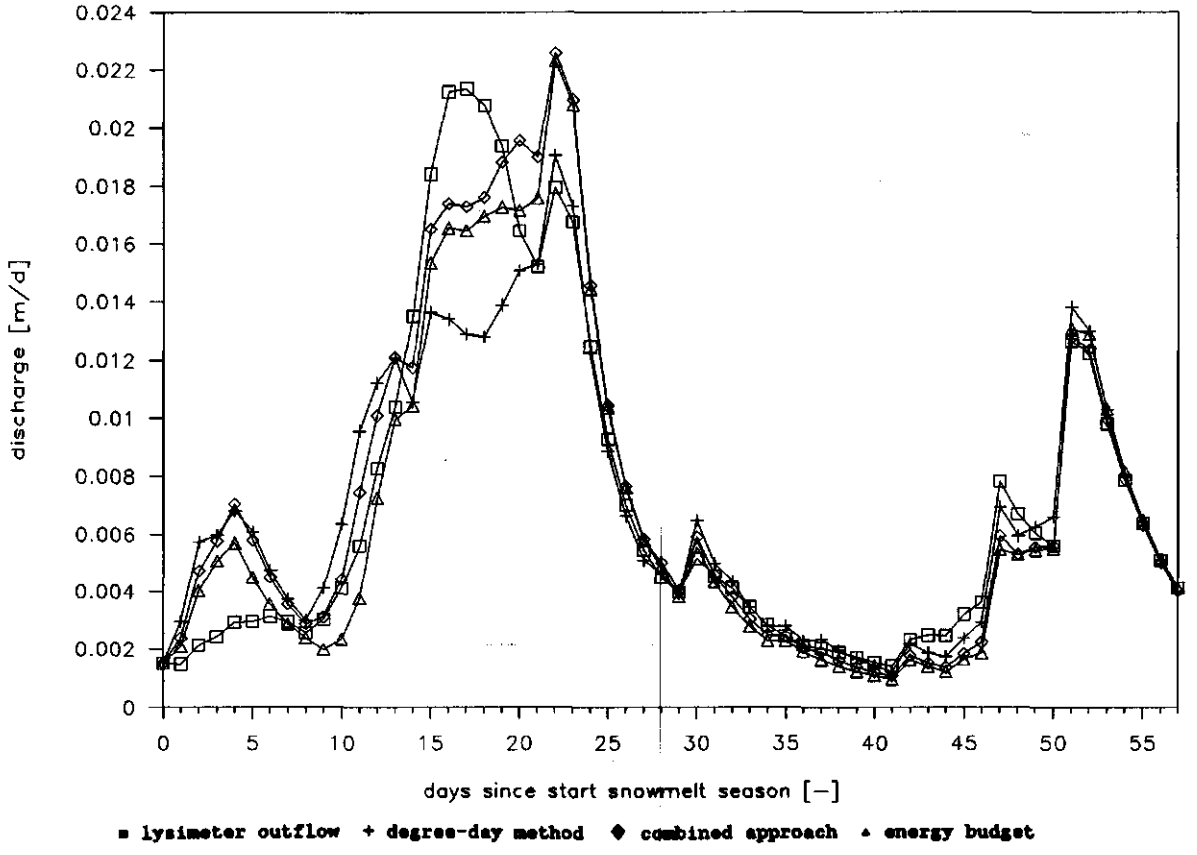

fig. 4.3.4.5. Artificial hydrographs for the Dischma basin from equations (49) and (50) with discharges converted to equivalent water depths; Inputs are measured lysimeter outflows and simulated snowmelt depths according to the original degree-day method (MBE = -1.6%; RMSE = 35%; CD = 82%), the restricted degree-day method (MBE = 4.0%; RMSE = 25%; CD = 91%) and the reduced energy budget method (MBE = -3.8%; RMSE = 25%; CD = 91%) throughout the 1985 snowmelt season at the Weissfluhjoch test site.

CHAPTER 5.

SUMMARY AND CONCLUSIONS

This investigation dealt with the development and operation of a simple radiation budget model at a point on a surface in snow covered mountainous terrain. Net radiation is usually the most important component of the surface energy balance in alpine environments, both with respect to its magnitude and with respect to its temporal and spatial variability. A positive energy balance at the snow surface will cause snowmelt once the snow pack is in thermal equilibrium. A radiation budget model can therefore provide an estimate of the snow surface energy balance and the associated snowmelt.

To allow easy incorporation into operational snowmelt runoff models like the Rango-Martinec Snowmelt Runoff Model (SRM), snowmelt factors should be simple with respect to the amount of required input parameters and their temporal resolution. Most currently available deterministic snowmelt runoff models employ a degree-day factor for computing the amount of snowmelt from a watershed. It is postulated that the incorporation of a radiation balance algorithm will provide a more physically based snowmelt factor than the presently applied temperature index methods, which may reduce the parameter variability associated with local calibrations and adjustments based on observations of snow properties or hydrological judgments of the model operator.

To maintain a high operational capability under a variety of atmospheric conditions and terrain configurations without the need for extensive measurements, a Radiation Budget Module (RBM) was developed based on broadband radiative transfer parameterizations instead of on more sophisticated spectral schemes. Topographic complexity associated with the effects of obstruction, reflection and emission by surfaces surrounding the model point is accounted for by means of conversion factors. The snow pack itself is treated as a black box, i.e. the complex melt associated processes underneath the snow surface are not modeled explicitly. It was found that isotropic or uniform radiance distributions provide reasonable approximations for the incident radiation components in a hypothetical terrain configuration.

The independent input variables required to drive RBM may be classified into three groups: (1) Fixed geographical parameters which need to be determined only once from topographic maps and/or digital elevation data: Latitude, longitude, altitude, slope, aspect and local horizon of the surface in question; (2) Temporal variables: Day of the year, time of the day and amount of days since the last snow accumulation event occured; (3) Atmospheric/ meteorological variables which need to be determined at least on a daily basis from ground truth or remote sensing measurements: Optical depth of the atmosphere, air pressure, surface temperature, air temperature, vapor pressure and mean fractional cloudcover (and/or duration of sunshine). RBM

provides means of estimating the first three atmospheric variables on a daily basis.

As a first step towards the verification of RBM, computed twenty minute values of incoming shortwave and net radiation for a whole day were compared with observations taken over a uniform wheat field under clear skies. RBM performed satisfactorily under these ideal topographic and atmospheric conditions. As a second step, computed daily averages of incoming shortwave radiation for a complete ablation period were compared with observations taken over an unobstructed horizontal snow covered surface in a Swiss alpine watershed under highly variable atmospheric conditions. Although RBM performed rather accurate on a seasonally averaged basis, the model could not explain the large variability of the measured values: It generally underpredicted high values and overpredicted low values. This can probably be associated with the rather unsophisticated manner in which radiation models based on daily average input variables are bound to account for the complicated radiative effects of cloudcover. A more realistic cloud treatment procedure will undoubtedly improve the simulation capacities of such models. As a final verification step within the scope of this investigation, computed daily averages of point snowmelt depth for a complete ablation period were compared with observed lysimeter outflows. Three different snowmelt prediction methods were compared: (1) The original degree-day method; (2) A combined approach which contains both a temperature index and the simulated radiation budget, referred to as the restricted degree-day method; (3) The reduced energy budget method which contains the radiation balance and bulk turbulent transfer parameterizations. In addition to a direct comparison, the simulated snowmelt depths and measured lysimeter outflows were used to generate artificial hydrographs for a complete watershed by means of the Snowmelt Runoff Model (SRM). Although all three methods performed equally well on a seasonally averaged basis, the original degree-day method could not explain the variability associated with snowmelt and the consequent runoff to the same extent as the other two methods. The restricted degree-day method performed even slightly better than the reduced energy budget method. These preliminary results indicate that the computed net radiation accounts for most of the observed temporal variability and that a combined temperature index - simulated radiation budget approach will provide a simple yet physically based snowmelt factor for operational snowmelt runoff modeling. However, additional development and testing of RBM both with respect to its radiative transfer algorithms and with respect to its snowmelt and runoff generating procedures remains necessary to further improve the model's operational accuracy.

Although this investigation deals with the development of a point radiation budget model, it is envisioned that distributed models using digital elevation data should become operational in the near future. This should provide more reliable estimates of snowmelt on a catchment scale, since net radiation accounts for most of the observed spatial and temporal variability. Until more accurate methods become available for the extrapolation of point measurements

over the whole of a catchment, turbulent transfer on this scale has to be accounted for by means of a temperature index. The hydrological character of the currently available operational snowmelt runoff models however, should become more distributed in order to take full advantage of the benefits of a snowmelt factor based on the radiation budget.

APPENDIX A.

DETERMINING RADIUS VECTOR, DECLINATION AND EQUATION OF TIME

The most common formula type for the parameterization of the ephemeris of the sun is the Fourier series representation, which considers the earth's radius vector, the sun's declination and the equation of time to be cyclic with a period of one year. Although it neglects the effects of the four year leap year cycle and other longer period variations, it provides approximations that comply with the accuracy required for purposes of modeling radiation [e.g., Spencer, 1971; Dozier, 1980; Bird and Riordan, 1986]. Such a Fourier series takes the form of a sum of sines and cosines of the day angle, which can generally be specified as follows (see end of each appendix for notation of symbols):

$$\alpha = 2 * \pi * (D - c_d) * (365 + c_l)^{-1} \qquad (A1)$$

In this formula, c_d is a small corection to the day number of the year (D on January 1 equals 1 and D on December 31 equals 365 or 366 for leap years), which takes different values from author to author but is always between zero and one; c_l may be set equal to 0.25 to account for the fact that one of every four years is a leap year. The factor $2*\pi*(365+c_l)^{-1}$ should be interpreted as the mean angular velocity of the earth in its orbit about the sun in units of radians per day.

The general functional form of a n-term Fourier series, either for the reciprocal of the square of the earth's radius vector, for the sun's declination (radians) or for the equation of time (radians) is the following [Dozier and Outcalt, 1979]:

$$r^{-2},\ \delta,\ E = \sum_{i=0}^{n-1} (a_i * \cos[i * \alpha] + b_i * \sin[i * \alpha]) \qquad (A2)$$

Spencer [1971] carried out Fourier analyses for all three of those astronomical variables, with c_d equal to one and c_l equal to zero, and yielded the cosine (a_i) and sine (b_i) coefficients presented in the second and third column of table A1. He evaluted the maximum errors of the obtained Fourier series to be 0.0001, 0.0006 radians and 0.0025 radians (about 34 seconds of time), respectively. Dozier and Outcalt [1979] on the other hand carried out Fourier analyses with both c_d and c_l equal to unity and obtained the coefficients for r and δ presented in the fourth and fifth column of table A1. They state that their series have accuracies of about four significant figures.

Blackadar [1989] proposed the application of a slightly adjusted day angle (c_d equal to 0.3 and c_l equal to 0.25) in combination with Spencer's Fourier coefficients for the solar declination. Although the variation of δ over the year is an order of magnitude larger than that of r or r^{-2}, a single value can be used for each day if an accuracy to the nearest degree in calculated solar zenith and azimuth angles is sufficient [Spencer, 1971].

	i	a_i (S)	b_i (S)	a_i (DO)	b_i (DO)
r^{-2}/r	0	1.000110	0.0	$0.1000108431*10^{1}$	0.0
	1	0.034221	0.001280	$-0.1673661579*10^{-1}$	$-0.4951856474*10^{-3}$
	2	0.000719	0.000077	$-0.1203091198*10^{-3}$	$-0.1790695747*10^{-4}$
	3	0.0	0.0	$0.3517325527*10^{-5}$	$-0.1608389648*10^{-5}$
δ	0	0.006918	0.0	$0.5796702596*10^{-2}$	0.0
	1	-0.399912	0.070257	$-0.3999070840*10^{0}$	$0.7359755022*10^{-1}$
	2	-0.006758	0.000907	$-0.6068166326*10^{-2}$	$0.7560534210*10^{-3}$
	3	-0.002697	0.001480	$-0.2363085071*10^{-2}$	$0.1389717739*10^{-2}$
E	0	0.000075	0.0	-	-
	1	0.001868	-0.032077	-	-
	2	-0.014615	-0.040849	-	-

Table A1. Fourier cosine (a_i) and sine (b_i) coefficients for the (reciprocal of the square of the) earth's radius vector (r^{-2}/r, [-]), for the sun's declination (δ, [radians]) and for the equation of time (E, [radians]) according to Spencer [1971] (S) and Dozier and Outcalt [1979] (DO), to be substituted in equation A2.

Whiteman and Allwine [1986] took a different approach for the determination of the radius vector of the earth and the declination of the sun and used the following convenient formulae, which were originally presented by McCullough [1968], in combination with a day angle based on values for c_d and c_l both equal to zero:

$$r = 1 - e * \cos[\alpha] \qquad \text{(A3)}$$

$$\delta = \arcsin[\sin[\delta_m] * \sin[l_c]] \qquad \text{(A4)}$$

$$l_c = \alpha - \alpha_o + 2 * e * (\sin[\alpha] - \sin[\alpha_o])$$

$$\alpha_o = 2 * \pi * D_o * 365^{-1}$$

In these expressions, e is the eccentricity of the earth's orbit, δ_m is the maximum solar declination (about 23.44°) and l_c is the true celestial longitude of the earth in its orbit about the sun as measured from the day number of the vernal equinox (D_o). It can be seen from the functional form of (A3) that α is in fact an approximation for the so-called true anomaly of the earth's orbit. Since the equation of time is the difference between the mean celestial longitude of the earth and the right ascension of the sun [Blackadar, 1984], which can both be defined in terms of the parameters used

in the above expressions, E can be expressed in the same manner as r and δ:

$$E = (l_c - dl_c) - \arctan[\cos[d_m] * \tan[l_c]] \quad \text{(A5)}$$

$$\begin{aligned} dl_c &= 2 * e * \sin[\alpha - dl_c] + 1.25 * e^2 * \sin[2 * (\alpha - dl_c)] \\ &= 2 * e * \sin[\alpha - dl_c] * (1 + 1.25 * e * \cos[\alpha - dl_c]) \\ &\approx 2 * e * \sin[\alpha] * (1 + 1.25 * e * \cos[\alpha]) \\ &\approx 2 * e * \sin[\alpha] \end{aligned} \quad \text{(A6)}$$

Here (l_c-dl_c) and $(\alpha-dl_c)$ stand for the mean celestial longitude and the mean anomaly, respectively. The maximum error in E obtained from (A5) and (A6) amounts about half a minute.

i	a_i	b_i
0	0.0	0.0
1	0.00839	-0.12193
2	-0.05391	-0.15699
3	-0.00154	-0.00657
4	-0.00222	-0.00370

Table A2. Fourier cosine (a_i) and sine (b_i) coefficients for the equation of time (E, [hr]) according to Whiteman and Allwine [1986], to be substituted in equation A2.

However, Whiteman and Allwine [1986] did not take this convenient approach for the determination of the equation of time, but rather carried out a Fourier analysis and obtained the cosine and sine coefficients for E expressed in hours presented in table A2. (based on c_d equal to 0.4 and c_l equal to zero). The maximum error in E evaluated by these Fourier coefficients is reported to amount about 25 seconds of time (i.e. about 0.0018 radians).

The third and most accurate approach for the parameterization of the ephemeris of the sun discussed here was implemented originally by Blackadar [1984; 1985b]. Taking the small year to year variations of the radius vector, the declination and the equation of time into account, he related the mean anomaly of the earth's orbit about the sun and the mean celestial longitude of the earth in (A3)-(A6) to the so-called Julian day number. This is the number of days (including fractions) since noon, Greenwich Mean Time, on November 24, 4714 B.C. (on our modern, Gregorian calendar). Sinott [1984] published a simple algorithm that converts a Gregorian calendar date into a Julian day number, which is not only required in order to be able to compute Blackadar's ephemeris formulae but provides also a convenient method to determine the number of any day of any year required for Spencer's and Whiteman and Allwine's formulae. Blackadar's ephemeris formulae together with Sinott's Julian date algorithm are implemented in the Radiation Budget Module, of which a code listing is presented in appendix E (see the appropriate subroutines).

Notation

α = Day angle [rad]
D = Day number of year [-]
c_d, c_l = Correction terms [-]
r = Radius vector of earth [-]
δ = Declination of sun [rad]
E = Equation of time [rad, hr]
i = Term counter in Fourier series [-]
a_i = Fourier cosine coefficient [-]
b_i = Fourier sine coefficient [-]
e = Eccentricity of earth's orbit about sun [$\approx$ 0.016728]
δ_m = Maximum declination of sun [$\approx$ 0.409095 rad]
l_c = True celestial longitude of earth in orbit about sun as measured from vernal equinox [rad]
α_o = Day angle of vernal equinox [rad]
D_o = Day number of vernal equinox [$\approx$ 80]
dl_c = Difference between true and mean celestial longitude [rad]

APPENDIX B.

DETERMINING THE WATER VAPOR AMOUNT AND THE EMISSIVITY OF THE ATMOSPHERE USING EXPONENTIAL DECAY FUNCTIONS

B.1. The Water Vapor Amount in the Atmosphere in a Vertical Path above a Surface

The actual (precipitable) water vapor amount in the atmosphere in a vertical path above an arbitrary surface can be approximated by the integral of the water vapor density between the surface altitude (h) and infinity, which can be seen as follows:

$$w_h = \int_0^{p_h} q * g^{-1} * dp = \int_0^{p_h} rho_v * (rho_a * g)^{-1} * dp \approx \int_h^{\infty} rho_v * dz \qquad (B1)$$

To simplify the determination of the integral at the upper limit, the water vapor density profile may be assumed to be given by an exponential decay with altitude (z), based on exponential decay functions for air temperature and vapor pressure [Brutsaert, 1975; 1982]:

$$rho_v = 0.622 * e_h * (R_d * T_h)^{-1} * \exp[-k_w * (z - h)] \quad ==> \qquad (B2)$$

$$w_h = 0.622 * e_h * (R_d * T_h)^{-1} * \int_h^{\infty} \exp[-k_w * (z - h)] * dz$$

$$= 0.622 * e_h * (R_d * T_h)^{-1} * \left[-k_w^{-1} * \exp[-k_w * (z - h)]\right]_h^{\infty}$$

$$= 0.622 * e_h * (k_w * R_d * T_h)^{-1} \qquad (B3)$$

The effective amount of water vapor scaled for the pressure and temperature effects can be determined in an analogous manner when the vertical pressure and temperature profiles are assumed to be given by exponential decay functions, which should be adequate in the lowest 10 km of the atmosphere [Brutsaert, 1975; 1982]:

$$p_z = p_h * \exp[-g * (R_d * T_o)^{-1} * (z - h)] \qquad (B4)$$

$$T_z = T_h * \exp[-\Gamma * T_o^{-1} * (z - h)] \quad ==> \qquad (B5)$$

$$w_{eh} = \int_h^\infty (p_z * p_h^{-1})^{Np} * (T_h * T_z^{-1})^{Nt} * rho_v * dz$$

$$= 0.622 * e_h * (R_d * T_h)^{-1} * \int_h^\infty exp[-k_{we} * (z - h)] * dz$$

$$= 0.622 * e_h * (k_{we} * R_d * T_h)^{-1} \qquad (B6)$$

$$k_{we} = k_w + (N_p * g * R_d^{-1} - N_t * \Gamma) * T_o^{-1} \qquad (B7)$$

$$(0.5 \leq N_p \leq 1.0;\ 0 \leq N_t \leq 0.5)$$

As denoted above, the usual practice is to take N_p between 0.5 and 1.0 (i.e. a pressure scaling ranging between square root and linear) and N_t between 0 and 0.5 (i.e. a temperature scaling ranging between zero and square root). For the purpose of computing water vapor absorption in the earth's atmosphere Lacis and Hansen [1974], Wang [1976] and Leckner [1978] included a (near) square root temperature scaling, but Wang noted that the effect is small. Brutsaert [1975, 1982] and Unsworth and Monteith [1975] therefore probably ignored the temperature effect completely for the purpose of computing the emission of the atmosphere due to water vapor. On the other hand, they took scaling for the pressure effect as a square root, whereas Leckner [1978] applied N_p equal to 0.9.

Since both (B3) and (B6) are based on average vertical profiles, they account for the decrease of the amount of water vapor above a surface with increasing altitude. As can be seen from equation (B2), the ratio of vapor pressure and air temperature decreases with increasing altitude, because vapor pressure, due to its strong temperature dependence, decreases much faster than air temperature.

B.2. Altitude Dependency of the Clear Sky Effective Atmospheric Emissivity

The following is a generalization of Brutsaert's [1975; 1982] derivation of the clear sky effective atmospheric emissivity as a function of screen level vapor pressure and air temperature from the integration of the equation for infrared radiative transfer in a plane stratified atmosphere by substituting exponential decay functions to approximate the vertical water vapor density (B2), air pressure (B4) and temperature (B5) profiles. It is shown that the functional form of Brutsaert's equation remains exactly the same at any altitude (h) in the atmosphere and that it therefore implicitly contains an altitude adjustment accounting for the fact that the water vapor amount above a certain level in the atmosphere decreases with increasing

altitude. His equation therefore makes any explicit altitude correction (as proposed by Marks and Dozier [1979] and Marks [1988]) superfluous when screen level values for vapor pressure and air temperature are substituted.

The clear sky atmospheric emission and emissivity can be defined in terms of the slab emissivity (ϵ_{slab}) as follows, respectively [e.g., Liou, 1980]:

$$L_{skyoh} = \epsilon_{skyoh} * \sigma * T_h^4 = \int_0^\infty \sigma * T_z^4 \frac{\delta \epsilon_{slab}}{\delta w_e} dw_e \quad <==>$$

$$\epsilon_{skyoh} = \int_0^\infty (T_z * T_h^{-1})^4 \frac{\delta \epsilon_{slab}}{\delta w_e} dw_e$$

$$= \int_0^\infty \exp[-4 * \Gamma * T_o^{-1} * (z - h)] \frac{\delta \epsilon_{slab}}{\delta w_e} dw_e \qquad (B8)$$

The slab emissivity can be conveniently approximated by a power function of the effective amount of water vapor in the air column from the level z down to the surface level h scaled for the pressure effect by means of a square root correction:

$$\epsilon_{slab} = A * w_{eslab}^m \quad ==> \frac{\delta \epsilon_{slab}}{\delta w_e} = m * A * w_{eslab}^{m-1} \qquad (B9)$$

$$dw_e = (p_z * p_h^{-1})^{1/2} * rho_v * dz$$

$$= 0.622 * e_h * (R_d * T_h)^{-1} * \exp[-k_{we} * (z - h)] * dz \qquad (B10)$$

$$w_{eslab} = \int_h^z dw_e$$

$$= 0.622 * e_h * (k_{we} * R_d * T_h)^{-1} * (1 - \exp[-k_{we} * (z - h)]) \qquad (B11)$$

$$k_{we} = k_w + g * (2 * R_d * T_o)^{-1} \qquad (B12)$$

Substituting equations (B9)-(B12) in (B8) and setting z-h equal to z' yields the following expression for the clear sky atmospheric emissivity:

$$\epsilon_{skyoh} = m * A * (0.622 * e_h * (k_{we} * R_d * T_h)^{-1})^m$$

$$* \int_0^\infty k_{we} * \exp[-k_{we}' * z'] * (1 - \exp[-k_{we} * z'])^{m-1} * dz' \qquad (B13)$$

$$k_{we}' = k_{we} + 4 * \Gamma * T_o^{-1} \qquad (B14)$$

The above integral can be conveniently expressed in terms of the complete beta function B(a,b) [Abramowitz and Stegun, 1964], when $k_{we}'*k_{we}^{-1}$, m and $\exp[-k_{we}*z']$ are substituted for a, b and t, respectively. This then yields Brutsaert's "derivable formula for longwave radiation from clear skies":

$$B(a,b) = \int_0^1 t^{a-1} * (1 - t)^{b-1} * dt$$

$$= \int_0^\infty k_{we} * \exp[-a * k_{we} * z'] * (1 - \exp[-k_{we} * z'])^{b-1} * dz' \quad ==>$$

$$\epsilon_{skyoh} = m * A * (0.622 * e_h * (k_{we} * R_d * T_h)^{-1})^m * B(k_{we}' * k_{we}^{-1}, m) \qquad (B15)$$

$$= m * A * w_{eh}^m * B(k_{we}' * k_{we}^{-1}, m) \approx 0.521 * w_{eh}^{1/7} \qquad (B16)$$

$$\approx 0.642 * (e_h * T_h^{-1})^{1/7} \qquad (B17)$$

The following altitude correction for the clear sky atmospheric emissivity based on the assumptions made for the derivation of (B15) can now be derived from equations (B2) and (B15):

$$\epsilon_{skyoz} = \epsilon_{skyoh} * \exp[-k_\epsilon * (z - h)] \qquad (B18)$$

$$k_\epsilon = m * k_w \approx k_w / 7 \approx 6.3 * 10^{-5}\ m^{-1} \qquad (B19)$$

It follows from (B19) that the emissivity of the atmosphere for average clear sky conditions decreases by about 6 percent per kilometer altitude increase.

In addition to Brutsaert's formula (B17), most of the other functional relationships between the effective emissivity of a cloudless atmosphere and the screen level air temperature and/or vapor pressure that have been developed over the past decades were discussed extensively in section 2.2.4. With the exception of Ångström's and Brunt's equations, they do not require extensive local calibrations to determine empirical parameters (e_h and T_h are expressed in the S.I. units pascal and kelvin, respectively):

$$\epsilon_{skyoh} = 9.39 * 10^{-6} * T_h^2 \quad \text{(B20)}$$

[Swinbank, 1963]

$$= 1 - 0.261 * \exp[-7.77 * 10^{-4} * (273 - T_h)^2] \quad \text{(B21)}$$

[Idso and Jackson, 1969]

$$= 1.08 * (1 - \exp[-(e_h / 100)^{Th/2016}]) \quad \text{(B22)}$$

[Satterlund, 1979]

$$= 0.7 + 5.95 * 10^{-7} * e_h * \exp[1500 * T_h^{-1}] \quad \text{(B23)}$$

[Idso, 1981]

Arguing that "in alpine areas the assumption of a standard atmosphere (which has been the basis for the derivation of Brutsaert's fromula, R.U.) is not valid", Marks and Dozier [1979] and Marks [1988] proposed the following adjusted scheme for the computation of ϵ_{skyoh} as a function of e_h, T_h and p_h in remote alpine areas (assuming a standard temperature lapse rate and a constant relative humidity):

$$\epsilon_{skyoh} = 0.642 * (e_o * T_o^{-1})^{1/7} * (p_h * p_o^{-1}) \quad \text{(B24)}$$

$$T_o = T_h + \Gamma * h$$

$$e_o = e_h * (e_s[T_o] * e_s[T_h]^{-1})$$

$$p_h * p_o^{-1} = \exp[-g * (\Gamma * R_d)^{-1} * \ln[T_o * T_h^{-1}]]$$

Although the derivations of (B20)-(B23) as opposed to that of (B17) are not based on vertical profiles for vapor pressure, air pressure and air temperature, their altitude dependency can be quantified when Brutsaert's [1975, 1982] typical exponential decay functions (equations (B2), (B4) and (B5) with k_w=4.4, $g/(R_d*T_o)$=1.3 and Γ/T_o=0.226*10^{-4}m^{-1}, respectively) are substituted.

h	e_h	T_h	p_h	ϵ_{skyoh} [-]					
[10^{3}m]	[Pa]	[K]	[10^{5}Pa]	(B20)	(B21)	(B17)	(B24)	(B22)	(B23)
0	1278	288	1.013	0.780	0.782	0.795	0.795	0.824	0.839
1	805	282	0.890	0.745	0.754	0.746	0.694	0.797	0.798
2	507	275	0.781	0.712	0.740	0.701	0.605	0.770	0.770
3	319	269	0.686	0.681	0.742	0.658	0.529	0.744	0.750
4	201	263	0.602	0.651	0.758	0.618	0.462	0.719	0.736
5	127	257	0.529	0.622	0.784	0.580	0.403	0.695	0.726

Table B1. Altitude dependency of clear sky effective atmospheric emissivities from different functional relationships using exponential decay functions for vertical vapor pressure, air temperature and air pressure profiles (RH_o = 75%).

For instance, it can be seen easily that substitution of (B5) in (B20) yields $k_\epsilon=2*\Gamma/T_o=4.52*10^{-5}$ m^{-1}, equivalent with a clear sky emissivity decay of about 4.5 percent per kilometer, which is slightly lower than follows from Brutsaert's formula. Since the vertical profiles that Marks proposed are very similar to the ones Brutsaert proposed, it follows directly from (B24) that the emissivity decay coefficient must approximately equal the pressure decay coefficient, i.e. $k_\epsilon \approx g/(R_d*T_o)=1.3*10^{-4}$ m^{-1}. The resulting 12 percent clear sky emissivity decay per kilometer is twice as much as results from Brutsaert's and almost three times as much as results from Swinbank's equation!

Table B1. gives the emissivities resulting from (B20)-(B24) for altitudes up to 5 kilometers, when the relative humidity at mean sea level is 75 percent. These figures confirm the observation of Aase and Idso [1978] that under moderate atmospheric conditions (B21) and (B17) adequately predict the clear sky effective atmospheric emissivity, whereas under freezing conditions the former tends to overestimate and the latter tends to underestimate. It can also be concluded that the linear pressure correction in (B24) causes an emissivity decay with altitude that is considerably stronger than that of the other equations, and that the scheme of Marks and Dozier [1979] is therefore likely to underestimate the atmospheric emissivity at high altitudes.

Notation

w	= Actual (precipitable) zenith path water vapor content of atmosphere [kgm^{-2}]
h	= Reference altitude above mean sea level [m]
q	= Specific humidity [-]
g	= Gravitational acceleration [≈ 9.81 ms^{-2}]
rho_v	= Water vapor density [kgm^{-3}]
rho_a	= Air density [kgm^{-3}]
p	= Air pressure [Pa]
z	= Altitude above mean sea level [m]
e	= Vapor pressure [Pa]
R_d	= Gas constant of dry air [≈ 287.04 $Jkg^{-1}K^{-1}$]
T	= Air temperature [K]
k_w	= Water vapor density decay coefficient [$\approx 4.4 * 10^{-4}$ m^{-1}]
T_o	= Mean air temperature at sea level [≈ 288.15 K]
Γ	= Temperature lapse rate [≈ 0.0065 Km^{-1}]
w_e	= Effective (scaled) zenith path water vapor content of atmosphere [kgm^{-2}]
N_p	= Scaling exponent for pressure [≈ 0.5]
N_t	= Scaling exponent for temperature [≈ 0.0]
k_{we}	= Effective water vapor density decay coefficient [$\approx 5.05 * 10^{-4}$ m^{-1}]
L_{skyo}	= Atmospheric emission for clear skies [Wm^{-2}]
ϵ_{skyo}	= Effective atmospheric emissivity for clear skies [-]
σ	= Stefan-Boltzmann's constant [$\approx 5.6697 * 10^{-8}$ $Wm^{-2}K^{-4}$]
ϵ_{slab}	= Emissivity of slab of water vapor with CO_2 [-]
A	= Factor of power function [≈ 0.54]
w_{eslab}	= Effective water vapor content of slab of air [kgm^{-2}]
m	= Exponent of power function [$\approx 1/7$]
k_{we}'	= Decay coefficient [$\approx 5.95 * 10^{-4}$ m^{-1}]

z' = Altitude above reference level [m]
$B(a,b)$ = Complete beta function with coefficients a and b [≈ 6.76]
t = Independent variable [-]
k_ϵ = Decay coefficient for clear sky effective atmospheric emissivity [≈ $6.3 * 10^{-5}$ m^{-1}]
p_o = Standard air pressure at mean sea level [≈ $1.01325 * 10^5$ Pa]
e_o = Vapor pressure at 288.15 K with 75% relative humidity [≈ 1278 Pa]

APPENDIX C.

DETERMINING THE ANGLE OF INCIDENCE OF DIRECT SOLAR RADIATION AT INCLINED SURFACES

The cosine of the incidence angle of direct solar radiation at an inclined surface can be given directly as a function of the sun's position in the sky as determined by its zenith and azimuth angles and of the geometry of the surface as determined by its inclination (slope) and azimuth (aspect) angles, as follows [e.g., Kondratyev, 1973]:

$$\begin{aligned}\cos[\theta_s'] &= \cos[S] * \cos[\theta_s] + \sin[S] * \sin[\theta_s] * \cos[\Phi_s - A] \\ &= \cos[S] * \cos[\theta_s] + \sin[S] * \sin[\theta_s] \\ &\quad * (\cos[A] * \cos[\Phi_s] + \sin[A] * \sin[\Phi_s])\end{aligned} \qquad (C1)$$

This equation can be transformed into a for some purposes more convenient functional form in which the sun's position is given indirectly as a function of the latitude of the surface, the date as determined by the solar declination and the time of the day as determined by the hour angle. The following expressions for the cosine of the solar zenith angle and the sine and cosine of the solar azimuth angle derived on the basis of spherical trigonometry [e.g., List, 1966; Kondratyev, 1973] must then be substituted in (C1):

$$\cos[\theta_s] = \sin[\Phi] * \sin[\delta] + \cos[\Phi] * \cos[\delta] * \cos[H] \qquad (C2)$$

$$\sin[\Phi_s] = -\cos[\delta] * \sin[H] * \sin^{-1}[\theta_s] \quad <==> \qquad (C3)$$

$$\sin[\theta_s] * \sin[\Phi_s] = -\cos[\delta] * \sin[H]$$

$$\cos[\Phi_s] = (\sin[\delta] - \sin[\Phi] * \cos[\theta_s]) * (\cos[\Phi] * \sin[\theta_s])^{-1} <==> (C4)$$

$$\sin[\theta_s] * \cos[\Phi_s] = (\sin[\delta] - \sin[\Phi] * \cos[\theta_s]) * \cos^{-1}[\Phi]$$

It is noted here for reasons of completeness that taking the quotient of (C3) and (C4) yields the same expression for the tangent of the solar azimuth angle as Iqbal [1983] presented [Blackadar, 1989]. Moreover, expressions for the solar zenith angle at true solar noon and for the hour angles at true sunrise and sunset at an unobstructed horizontal surface (i.e. neglecting the phenomena of atmospheric refraction and parallax that determine the apparent sunrise and sunset) can easily be derived from (C2) by setting H equal to zero ($=> \theta_s = |\Phi - \delta|$) and θ_s equal to $\pi/2$ ($=> H_{set,rise} = \pm\arccos[-\tan[\Phi]*\tan[\delta]]$), respectively. The latter allows (C2) to be integrated analytically between solar noon (H=0) and sunset ($H=H_{set}$) to yield an expression ($\sin[\Phi]*\sin[\delta]*H_{set} + \cos[\Phi]*\cos[\delta]*\sin[H_{set}]$) which after multiplication with the factor $S_o*(\pi*r^2)^{-1}$ determines the average daily radiation reaching a hypothetical horizontal

surface at the top of the atmosphere (with the minor approximations that δ and r are constant during the day). See figure 2.1.1.

Substitution of (C2)-(C4) in (C1) yields the same formula as Garnier and Ohmura [1968, 1970] developed on the basis of a coordinate transformation following the principles of vector algebra. In this expression, latitudes and declinations north of the equator are taken as positive and south of the equator as negative, the hour angle is measured from solar noon positively towards west and negatively towards east, and lastly azimuths are measured from north through east:

$$\begin{aligned}\cos[\theta_s'] = &(\cos[S] * \sin[\Phi] + \sin[S] * \cos[A] * \cos[\Phi]) * \sin[\delta] \\ &+ (\cos[S] * \cos[\Phi] * \cos[H] - \sin[S] * \sin[A] * \sin[H] \\ &- \sin[S] * \cos[A] * \sin[\Phi] * \cos[H]) * \cos[\delta] \qquad \text{(C5)}\end{aligned}$$

When the surface inclination angle is set equal to zero in (C5), (C2) can easily be obtained. The incidence angle of direct solar radiation at a horizontal surface by definition namely equals the solar zenith angle.

Notation[1]

θ_s' = Incidence angle of direct solar radiation at inclined surface
S = Surface inclination angle or slope
θ_s = Solar zenith angle or incidence angle of direct solar radiation at horizontal surface
Φ_s = Solar azimuth angle
A = Surface azimuth angle or aspect
Φ = Latitude of surface
δ = Declination of sun
H = Hour angle

[1] All angles are expressed in units of radians [rad]

APPENDIX D.

DERIVING ANISOTROPY FACTORS FROM RADIANCE DISTRIBUTION FUNCTIONS

D.1. Background Solar Sky Radiance

Several authors have described the background diffuse shortwave radiation field by a fictitious radiance distribution linear in the cosine of the zenith angle [e.g., Steven and Unsworth, 1979; 1980; Arnfield, 1982]:

$$K[\theta] = K[0] * (1 + b_k * \cos[\theta]) * (1 + b_k)^{-1} \quad <==>$$
$$K[\mu] = K[1] * (1 + b_k * \mu) * (1 + b_k)^{-1} \; ; \; \mu = \cos[\theta] \qquad (D1)$$

In these equations K[0] and K[1] denote the radiance from the zenith and not the mean radiance from the entire spherical solid angle, which Olyphant [1986b] incorrectly assumed. The total amount of background solar sky radiation reaching an unobstructed horizontal surface is the hemispherical integration of the radiance distribution function:

$$K_{dif} = \int_0^{2\pi} \int_0^{\pi/2} K[\theta] * \sin[\theta] * \cos[\theta] * d\theta * d\Phi$$

$$= 2\pi * \int_0^1 K[\mu] * \mu * d\mu$$

$$= 2\pi * K[1] * (1 + b_k)^{-1} * \int_0^1 (1 + b_k * \mu) * \mu * d\mu$$

$$= 2\pi * K[1] * (1 + b_k)^{-1} * \left[\mu^2/2 + b_k * \mu^3/3 \right]_0^1$$

$$= \pi * K[1] * (1 + b_k * 2/3) * (1 + b_k)^{-1} \qquad (D2)$$

The anisotropy factor for background solar sky radiation is by definition the ratio of the equivalent flux density from a particular solid angle to the total amount of diffuse radiation reaching an unobstructed horizontal surface [Dozier and Frew, 1989]:

$$\Omega_k[\mu] = \pi * K[\mu] * K_{dif}^{-1}$$
$$= (1 + b_k * \mu) * (1 + b_k * 2/3)^{-1} \qquad (D3)$$

It can be seen from the above equation that the anisotropy factor becomes unity when μ equals 2/3, i.e. when θ equals $\arccos[2/3] \approx 48.2°$. The equivalent flux density from this representative angle equals the total hemispherically integrated amount of diffuse sky radiation.

D.2. Atmospheric Emittance

Unsworth and Monteith [1975] presented a radiance distribution function for incoming longwave radiation in terms of the apparent (or equivalent) emissivity and the zenith optical water path of the atmosphere, i.e. the effective water vapor amount scaled for the pressure effect (by a square root correction as determined by (B6) and (B12)):

$$\epsilon_e[\theta] = a + b_l * \ln[w_e * \cos^{-1}[\theta]] \quad <==>$$
$$\epsilon_e[\mu] = a + b_l * \ln[w_e * \mu^{-1}] \tag{D4}$$

In these equations the secant approximation is used to account for the relative path length for water vapor because of its easy integrability. The atmospheric emissivity is consequently given by the hemispherical integration of the apparent emissivity of each solid angle, which follows the derivation of (D2):

$$\epsilon_{sky} = 2 * \int_0^1 \epsilon_e[\mu] * \mu * d\mu$$

$$= 2 * \int_0^1 (a + b_l * (\ln[w_e] - \ln[\mu])) * \mu * d\mu$$

$$= 2 * (a + b_l * \ln[w_e]) * \left[\mu^2/2 \right]_0^1$$

$$- 2 * b_l * \left[\mu^2/2 * (\ln[\mu] - 1/2) \right]_0^1$$

$$= a + b_l * \ln[w_e] + b_l/2 = a + b_l * (1/2 + \ln[w_e]) \tag{D5}$$

The anisotropy factor for atmospheric emittance is defined as the ratio of the apparent emissivity to the atmospheric emissivity:

$$\Omega_l[\mu] = \epsilon_e[\mu] * \epsilon_{sky}^{-1}$$
$$= (a + b_l * (\ln[w_e] - \ln[\mu])) * (a + b_l * (\ln[w_e] + 1/2))^{-1} \tag{D6}$$

It can be seen from this equation that the representative angle for the incoming longwave radiation field (the angle for which the anisotropy factor becomes unity) is determined by setting $\ln[\mu]$ equal to -1/2, i.e. θ equal to $\arccos[\exp[-1/2]] \approx 52.7°$.

Since ϵ_{sky} can easily be determined with reasonable accuracy from the screen level vapor pressure and/or air temperature and the mean fractional cloudcover, (D5) can be used for the convenient elimination a and w_e from (D6):

$$a = \epsilon_{sky} - b_1 * (1/2 + \ln[w_e]) \quad ==> \tag{D7}$$

$$\epsilon_e[\mu] = \epsilon_{sky} - b_1 * (1/2 + \ln[\mu]) \quad ==> \tag{D8}$$

$$\Omega_1[\mu] = 1 - b_1 * \epsilon_{sky}^{-1} * (1/2 + \ln[\mu]) \tag{D9}$$

Until this point basically the method proposed by Unsworth and Monteith [1975] has been followed. However, they stated that (D8) "clearly does not represent the variation of the emissivity at very large (zenith, R.U.) angles, since it fails to predict that emissivity tends to unity as θ approaches 90°". The reason for this deviation is that the secant approximation for the relative path length for water vapor (which has been the basis for the derivation of (D5)-(D9)) neglects the curvature of the earth and its atmosphere. Instead of approaching unity for large zenith angles, the apparent emissivity as determined by (D8) tends to infinity. Brunt [1932] inferred from his measurements of the angular distribution of incoming longwave radiation that "... just above the horizon, we should expect to find the amount of radiation practically independent of vapor pressure, since a horizontal cylinder of the atmosphere will always contain enough water vapor to radiate effectively as a black body ...". Although setting the apparent emissivity equal to unity for θ equal to $\pi/2$ radians may lead to a slight overestimation of the radiance at large zenith angles because the screen level air temperature will generally be higher than the mean temperature of the radiating layer, below inversions (which occur frequently in snow covered mountainous terrain, particularly during the snowmelt season) it leads to an underestimation because the screen level air temperature is lower than the mean temperature of the radiating layer [Unsworth and Monteith, 1975]. It is therefore assumed that the approximation that $\epsilon_e[\pi/2]$ equals unity represents the average atmospheric conditions with reasonable accuracy. This makes it possible to eliminate the remaining empirical coefficient (b_1) and derive a standard longwave radiation distribution that is solely a function of the atmospheric emissivity. Hence, it is obvious that the secant approximation for the relative path length for water vapor has to be abandonned in favor of an expression that is more accurate at large zenith angles.

The following empirical formula has the same functional form as Rodgers' [1967] expression for the relative path length for ozone [Lacis and Hansen,

1974], which allows easier integration than the form of Kasten's [1966] formula:

$$M_w = M_w[0] * ((M_w[0]^2 - 1) * \mu^2 + 1)^{-1/2} \qquad \text{(D10)}$$

For the purpose of computing the absorption of solar (shortwave) radiation in the atmosphere by water vapor, the maximum relative path length ($M_w[0]$) has a value of about 75. However, emission of radiation by water vapor occurs in the thermal (longwave) region of the electromagnetic spectrum, where no appreciable refraction takes place. Hence, $M_w[0]$ in (D10) will most likely have a lower value than 75, although the influence of its magnitude on the computation of the atmospheric emissivity is small (equation (D12)).

The derivation of the revised anisotropy factor for atmospheric emittance on the basis of (D10) and the assumption that $\epsilon_e[\pi/2]$ equals unity basically follows that of (D4)-(D9):

$$\epsilon_e[\mu] = a + b_1 * \ln[w_e * M_w] \quad ==> \qquad \text{(D11)}$$

$$\epsilon_{sky} = 2 * \int_0^1 (a + b_1 * (\ln[w_e] + \ln[M_w])) * \mu * d\mu$$

$$= a + b_1 * \ln[w_e] + 2 * b_1 * \int_0^1 \ln[M_w] * \mu * d\mu$$

$$= a + b_1 * \ln[w_e * M_w[0]]$$

$$- b_1 * \int_0^1 \ln[(M_w[0]^2 - 1) * \mu^2 + 1] * \mu * d\mu$$

$$\mu' = (M_w[0]^2 - 1) * \mu^2 + 1 \quad ==> d\mu' = 2 * (M_w[0]^2 - 1) * \mu * d\mu \quad ==>$$

$$\epsilon_{sky} = a + b_1 * \ln[w_e + M_w[0]]$$

$$- b_1 * (2 * (M_w[0]^2 - 1))^{-1} * \int_1^{M_w[0]^2} \ln[\mu'] * d\mu'$$

$$= a + b_1 * \ln[w_e + M_w[0]]$$

$$- b_1 * (2 * (M_w[0]^2 - 1))^{-1} * \left[\mu' * \ln[\mu'] - \mu' \right]_1^{M_w[0]^2}$$

$$= a + b_1 * \ln[w_e + M_w[0]]$$

$$+ b_1 * (1/2 - (1 - M_w[0]^{-2})^{-1} * \ln[M_w[0]])$$

$$= a + b_1 * ((1/2 - (M_w[0]^2 - 1)^{-1} * \ln[M_w[0]]) + \ln[w_e]) \qquad \text{(D12)}$$

$$\approx a + b_l * (0.5 + \ln[w_e]) \quad ==> \tag{D5}$$

$$a = \epsilon_{sky} - b_l * (0.5 + \ln[w_e]) \quad ==> \tag{D7}$$

$$\epsilon_e[\mu] = \epsilon_{sky} - b_l * (0.5 - \ln[M_w]) \quad ==> \tag{D13}$$

$$\epsilon_e[0] = \epsilon_{sky} - b_l * (0.5 - \ln[M_w[0]]) = 1 \quad <==>$$

$$b_l = (1 - \epsilon_{sky}) * (\ln[M_w[0]] - 0.5)^{-1} \quad ==> \tag{D14}$$

$$\epsilon_e[\mu] = \epsilon_{sky} - (\epsilon_{sky} - 1) * (0.5 - \ln[M_w]) * (0.5 - \ln[M_w[0]])^{-1} \tag{D15}$$

$$\Omega_l[\mu] = 1 - (1 - \epsilon_{sky}^{-1}) * (0.5 - \ln[M_w]) * (0.5 - \ln[M_w[0]])^{-1} \tag{D16}$$

Since (D12) approximately equals (D5), it may be concluded that the hemispherical integration of (D10) is not significantly different from that of the secant approximation for the relative path length for water vapor. However, application of (D10) will yield more accurate values for the apparent emissivity at large zenith angles and moreover, it is necessary in order to be able to derive b_l as a function of ϵ_{sky} (equation (D14)). The only empirical coefficient remaining in the formulation of the anisotropy factor for atmospheric emittance (D16) consequently is the atmospheric emissivity, which can be determined from (B16) (as a function of the scaled water vapor amount) or (B17) (as a function of vapor pressure and air temperature) and the mean fractional cloudcover. Application of typical values for ϵ_{sky} (roughly ranging between 0.6 and 1 as can be gathered from table B1.) yields values for a (from (D7)) and b_l (from D(14)) that fall within the ranges mentioned by Unsworth and Monteith [1975], which are based on extensive measurements.

Notation

K = Background solar sky radiance [$Wm^{-2}sr^{-1}$]
Θ = Zenith angle [rad]
b_k = Coefficient for background solar sky radiance distribution [-]
μ = Cosine of zenith angle [-]
K_{dif} = Background solar sky radiation [Wm^{-2}]
Φ = Azimuth angle [rad]
Ω_k = Anisotropy factor for background solar sky radiance [-]
ϵ_e = Equivalent emissivity [-]
a, b_l = Coefficients for equivalent emissivity distribution [-]
w_e = Effective (scaled) zenith path water vapor content of atmosphere [kgm^{-2}]
ϵ_{sky} = Effective atmospheric emissivity [-]
Ω_l = Anisotropy factor for atmospheric emittance [-]
M_w = Relative path length for water vapor [-]
μ' = Integration variable [-]

APPENDIX E.

DEVELOPED SOFTWARE

E.1. Microsoft QuickBASIC Computer Program FACTORS

```
'*********************************************************************
'* program:   conversion FACTORS                                     *
'* objective: computing sky view factor (Vd) and terrain             *
'*            configuration factor (Vt) for infinitely long V-       *
'*            shaped valley as functions of different radiance       *
'*            distributions (anisotropy factors Omega) and site      *
'*            elevations above valley floor                          *
'* interface: parameters defined in program;                         *
'*            output to terminal screen                              *
'* author:    Remko Uijlenhoet                                       *
'* date:      August 2, 1989                                         *
'*********************************************************************
'BEGIN FACTORS

'* definitions and declarations *

CONST pi# = 3.141592654# '* pi [-]                                   *
CONST rad = pi / 180     '* radians per degree [rad/deg]             *
CONST A = 0 * rad        '* slope azimuth [rad]                      *
CONST Dsite = 0          '* horizontal distance from site to         *
                         '*   slope base [m]                         *
CONST S = 60 * rad       '* slope inclination [rad]                  *
CONST S2 = 60 * rad      '* inclination of facing slope [rad]        *
CONST Yridge = 100       '* ridge top elevation [m]                  *
CONST Yridge2 = 100      '* elevation of facing ridge top [m]        *
CONST stepphi0 = pi / 18 '* initial azimuthal integration            *
                         '*   increment [rad]                        *
CONST stepZ0 = pi / 18   '* initial zenith integration increment     *
                         '*   [rad]                                  *
CONST stepY0 = 100       '* initial increment of site elevation      *
                         '*   [m]                                    *
CONST startphi = 0       '* azimuth at start of integration [rad]    *
CONST stopphi = 2 * pi   '* azimuth at end of integration [rad]      *
CONST startZ = 0         '* zenith at start of integration [rad]     *
CONST startY = 0         '* lowest site elevation [m]                *
CONST stopY = Yridge     '* heighest site elvation [m]               *
COMMON SHARED Y          '* site elevation [m]                       *

DECLARE FUNCTION ARCTAN (x1, x2)
DECLARE FUNCTION HfunctionA (phi)
DECLARE FUNCTION HfunctionB (phi)
DECLARE FUNCTION Omegak (Z, phi, mc)
DECLARE FUNCTION Omegal (Z, phi, mc)
DECLARE FUNCTION PSIfunction (phi)
DECLARE FUNCTION reduce (angle, interval)
DECLARE FUNCTION simpson (stepno%, stepmax%)
```

```
'* main program *

CLS
PRINT "   Y       VdHm      Vdiso       Vdko       Vdkc       Vdlo     ";
PRINT "  Vdlc          Vt"
PRINT " [m]        [-]        [-]        [-]        [-]        [-]     ";
PRINT "   [-]         [-]"
PRINT "-------------------------------------------------------------";
PRINT "----------------"
stepphimax% = 2 * CINT((stopphi - startphi) / (2 * stepphi0))
stepphi = (stopphi - startphi) / stepphimax%
IF stopY > startY THEN
   stepYmax% = CINT((stopY - startY) / stepY0)
   stepY = (stopY - startY) / stepYmax%
ELSE
   stepYmax% = 0
END IF
Y = startY

'* (1) compute conversion factors for all site elevations (Y)      *
'*     from startY to stopY with increment stepY                    *

FOR stepYno% = 0 TO stepYmax%
   Hmean = 0
   Vdiso = 0: Vdko = 0: Vdkc = 0: Vdlo = 0: Vdlc = 0
   Vt = 0
   phi = startphi

   '* (1.1) perform integration over all azimuth angles (phi)      *
   '*       from startphi to stopphi with increment stepphi        *

   FOR stepphino% = 0 TO stepphimax%
      deltaphi = simpson(stepphino%, stepphimax%)
      deltaphi = deltaphi * stepphi / (2 * pi)
      H = HfunctionB(phi)
      Hmean = Hmean + deltaphi * H
      PSI = PSIfunction(phi)
      IF Y >= Yridge THEN
         slope = 0
      ELSE
         slope = S
      END IF
      factorA = TAN(slope) * COS(phi - A)
      termVdA = SIN(H) ^ 2
      termVdB = H - SIN(H) * COS(H)
      termVtA = SIN(PSI) ^ 2 - termVdA
      termVtB = PSI - SIN(PSI) * COS(PSI) - termVdB
      intphiVdiso = termVdA + factorA * termVdB
      intphiVt = termVtA + factorA * termVtB
      Vdiso = Vdiso + deltaphi * COS(slope) * intphiVdiso
      Vt = Vt + deltaphi * COS(slope) * intphiVt
      stopZ = H
      IF stopZ - startZ > 0 THEN
         IF stopZ - startZ < stepZ0 THEN
            stepZ = (stopZ - startZ) / 2
         ELSE
            stepZ = stepZ0
         END IF
         stepZmax% = 2 * CINT((stopZ - startZ) / (2 * stepZ))
         stepZ = (stopZ - startZ) / stepZmax%
         intphiVdko = 0: intphiVdkc = 0
         intphiVdlo = 0: intphiVdlc = 0
         Z = startZ
```

```
         '* (1.1.1) perform integration over all zenith angles    *
         '*         (Z) from startZ to stopZ with increment stepZ *

         FOR stepZno% = 0 TO stepZmax%
            deltaZ = simpson(stepZno%, stepZmax%) * stepZ
            factorB = SIN(2 * Z) + factorA * (1 - COS(2 * Z))
            intZVdko = Omegak(Z, phi, 0) * factorB
            intZVdkc = Omegak(Z, phi, 1) * factorB
            intZVdlo = Omegal(Z, phi, 0) * factorB
            intZVdlc = Omegal(Z, phi, 1) * factorB
            intphiVdko = intphiVdko + deltaZ * intZVdko
            intphiVdkc = intphiVdkc + deltaZ * intZVdkc
            intphiVdlo = intphiVdlo + deltaZ * intZVdlo
            intphiVdlc = intphiVdlc + deltaZ * intZVdlc
            Z = Z + stepZ
         NEXT stepZno%
         Vdko = Vdko + deltaphi * COS(slope) * intphiVdko
         Vdkc = Vdkc + deltaphi * COS(slope) * intphiVdkc
         Vdlo = Vdlo + deltaphi * COS(slope) * intphiVdlo
         Vdlc = Vdlc + deltaphi * COS(slope) * intphiVdlc
      END IF
      phi = phi + stepphi
   NEXT stepphino%
   VdHm = SIN(Hmean) ^ 2
   PRINT USING " ### "; Y;
   PRINT USING " #.###### "; VdHm; Vdiso; Vdko; Vdkc; Vdlo;
   PRINT USING " #.###### "; Vdlc; Vt
   Y = Y + stepY
NEXT stepYno%
Vdinfinite = COS((S + S2) / 2) ^ 2
Vtinfinite = 1 - Vdinfinite
PRINT "------------------------------------------------------------";
PRINT "----------------"
PRINT "   Vdinfinite [-]: ";
PRINT USING " #.###### "; Vdinfinite
PRINT "   Vtinfinite [-]: ";
PRINT USING " #.###### "; Vtinfinite
IF S2 = 0 THEN
   dummyA = COS(S / 2) ^ 2
   dummyB = SIN(S) - S * COS(S) - pi * SIN(S / 2) ^ 2
   VdkoSOC = dummyA + 2 * bko * dummyB / ((2 * bko + 3) * pi)
   VdkcSOC = dummyA + 2 * bkc * dummyB / ((2 * bkc + 3) * pi)
   PRINT "   VdkoSOC [-]:    ";
   PRINT USING " #.###### "; VdkoSOC
   PRINT "   VdkcSOC [-]:    ";
   PRINT USING " #.###### "; VdkcSOC
END IF
END'FACTORS
```

```
'*********************************************************************
'* function:  ARCTANgent                                             *
'* objective: computing arctangent of quotient of x1 and x2;         *
'*            resulting value between -pi/2 and pi/2                 *
'*********************************************************************
FUNCTION ARCTAN (x1, x2)
IF x2 = 0 THEN
   ARCTAN = SGN(x1) * pi / 2
ELSE
   ARCTAN = ATN(x1 / x2)
END IF
END FUNCTION'ARCTAN

'*********************************************************************
'* function:  HfunctionA, horizon function A                         *
'* objective: computing zenith angle of local horizon of             *
'*            infinitely long slope in V-shaped valley as            *
'*            function of azimuth (phi), surface azimuth (A) and     *
'*            inclinations of facing slopes (S, S2)                  *
'*********************************************************************
FUNCTION HfunctionA (phi)
IF COS(phi - A) <= 0 THEN
   Hfunction = ARCTAN(-1, TAN(S) * COS(phi - A))
ELSE
   Hfunction = ARCTAN(1, TAN(S2) * COS(phi - A))
END IF
HfunctionA = reduce(Hfunction, pi)
END FUNCTION'HfunctionA

'*********************************************************************
'* function:  HfunctionB, horizon function B                         *
'* objective: computing zenith angle of local horizon of point at    *
'*            slope in V-shaped valley as function of azimuth        *
'*            (phi), surface azimuth (A) and inclination (S),        *
'*            site elevation (Y), ridge top elevations of facing     *
'*            slopes (Yridge, Yridge2) and HfunctionA                *
'*********************************************************************
FUNCTION HfunctionB (phi)
Ha = HfunctionA(phi)
phi2 = reduce(phi + pi, 2 * pi)
Ha2 = HfunctionA(phi2)
IF COS(phi - A) <= 0 THEN
   IF Y >= Yridge THEN
      HfunctionB = pi / 2
   ELSE
      HfunctionB = Ha
   END IF
ELSE
   IF Y >= Yridge2 THEN
      HfunctionB = pi / 2
   ELSEIF S = 0 THEN
      dummyA = Dsite / (Yridge2 * COS(phi - A))
      HfunctionB = ATN(TAN(Ha) + dummyA)
   ELSE
      dummyA = Yridge2 / (Yridge2 - Y)
      dummyB = Y / (Yridge2 - Y)
      HfunctionB = ATN(dummyA * TAN(Ha) + dummyB * TAN(Ha2))
   END IF
END IF
END FUNCTION'HfunctionB
```

```
'*****************************************************************
'* function:  Omegak                                             *
'* objective: defining anisotropy factor for background solar sky *
'*            radiance as function of zenith (Z), azimuth (phi),  *
'*            fractional cloudcover (mc) and surface albedo       *
'*            (albedo)                                            *
'*****************************************************************
FUNCTION Omegak (Z, phi, mc)
SHARED bko, bkc
CONST albedo = .17
bko = -.87
bkc = 2 * (1 - albedo) / (1 + 2 * albedo)
mu = COS(Z)
Omegako = (1 + bko * mu) / (1 + bko * 2 / 3)
Omegakc = (1 + bkc * mu) / (1 + bkc * 2 / 3)
Omegak = (1 - mc) * Omegako + mc * Omegakc
END FUNCTION'Omegak

'*****************************************************************
'* function:  Omegal                                             *
'* objective: defining anisotropy factor for atmospheric         *
'*            emittance as function of zenith (Z), azimuth (phi), *
'*            fractional cloudcover (mc) and clear sky effective  *
'*            atmospheric emissivity (eskyo)                      *
'*****************************************************************
FUNCTION Omegal (Z, phi, mc)
CONST Mw0 = 75, kl = .22, eskyo = .7
esky = (1 + kl * mc * mc) * eskyo
bl = (1 - esky) / (LOG(Mw0) - .5)
mu = COS(Z)
Mw = Mw0 / SQR((Mw0 ^ 2 - 1) * mu ^ 2 + 1)
Omegal = 1 - bl * (.5 - LOG(Mw)) / esky
END FUNCTION'Omegal

'*****************************************************************
'* function:  PSIfunction                                        *
'* objective: computing zenith angle of sunray parallel to slope *
'*            in V-shaped valley as function of azimuth (phi),    *
'*            surface azimuth (A) and inclination (S), site       *
'*            elevation (Y), ridge top elevation of facing slope  *
'*            (Yridge2) and HfunctionB                            *
'*****************************************************************
FUNCTION PSIfunction (phi)
Hb = HfunctionB(phi)
IF COS(phi - aspect) <= 0 THEN
   PSIfunction = Hb
ELSE
   IF Y >= Yridge THEN
      PSIfunction = pi / 2
   ELSE
      dummyA = ARCTAN(-1, TAN(S) * COS(phi - A))
      PSIfunction = reduce(dummyA, pi)
   END IF
END IF
END FUNCTION'PSIfunction

'*****************************************************************
'* function:  reduce                                             *
'* objective: reducing value of angle to value between 0 and     *
'*            interval                                           *
'*****************************************************************
FUNCTION reduce (angle, interval)
modulus = INT(angle / interval)
reduce = angle - modulus * interval
END FUNCTION'reduce
```

```
'*********************************************************************
'* function:  simpson                                                *
'* objective: computing coefficients for numerical integration       *
'*            according to Simpson's 1/3 rule from number of         *
'*            integration steps already performed (stepno%) and      *
'*            total number of integration steps (stepmax%)           *
'*********************************************************************
FUNCTION simpson (stepno%, stepmax%)
IF stepno% = 0 OR stepno% = stepmax% THEN
   simpson = 1 / 3
ELSEIF 2 * INT(stepno% / 2) <> stepno% THEN
   simpson = 4 / 3
ELSE
   simpson = 2 / 3
END IF
END FUNCTION'simpson
```

E.2. Microsoft QuickBASIC Computer Program RBM

```
'*********************************************************************
'* program:   RBM, Radiation Budget Module                           *
'* objective: computing diurnal variation in radiation balance       *
'*            of obstructed point at inclined surface                *
'* interface: input from data-file RBMIN.DAT on current directory;*
'*            remaining parameters defined in main module;           *
'*            output to data-file RBMOUT.DAT on current directory    *
'*            and/or to terminal screen                              *
'* author:    Remko Uijlenhoet                                       *
'* date:      July 7, 1989                                           *
'*********************************************************************
'BEGIN RBM

'* parameter definitions *

CONST pi# = 3.141592654#       '* pi [-]                              *
CONST rad# = pi / 180          '* radians per degree [rad/deg]        *
CONST deg# = 2 * pi / 1440     '* radians per minute [rad/min]        *
CONST month = 4, day = 10, year = 1989
                               '* date of measurements [m;d;y]        *
CONST lat = 33.075 * rad       '* site latitude [rad N]               *
CONST lon = 111.983 * rad      '* site longitude [rad W]              *
CONST aspect = 0 * rad         '* slope azimuth angle [rad]           *
CONST slope = 0 * rad          '* slope inclination angle [rad]       *
CONST hsite = 358              '* site altitude [m]                   *
CONST a = .1                   '* average surface albedo [-]          *
CONST atrn = a                 '* average terrain albedo [-]          *
CONST e = .95                  '* average surface emissivity [-]      *
CONST etrn = e                 '* average terrain emissivity [-]      *
CONST mc = 0                   '* mean fractional cloudcover [-]      *
CONST askyo = .1               '* effective clear sky albedo [-]      *
CONST askyc = .5               '* effective overcast sky albedo [-]   *
CONST asky = (1 - mc) * askyo + mc * askyc
                               '* effective sky albedo [-]            *
CONST kl = .22                 '* longwave cloudcover correction      *
                               '*   coefficient [-]                   *
CONST cloudlw = 1 + kl * mc * mc '* longwave cloudcover               *
                               '*   correction [-]                    *
CONST ksa = .39, ksb = .38     '* shortwave cloudcover correction     *
CONST ks = ksa + ksb * mc      '*   coefficients [-]                  *
CONST cloudsw = 1 - ks * mc    '* shortwave cloudcover correction     *
                               '*   [-]                               *
CONST Aoc = .02                '* average absorptivity of ozone [-]   *
CONST Awc = .07                '* average absorptivity of water       *
                               '*   vapor [-]                         *
CONST trans = .75              '* average zenith path atmospheric     *
                               '*   transmissivity [-]                *
CONST dt = 20                  '* simulation time step [min]          *
CONST dH = deg * dt            '* angular equivalent of dt [rad]      *
CONST length% = 1000           '* array length [-]                    *
CONST muHrise# = -.014539      '* cosine of solar zenith angle at     *
                               '*   apparent sunrise [-]              *
CONST accuracy = .01           '* iteration accuracy [%]              *
CONST countmax = 100           '* maximum number of iterations [-]    *
CONST g = 9.81                 '* gravitational acceleration [m/s2]   *
CONST kelvin = 273.15          '* freezing temperature of water [K]   *
CONST kw = .00044              '* water vapor density decay           *
                               '*   coefficient [/m]                  *
CONST lapse = .0065            '* lapse rate [K/m]                    *
CONST Rd = 287.04              '* gas constant of dry air [J/kg/K]    *
CONST sigma = 5.6697E-08       '* Stefan-Boltzmann's constant         *
                               '*   [W/m2/K4]                         *
CONST S0 = 1365                '* solar constant [W/m2]               *
```

```
'* array declarations *

OPTION BASE 1
DIM dummyA(length), dummyB(length), dummyC(length), dummyD(length)
DIM dummyE(length), dummyF(length), dummyG(length), dummyH(length)
DIM dummyI(length), dummyJ(length), dummyK(length), dummyL(length)
                              '* dummy variables [?]                  *
DIM Hm(length)                '* hour angle at measurement [rad]      *
                              '* measurements:                        *
DIM Ktotm(length)             '*   global radiation [W/m2]            *
DIM Rnm(length)               '*   net radiation [W/m2]               *
DIM Ta(length)                '*   air temperature [K]                *
DIM Ts(length)                '*   soil temperature 1 [K]             *
DIM TsB(length)               '*   soil temperature 2 [K]             *
DIM Tc(length)                '*   canopy temperature [K]             *
DIM ea(length)                '*   vapor pressure [Pa]                *
                              '* corrections:                         *
DIM KtotmB(length)            '*   corrected global radiation         *
                              '*   [W/m2]                             *
DIM RnmB(length)              '*   corrected net radiation [W/m2]     *
DIM TcB(length)               '*   corrected canopy temperature [K]*
                              '* simulations [W/m2]:                  *
DIM Ko(length)                '*   extraterrestrial radiation         *
DIM Kdir(length)              '*   direct insolation                  *
DIM Kdif(length)              '*   diffuse sky radiation              *
DIM Ksct(length)              '*   radiation scattered downward       *
                              '*     from direct beam                 *
DIM Kbck(length)              '*   backscatter from atmosphere        *
DIM Ktrn(length)              '*   reflection from adjacent terrain*
DIM Ktot(length)              '*   global radiation                   *
DIM Kn(length)                '*   net shortwave radiation            *
DIM Lsky(length)              '*   emission from atmosphere           *
DIM Ltrn(length)              '*   emission from adjacent terrain     *
DIM Lsfc(length)              '*   surface emission                   *
DIM Rn(length)                '*   net radiation                      *
DIM asfc(length)              '*   instantaneous surface albedo [-]*

'* common area declarations *

COMMON SHARED anom AS DOUBLE  '* true anomaly [rad]                   *
COMMON SHARED clon AS DOUBLE  '* true celestial longitude [rad]       *
COMMON SHARED cor AS DOUBLE   '* time correction [d]                  *
COMMON SHARED dclon AS DOUBLE'* difference between true and mean     *
                              '*   celestial longitude [rad]         *
COMMON SHARED dec             '* declination [rad]                    *
COMMON SHARED jday AS DOUBLE  '* Julian day number [d]               *
COMMON SHARED jdayreduced AS DOUBLE '* reduced Julian day number     *
                              '*   [d]                               *
COMMON SHARED manom AS DOUBLE'* mean anomaly [rad]                   *
COMMON SHARED mclon AS DOUBLE'* mean celestial longitude [rad]       *
COMMON SHARED rv              '* earth's radius vector [-]           *
COMMON SHARED storeA, storeB  '* storage variables [-]               *
```

```
'* function and subroutine declarations *

DECLARE FUNCTION albedo (Z, Tk, choice)
DECLARE FUNCTION Ao (Z, D)
DECLARE FUNCTION ARCCOS (x, y)
DECLARE FUNCTION ARCSIN (x, y)
DECLARE FUNCTION ARCTAN (x, y)
DECLARE FUNCTION Aw (Z, ea, Ta)
DECLARE FUNCTION coefficient (Kt)
DECLARE FUNCTION horizon (phi)
DECLARE FUNCTION julianday (month, day, year)
DECLARE FUNCTION LOG10 (x)
DECLARE FUNCTION reduce (angle, interval)
DECLARE SUB average (inarray(), outarray(), ibegin, iend,
  sublength)
DECLARE SUB factors (mc, VdK, Vdl, Vtrn)
DECLARE SUB position (jday AS DOUBLE, dec, rv, eq)
DECLARE SUB localriseset (Hlocal, azlocal, altlocal, Hguess)
DECLARE SUB statistics (Carray(), Marray(), MBE, RMSE, NASH,
  ibegin, iend)
DECLARE SUB time (angle, sign$, hour, min, sec)

'* main program *

'* (1) Input data from measurements-file "RBMIN.DAT" *

OPEN "RBMIN.DAT" FOR INPUT AS #1
t% = 1
DO UNTIL EOF(1)
   INPUT #1, Hm(t%), Ktotm(t%), KtotmB(t%), Rnm(t%), RnmB(t%), Ta(t%), Ts(t%),
TsB(t%), Tc(t%), TcB(t%), ea(t%)
   t% = t% + 1
LOOP
CLOSE #1
Hstart = Hm(1) * rad + dH / 2
tmax = t% - 1
dtin = (Hm(tmax) - Hm(1)) * rad / ((tmax - 1) * deg)
IF dtin < dt THEN
   FOR t% = 1 TO tmax
      dummyA(t%) = Ktotm(t%)
      dummyB(t%) = KtotmB(t%)
      dummyC(t%) = Rnm(t%)
      dummyD(t%) = RnmB(t%)
      dummyE(t%) = Ta(t%)
      dummyF(t%) = Ts(t%)
      dummyG(t%) = TsB(t%)
      dummyH(t%) = Tc(t%)
      dummyI(t%) = TcB(t%)
      dummyJ(t%) = ea(t%)
   NEXT t%
   sublength = CINT(dt / dtin)
   nmax = INT(tmax / sublength)
   ibegin = 1: iend = sublength * nmax
   'iend = tmax: ibegin = iend - sublength * nmax + 1
   Hstart = Hm(ibegin) * rad + dH / 2
   CALL average(dummyA(), Ktotm(), ibegin, iend, sublength)
   CALL average(dummyB(), KtotmB(), ibegin, iend, sublength)
   CALL average(dummyC(), Rnm(), ibegin, iend, sublength)
   CALL average(dummyD(), RnmB(), ibegin, iend, sublength)
   CALL average(dummyE(), Ta(), ibegin, iend, sublength)
   CALL average(dummyF(), Ts(), ibegin, iend, sublength)
   CALL average(dummyG(), TsB(), ibegin, iend, sublength)
   CALL average(dummyH(), Tc(), ibegin, iend, sublength)
   CALL average(dummyI(), TcB(), ibegin, iend, sublength)
   CALL average(dummyJ(), ea(), ibegin, iend, sublength)
END IF
```

```
'* (2) diurnal variation in instantaneous radiation                *
'*     characteristics for dt minute intervals, starting when     *
'*     hour angle equals Hstart                                   *

jday = julianday(month, day, year)
jday0 = julianday(1, 1, year)
D = jday - jday0 + 1
CALL position(jday, dec, rv, eq)
CALL factors(mc, VdK, Vdl, Vtrn)
storeA = SIN(lat) * SIN(dec)
storeB = COS(lat) * COS(dec)
dummyA = SIN(slope) * COS(aspect)
dummyB = SIN(slope) * SIN(aspect)
storeC = storeA * COS(slope) + COS(lat) * SIN(dec) * dummyA
storeD = storeB * COS(slope) - SIN(lat) * COS(dec) * dummyA
storeE = -COS(dec) * dummyB
H0 = ARCCOS(-storeA, storeB)
Hrise = -ARCCOS(muHrise - storeA, storeB)
H = Hstart
FOR n% = 1 TO nmax

   '* (2.1) instantaneous shortwave radiation characteristics     *

   IF H0 > 0 THEN
      mu = storeA + storeB * COS(H)
      dummyA = H0 * storeA + storeB * SIN(H0)
      Kotot = S0 * dummyA / (pi * rv ^ 2)
      IF mu > 0 THEN

         '* (2.1.1) direct solar radiation                         *

         Z = ARCCOS(mu, 1)
         refraction = .15 * (93.885 - Z / rad) ^ -1.253
         airmass0 = 1 / (mu + refraction)
         Prel = (1 + lapse * hsite / Ta(n%)) ^ (-g / (lapse * Rd))
         airmass = Prel * airmass0
         Ko(n%) = (S0 / rv ^ 2) * mu
         Kdir(n%) = Ko(n%) * trans ^ airmass
         dummyA = mu * SIN(lat) - SIN(dec)
         dummyB = SIN(Z) * COS(lat)
         az = pi + SGN(H) * ARCCOS(dummyA, dummyB)
         IF Z < horizon(az) THEN
            boolean = 1
            IF Kdir(n% - 1) = 0 THEN
               nrise = n%
               Hguess = H - dH / 2
               CALL localriseset(Hlocal, azlocal, altlocal, Hguess)
               Hriselocal = Hlocal
               azriselocal = azlocal
               altriselocal = altlocal
            END IF
         ELSE
            boolean = 0
            IF Kdir(n% - 1) > 0 THEN
               nset = n%
               Hguess = H - dH / 2
               CALL localriseset(Hlocal, azlocal, altlocal, Hguess)
               Hsetlocal = Hlocal
               azsetlocal = azlocal
               altsetlocal = altlocal
            END IF
         END IF
         'dummyA = COS(slope) * mu
         'mus = dummyA + SIN(slope) * SIN(Z) * COS(az - aspect)
         mus = storeC + storeD * COS(H) + storeE * SIN(H)
         Vdir = boolean * mus / mu
         Kdir(n%) = Vdir * Kdir(n%)
```

```
        '* (2.1.2) diffuse sky radiation and global radiation    *

        Cz = .5 * mu ^ (1 / 3)
        Cs = 1 + mu ^ 2 * SIN(Z) ^ 3
        'dummyA = (1 - Awc - Awo) * Ko(n%)
        dummyA = (1 - Aw(Z, ea(n%), Ta(n%)) - Ao(Z, D)) * Ko(n%)
        Ksct(n%) = Cz * Cs * (dummyA - Kdir(n%))
        Kbck(n%) = (Kdir(n%) + Ksct(n%)) / (1/(atrn * askyo) - 1)
        Kdif(n%) = Ksct(n%) + Kbck(n%)
        Ktot(n%) = Kdir(n%) + Kdif(n%)
        Tk = Kdif(n%) / Ktot(n%)
        IF mc > 0 THEN
           Ktot(n%) = cloudsw * Ktot(n%)
           Kt = Ktot(n%) / Ko(n%)
           Tk = coefficient(Kt)
           Kdif(n%) = Tk * Ktot(n%)
           Kdir(n%) = Ktot(n%) - Kdif(n%)
           Kbck(n%) = atrn * asky * Ktot(n%)
           Ksct(n%) = Kdif(n%) - Kbck(n%)
        END IF
        F = 1 - Tk ^ 2
        Cs = 1 + F * mu ^ 2 * SIN(Z) ^ 3
        Css = 1 + boolean * F * mus ^ 2 * SIN(Z) ^ 3
        Ksct(n%) = VdK * (Css / Cs) * Ksct(n%)
        Kbck(n%) = VdK * Kbck(n%)
        Kdif(n%) = Ksct(n%) + Kbck(n%)
        Ktrn(n%) = Vtrn * atrn * Ktot(n%)
        Ktot(n%) = Kdir(n%) + Kdif(n%) + Ktrn(n%)
        asfc(n%) = albedo(Z, Tk, 1)
        Kn(n%) = (1 - asfc(n%)) * Ktot(n%)
     END IF
  ELSEIF H0 <= 0 OR mu <= 0 THEN
     Ko(n%) = 0: Kdir(n%) = 0: Kdif(n%) = 0: Ksct(n%) = 0
     Kbck(n%) = 0: Ktrn(n%) = 0: Ktot(n%) = 0: Kn(n%) = 0
  END IF

  '* (2.2) instantaneous longwave radiation and net radiation    *
  '*       characteristics                                       *

  'esky = .00000939# * Ta(n%) ^ 2
  'esky = 1 - .261 * EXP(-.000777 * (273 - Ta(n%)) ^ 2)
  'esky = .642 * (ea(n%) / Ta(n%)) ^ (1 / 7)
  esky = 1.08 * (1 - EXP(-(ea(n%) / 100) ^ (Ta(n%) / 2016)))
  'esky = .7 + .000000595# * ea(n%) * EXP(1500 / Ta(n%))
  Lsky(n%) = Vdl * cloudlw * esky * sigma * Ta(n%) ^ 4
  Lsfc(n%) = e * sigma * TcB(n%) ^ 4
  Ltrn(n%) = Vtrn * etrn * sigma * TcB(n%) ^ 4
  Ln = e * (Lsky(n%) + Ltrn(n%)) - Lsfc(n%)
  Rn(n%) = Kn(n%) + Ln
  IF H <= 0 AND H + dH > 0 THEN
     nnoon = n%
  END IF
  H = H + dH
NEXT n%
```

```
'* (3) assessment of model performance                                  *

CALL statistics(Ktot(), Ktotm(), MBE1, RMSE1, NASH1, nrise, nmax)
CALL statistics(Ktot(), KtotmB(), MBE2, RMSE2, NASH2, nrise, nmax)
CALL statistics(Rn(), Rnm(), MBE3, RMSE3, NASH3, 1, nmax)
CALL statistics(Rn(), RnmB(), MBE4, RMSE4, NASH4, 1, nmax)
CALL average(Ko(), dummyA(), 1, nnoon, nnoon)
CALL average(Ktot(), dummyB(), 1, nnoon, nnoon)
CALL average(Kdir(), dummyC(), 1, nnoon, nnoon)
CALL average(Kdif(), dummyD(), 1, nnoon, nnoon)
CALL average(Ksct(), dummyE(), 1, nnoon, nnoon)
CALL average(Kbck(), dummyF(), 1, nnoon, nnoon)
CALL average(Ktrn(), dummyG(), 1, nnoon, nnoon)
CALL average(Kn(), dummyH(), 1, nnoon, nnoon)
CALL average(Lsky(), dummyI(), 1, nnoon, nnoon)
CALL average(Ltrn(), dummyJ(), 1, nnoon, nnoon)
CALL average(Lsfc(), dummyK(), 1, nnoon, nnoon)
CALL average(Rn(), dummyL(), 1, nnoon, nnoon)

'* (4) resulting data to output-file "RBMOUT.DAT" on current       *
'*     directory and/or to terminal screen                          *

CLS
PRINT "simulation results:"
PRINT
PRINT "day number of year [-]:              ";
PRINT USING " #### "; D
PRINT "solar declination [deg]:             ";
PRINT USING " ####.#### "; dec / rad
PRINT "earth's radius vector [-]:           ";
PRINT USING " ####.#### "; rv
CALL time(eq / rad, sign$, hour, min, sec)
PRINT "equation of time [hr;min;sec]:       ";
PRINT sign$; hour; min; sec
PRINT "extraterrestrial radiation [W/m2]:   ";
PRINT USING " ####.#### "; Kotot
PRINT "hour angle at sunrise [deg]:         ";
PRINT USING " ####.#### "; Hrise / rad
PRINT "half day length [deg]:               ";
PRINT USING " ####.#### "; H0 / rad
PRINT "start of simulation [deg]:           ";
PRINT USING " ####.#### "; Hstart / rad
PRINT "number of input time steps [-]:      ";
PRINT USING " #### "; tmax
PRINT "input time step [min]:               ";
PRINT USING " ####.#### "; dtin
PRINT "number of simulated time steps [-]: ";
PRINT USING " #### "; nmax
PRINT "time step number at sunrise [-]:     ";
PRINT USING " #### "; nrise
PRINT "time step number at solar noon [-]: ";
PRINT USING " #### "; nnoon
PRINT
PRINT "Press any key to continue"
DO
   keystroke$ = INKEY$
LOOP UNTIL LEN(keystroke$) <> 0
```

```
CLS
PRINT "simulated daily average radiation budget [W/m2]:"
PRINT
PRINT "Ko:        "; : PRINT USING " ####.## "; dummyA(1)
PRINT "Ktot:      "; : PRINT USING " ####.## "; dummyB(1)
PRINT "  Kdir:    "; : PRINT USING " ####.## "; dummyC(1)
PRINT "  Kdif:    "; : PRINT USING " ####.## "; dummyD(1)
PRINT "    Ksct:  "; : PRINT USING " ####.## "; dummyE(1)
PRINT "    Kbck:  "; : PRINT USING " ####.## "; dummyF(1)
PRINT "  Ktrn:    "; : PRINT USING " ####.## "; dummyG(1)
asfc = 1 - dummyH(1) / dummyB(1)
PRINT "asfc [-]: "; : PRINT USING " ####.## "; asfc
PRINT "Lsky:      "; : PRINT USING " ####.## "; dummyI(1)
PRINT "Ltrn:      "; : PRINT USING " ####.## "; dummyJ(1)
PRINT "Lsfc:      "; : PRINT USING " ####.## "; dummyK(1)
PRINT "Rn:        "; : PRINT USING " ####.## "; dummyL(1)
PRINT
PRINT "assessment of model performance:"
PRINT
PRINT "                    MBE [%]  RMSE [%] NASH [%]"
PRINT
PRINT "Ktot vs. Ktotm:  "; : PRINT USING " ###.### "; MBE1; RMSE1; NASH1
PRINT "Ktot vs. KtotmB: "; : PRINT USING " ###.### "; MBE2; RMSE2; NASH2
PRINT "Rn   vs. Rnm:    "; : PRINT USING " ###.### "; MBE3; RMSE3; NASH3
PRINT "Rn   vs. RnmB:   "; : PRINT USING " ###.### "; MBE4; RMSE4;
  NASH4
OPEN "RBMOUT.DAT" FOR OUTPUT AS #2
H = Hstart
FOR n% = 1 TO nmax
   PRINT #2, USING "####.##"; H / rad; Ta(n%); TcB(n%); ea(n%); Ko(n%);
                              Ktot(n%); Ktotm(n%); Rn(n%); RnmB(n%)
   H = H + dH
NEXT n%
CLOSE #2
END' RBM
```

```
'*********************************************************************
'* subroutine: albedo                                                *
'* objective:  computing albedo of wheat field as function of        *
'*             solar zenith angle (Z), ratio of diffuse to global    *
'*             radiation (Tk) and albedo with sun in zenith          *
'*             (albedo0)                                             *
'*********************************************************************
FUNCTION albedo (Z, Tk, choice)
CONST Cd = .8
albedo0 = a
IF choice = 1 THEN
   factor = 1 + 2.5 * (1.25 - Tk) * (1 - albedo0) * SIN(1.5 * Z)
ELSEIF choice = 2 THEN
   mu = COS(Z)
   factor = (1 + Cd) / (1 + Cd * mu)
ELSE
   factor = 1
END IF
albedo = albedo0 * factor
END FUNCTION'albedo

'*********************************************************************
'* function:  Ao, ozone absorptivity                                 *
'* objective: computing absorptivity of ozone as function of         *
'*            solar zenith angle (Z), day number of year (D) and     *
'*            latitude (lat) and longitude (lon) of site             *
'*********************************************************************
FUNCTION Ao (Z, D)
Mo = 35 / SQR(1224 * COS(Z) ^ 2 + 1)
IF lat > 0 THEN
   c1 = .15: c2 = .04: c3 = -30: c4 = 3: c6 = 1.28
   IF lon < 0 THEN
      c5 = 20 * rad
   ELSE
      c5 = 0
   END IF
ELSE
   c1 = .1: c2 = .03: c3 = 152.625: c4 = 2: c5 = -75 * rad
   c6 = 1.5
END IF
dummyA = c1 + c2 * SIN(2 * pi * (D + c3) / 365.25)
dummyB = (dummyA - .02 * SIN(c4 * (lon + c5))) * SIN(c6 * lat) ^ 2
o = .235 + dummyB
'o = .31 + .1 * SIN(lat)
dummyC = 1 + .042 * Mo * o + .000323 * (Mo * o) ^ 2
Aovis = .02118 * Mo * o / dummyC
dummyD = 1.082 * Mo * o / (1 + 138.6 * Mo * o) ^ .805
Aouv = dummyD + .0658 * Mo * o / (1 + (103.6 * Mo * o) ^ 2)
Ao = Aovis + Aouv
END FUNCTION'Ao
```

```
'*********************************************************************
'* function:  ARCCOS, ARCCOSine                                      *
'* objective: computing arccosine of quotient of x and y;            *
'*            resulting value within interval 0 <= ARCCOS <= pi      *
'*********************************************************************
FUNCTION ARCCOS (x, y)
IF y = 0 THEN
   dummyA = SGN(x)
ELSE
   dummyA = x / y
   IF ABS(dummyA) > 1 THEN
      dummyA = SGN(dummyA)
   END IF
END IF
dummyB = ARCTAN(SQR(1 - dummyA ^ 2), dummyA)
IF dummyB < 0 OR dummyA = -1 THEN
   dummyB = dummyB + pi
END IF
   ARCCOS = dummyB
END FUNCTION'ARCCOS

'*********************************************************************
'* function:  ARCSIN, ARCSINe                                        *
'* objective: computing arcsine of quotient of x and y;              *
'*            resulting value within interval -pi / 2 <= ARCSIN      *
'*            <= pi / 2                                              *
'*********************************************************************
FUNCTION ARCSIN (x, y)
IF y = 0 THEN
   dummyA = SGN(x)
ELSE
   dummyA = x / y
   IF ABS(dummyA) > 1 THEN
      dummyA = SGN(dummyA)
   END IF
END IF
ARCSIN = ARCTAN(dummyA, SQR(1 - dummyA ^ 2))
END FUNCTION'ARCSIN

'*********************************************************************
'* function:  ARCTAN, ARCTANgent                                     *
'* objective: computing arctangent of quotient of x and y;           *
'*            resulting value within interval -pi / 2 <= ARCTAN      *
'*            <= pi / 2                                              *
'*********************************************************************
FUNCTION ARCTAN (x, y)
IF y = o THEN
   ARCTAN = SGN(x) * pi / 2
ELSE
   ARCTAN = ATN(x / y)
END IF
END FUNCTION'ARCTAN
```

```
'*********************************************************************
'* subroutine: average                                               *
'* objective:  computing averages (outarray) of all subsets with     *
'*             length sublength within element range ibegin until    *
'*             iend of given data set (inarray)                      *
'*********************************************************************
SUB average (inarray(), outarray(), ibegin, iend, sublength)
outlength = CINT((iend - ibegin + 1) / sublength)
FOR j% = 1 TO outlength
   outarray(j%) = 0
   istart = ibegin + (j% - 1) * sublength
   istop = ibegin - 1 + j% * sublength
   FOR i% = istart TO istop
      outarray(j%) = outarray(j%) + inarray(i%)
   NEXT i%
   outarray(j%) = outarray(j%) / sublength
NEXT j%
END SUB'average

'*********************************************************************
'* function:  Aw, water vapor absorptivity                           *
'* objective: computing absorptivity of water vapor as function      *
'*            of solar zenith angle (Z), vapor pressure (ea) and     *
'*            air temperature (Ta)                                   *
'*********************************************************************
FUNCTION Aw (Z, ea, Ta)
Mw = 1 / (COS(Z) + .0548 * (92.65 - Z / rad) ^ -1.452)
w = .622 * ea / (kw * Rd * Ta)
dummyA = .5149 * LOG10(Mw * w) - .0345 * (LOG10(Mw * w)) ^ 2
Aw = 10 ^ (-1.6754 + dummyA)
END FUNCTION'Aw

'*********************************************************************
'* function:  coefficient                                            *
'* objective: determining ratio of diffuse to global radiation       *
'*            from ratio of global to extraterrestrial radiation     *
'*            (Kt)                                                   *
'*********************************************************************
FUNCTION coefficient (Kt)
IF Kt <= .22 THEN
   coefficient = 1 - .09 * Kt
ELSEIF Kt <= .8 THEN
   dummyA = .9511 - .1604 * Kt + 4.388 * Kt ^ 2
   coefficient = dummyA - 16.638 * Kt ^ 3 + 12.336 * Kt ^ 4
ELSE
   coefficient = .165
END IF
END FUNCTION'coefficient

'*********************************************************************
'* subroutine: factors                                               *
'* objective:  computing sky view factors for background solar       *
'*             sky radiation (Vdk) and atmospheric emission (Vdl)    *
'*             and terrain configuration factor (Vtrn) as function*
'*             of local topography and fractional cloudcover (mc)    *
'*********************************************************************
SUB factors (mc, VdK, Vdl, Vtrn)
VdK = 1
Vdl = 1
Vtrn = 0
END SUB'factors
```

```
'*********************************************************************
'* function:  horizon                                                *
'* objective: computing zenith angle of local horizon as function *
'*            of local topography and azimuth (phi) relative to   *
'*            north                                               *
'*********************************************************************
FUNCTION horizon (phi)
horizon = pi / 2
END FUNCTION'horizon

'*********************************************************************
'* function:  julianday                                              *
'* objective: computing Julian day number from Gregorian calendar *
'*            date as defined by month, day and year number       *
'*********************************************************************
FUNCTION julianday (month, day, year)
dummyA = 367 * (year - 1980)
dummyA = dummyA - INT(7 * (year + INT((month + 9) / 12)) / 4)
dummyB = SGN(month - 9)
dummyC = ABS(month - 9)
dummyD = INT((year + dummyB * INT(dummyC / 7)) / 100)
dummyA = dummyA - INT(3 * (dummyD + 1) / 4)
dummyA = dummyA + INT(275 * month / 9) + day - .5
julianday = dummyA + 2447689
END FUNCTION'julianday

'*********************************************************************
'* subroutine: localriseset                                          *
'* objective:  computing hour angle (Hlocal), solar azimuth       *
'*             (azlocal), and solar altitude (altlocal) at local  *
'*             sun rise or set by means of iteration procedure    *
'*             with initial guess for hour angle (Hguess)         *
'*********************************************************************
SUB localriseset (Hlocal, azlocal, altlocal, Hguess)
muguess = storeA + storeB * COS(Hguess)
Zguess = ARCCOS(muguess, 1)
Zold = Zguess
improve = 2 * accuracy
count = 0
DO UNTIL improve <= accuracy OR count = countmax
   dummyA = COS(Zold) * SIN(lat) - SIN(dec)
   dummyB = SIN(Zold) * COS(lat)
   azlocal = pi + SGN(Hguess) * ARCCOS(dummyA, dummyB)
   Znew = (Zold + horizon(azlocal)) / 2
   Hlocal = SGN(Hguess) * ARCCOS(COS(Znew) - storeA, storeB)
   altlocal = pi / 2 - Znew
   improve = 100 * ABS(Znew / Zold - 1)
   Zold = Znew
   count = count + 1
LOOP
IF count = countmax THEN
   Hlocal = Hguess
   dummyA = muguess * SIN(lat) - SIN(dec)
   dummyB = SIN(Zguess) * COS(lat)
   azlocal = pi + SGN(Hguess) * ARCCOS(dummyA, dummyB)
   altlocal = pi / 2 - Zguess
END IF
END SUB'localriseset
```

```
'*************************************************************************
'* function:  LOG10                                                      *
'* objective: computing decimal logarithm of x                           *
'*************************************************************************
FUNCTION LOG10 (x)
IF x > 0 THEN
   LOG10 = LOG(x) / LOG(10)
END IF
END FUNCTION'LOG10

'*************************************************************************
'* subroutine: position, solar position                                  *
'* objective:  computing solar position at local noon                    *
'*             from Julian day number (jday): declination (dec),         *
'*             radius vector (rv) and equation of time (eq)              *
'*************************************************************************
SUB position (jday AS DOUBLE, dec, rv, eq)
CONST parA# = 6.23471229#, parB# = .01720197#, parC# = 4.88376619#
CONST parD# = .017202791#, parE# = .016728, parF# = .409095
jdayreduced = jday - 2444239 + lon / (2 * pi)
cor = 2.2E-08 * jdayreduced + .00059
jdayreduced = jdayreduced + cor
manom = parA + parB * jdayreduced
mclon = parC + parD * jdayreduced
mclon = mclon - 2 * pi * INT(mclon / (2 * pi))
dclon = 2 * parE * SIN(manom) + 1.25 * parE ^ 2 * SIN(2 * manom)
anom = manom + dclon
clon = mclon + dclon
rv = (1 - parE ^ 2) / (1 + parE * COS(anom))
dec = ARCSIN(SIN(clon) * SIN(parF), 1)
mclon = mclon - pi * INT(mclon / pi)
asce = ARCTAN(SIN(clon) * COS(parF), COS(clon))
asce = reduce(asce, pi)
eq = mclon - asce
END SUB'position

'*************************************************************************
'* function:  reduce                                                     *
'* objective: reducing value of angle to interval 0 <= angle <=          *
'*            interval                                                   *
'*************************************************************************
FUNCTION reduce (angle, interval)
MODULUS = INT(angle / interval)
reduce = angle - MODULUS * interval
END FUNCTION'reduce
```

```
'*********************************************************************
'* subroutine: statistics                                            *
'* objective:  computing mean bias error (MBE), root mean square     *
'*             error (RMSE) and coefficient of determination         *
'*             (NASH) of calculated data set (Carray) vs.            *
'*             measured data set (Marray) from element ibegin to     *
'*             element iend                                          *
'*********************************************************************
SUB statistics (Carray(), Marray(), MBE, RMSE, NASH, ibegin, iend)
DIM dummyA(1), dummyB(1), dummyC(1), dummyD(1)
DIM CminusMarray(length), CminusMarraySQR(length)
DIM MminusMarraySQR(length)
sublength = iend - ibegin + 1
CALL average(Marray(), dummyA(), ibegin, iend, sublength)
FOR i% = ibegin TO iend
   CminusMarray(i%) = Carray(i%) - Marray(i%)
   CminusMarraySQR(i%) = CminusMarray(i%) ^ 2
   MminusMarraySQR(i%) = (dummyA(1) - Marray(i%)) ^ 2
NEXT i%
CALL average(CminusMarray(), dummyB(), ibegin, iend, sublength)
MBE = 100 * dummyB(1) / ABS(dummyA(1))
CALL average(CminusMarraySQR(), dummyC(), ibegin, iend, sublength)
RMSE = 100 * SQR(dummyC(1)) / ABS(dummyA(1))
CALL average(MminusMarraySQR(), dummyD(), ibegin, iend, sublength)
NASH = 100 * (1 - dummyC(1) / dummyD(1))
END SUB'statistics

'*********************************************************************
'* subroutine: time                                                  *
'* objective:  converting angular time (angle, [deg]) to             *
'*             hours (hour), minutes (min) and seconds (sec)         *
'*********************************************************************
SUB time (angle, sign$, hour, min, sec)
IF angle < 0 THEN
   sign$ = "-"
ELSE
   sign$ = "+"
END IF
dummyA = ABS(angle) * 24 / 360
hour = INT(dummyA)
dummyB = (dummyA - hour) * 60
min = INT(dummyB)
dummyC = (dummyB - min) * 60
sec = CINT(dummyC)
IF sec = 60 THEN
   min = min + 1
   sec = 0
   IF min = 60 THEN
      hour = hour + 1
      min = 0
   END IF
END IF
END SUB'time
```

REFERENCES

Aase, J.K. and S.B. Idso [1978], "A comparison of two formula types for calculating long-wave radiation from the atmosphere", Water Resources Research (14), pp. 623-625.

Abramowitz, M. and I.A. Stegun (editors) [1964], "Handbook of mathematical functions", Applied Mathematics Series vol. 55, National Bureau of Standards, Washington, D.C., pp. 255-270.

Ambach, W. [1988], "Interpretation of the positive-degree-days factor by heat balance characteristics - West Greenland", Nordic Hydrology (19), pp. 217-224.

Arnfield, A.J. [1982], "Estimation of diffuse irradiance on sloping, obstructed surfaces: an error analysis", Archiv für Meteorologie, Geophysik und Bioklimatologie B(30), pp. 303-320.

Barkstrom, B.E., E.F. Harrison and R.B. Lee, III [1990], "Earth Radiation Budget Experiment. Preliminary seasonal results", EOS, Transactions of the American Geophysical Union (71), pp. 297, 304-305.

Becker, C.F. and J.S. Boyd [1957], "Solar radiation availability on surfaces in the United States as affected by season, orientation, latitude, altitude and cloudiness", Solar Energy (1), pp. 13-21.

Bird, R.E. and C. Riordan [1986], "Simple solar spectral model for direct and diffuse irradiance on horizontal and tilted planes at the earth's surface for cloudless atmospheres", Journal of Climate and Applied Meteorology (25), pp. 87-97.

Blackadar, A.K. [1984], "A computer almanac", in A.K. Blackadar (editor), "Using your computer", Weatherwise, October 1984, pp. 257-260.

Blackadar, A.K. [1985a], "Fine-tuning the almanac", in A.K. Blackadar (editor), "Using your computer", Weatherwise, August 1985, pp. 213-214.

Blackadar, A.K. [1985b], "Solar energy budget", in A.K. Blackadar (editor), "Using your computer", Weatherwise, October 1985, pp. 263-266.

Blackadar, A.K. [1989], "Solar declination, altitude and azimuth", in A.K. Blackadar (editor), "Using your computer", Weatherwise, April 1989, p.113.

Briegleb, B.P., P. Minnis, V. Ramanathan and E. Harrison [1986], "Comparison of regional clear-sky albedos inferred from satellite observations and model computations", Journal of Climate and Applied Meteorology (25), pp. 214-226.

Bristow, K.L. and G.S. Campbell [1984], "On the relationship between incoming solar radiation and daily maximum and minimum temperature", Agricultural and Forest Meteorology (31), pp. 159-166.

Brunt, D. [1932], "Notes on radiation in the atmosphere. I.", Quarterly Journal of the Royal Meteorological Society (58), pp. 389-420.

Brutsaert, W. [1975], "On a derivable formula for long-wave radiation from clear skies", Water Resources Research (11), pp. 742-744.

Brutsaert, W. [1982], "Evaporation into the atmosphere. Theory, history and applications", D. Reidel Publishing Company, Dordrecht, 299 pp.

Charbonneau, R., J.-P. Lardeau and C. Obled [1981], "Problems of modelling a high mountainous drainage basin with predominant snow yields", Hydrological Sciences Bulletin (26), pp. 345-361.

Dozier, J. [1980], "A clear-sky spectral solar radiation model for snow-covered mountainous terrain", Water Resources Research (16), pp. 709-718.

Dozier, J. [1987], "Recent research in snow hydrology", Reviews of Geophysics (25), pp. 153-161.

Dozier, J. and S.I. Outcalt [1979], "An approach toward energy balance simulation over rugged terrain", Geographical Analysis (11), pp. 65-85.

Dozier, J., R.E. Davis and A.W. Nolin [1989], "Reflectance and transmittance of snow at high spectral resolution", in Proceedings of 1989 International Geosciences and Remote Sensing Symposium (IGARSS), Vancouver, pp. 662-664.

Dozier, J. and J. Frew [1989], "Rapid calculation of terrain parameters for radiation modeling from digital elevation data", in Proceedings of 1989 International Geosciences and Remote Sensing Symposium (IGARSS), Vancouver, pp. 1769-1774.

Erbs, D.G., S.A. Klein and J.A. Duffie [1982], "Estimation of the diffuse radiation fraction for hourly, daily and monthly-average global radiation", Solar Energy (28), pp. 293-302.

Eyton, J.R. [1989], "Low-relief topographic enhancement in a Landsat snow-cover scene", Remote Sensing of the Environment (27), pp. 105-118.

Feldman, P. and T. Rugg [1988], "Using QuickBASIC 4", Que Corporation, Carmel, Indiana, 713 pp.
Fritz, S. [1951], "Solar radiant energy and its modification by the earth and its atmosphere", Compendium of Meteorology, American Meteorological Society, Boston, pp. 13-33.
Fritz, S. [1955][1], "Illuminance and luminance under overcast skies", Journal of the Optical Society of America (45), pp. 820-825.
Garnier, B.J. and A. Ohmura [1968], "A method of calculating the direct shortwave radiation income of slopes", Journal of Applied Meteorology (7), pp. 796-800.
Garnier, B.J. and A. Ohmura [1970], "The evaluation of surface variations in solar radiation income", Solar Energy (13), pp. 21-34.
Geiger, R. [1959], "The climate near the ground", translated from German by M.N. Stewart and others, Harvard University Press, Cambridge, Massachusetts, 494 pp.
Goudriaan, J. [1977][1], "Crop micrometeorology: a simulation study", Centre for Agricultural Publishing and Documentation, Wageningen, 258 pp.
Granger, R.J. and D.H. Male [1978], "Melting of a prairie snowpack", Journal of Applied Meteorology (17), pp. 1833-1842.
Hay, J.E. and J.A. Davies [1978], "Calculation of the solar radiation incident on an inclined surface", in J.E. Hay and T.K. Won (editors), in Proceedings of the first Canadian solar radiation data workshop, Toronto, 1978, pp. 59-72.
Horn, B.K.P. and R.W. Sjoberg [1979], "Calculating the reflectance map", Applied Optics (18), pp. 1770-1779.
Idso, S.B. [1981], "A set of equations for full spectrum and 8- to 14-μm and 10.5- to 12.5-μm thermal radiation from cloudless skies", Water Resources Research (17), pp. 295-304.
Idso, S.B. and R.D. Jackson [1969], "Thermal radiation from the atmosphere", Journal of Geophysical Research (74), pp. 5397-5403.
Iqbal, M. [1983][1], "An introduction to solar radiation", Academic Press, New York. Isard, S.A. [1983], "Estimating potential direct insolation to alpine terrain", Arctic and Alpine Research (15), pp. 77-89.
Kasten, F. [1966], "A new table and approximation formula for the relative optical airmass", Archiv für Meteorologie, Geophysik und Bioklimatologie B(14), pp. 206-223.
Katwijk, V.F. van and A. Rango [1988], "A procedure for forecasting runoff from an alpine watershed with the Snowmelt Runoff Model", USDA-ARS Hydrology Laboratory Technical Report no. 12, 57 pp. plus appendices.
Kimball, B.A., S.B. Idso and J.K. Aase [1982], "A model for thermal radiation from partly cloudy and overcast skies", Water Resources Research (18), pp. 931-936.
Kimball, H.H. [1928], "Amount of solar radiation that reaches the surface of the earth on the land and on the sea, and methods by which it is measured", Monthly Weather Review (56), pp. 393-398.
Klucher, T.M. [1979], "Evaluation of models to predict insolation on tilted surfaces", Solar Energy (23), pp. 111-114.
Kondratyev, K. Ya. (editor) [1973], "Radiation characteristics of the atmosphere and the earth's surface", translated from Russian by V. Pandit, Amerind Publishing Company Pvt. Ltd., New Delhi, pp. 311-463.
Kondratyev, K. Ya., V.I. Korzov, V.V. Mukhenberg and L.N. Dyachenko [1982], "The shortwave albedo and the surface emissivity", in P.S. Eagleson (editor), Papers presented at the JSC study conference on land surface processes in atmospheric general circulation models, Greenbelt, Maryland, January 1981, Cambridge University Press, Cambridge, Massachusetts, pp. 463-514.
Kondratyev, K. Ya. and M.P. Manolova [1960], "The radiation balance of slopes", Solar Energy (4), pp. 14-19.
Kuusisto, E. [1980], "On the values and variability of degree-day melting factor in Finland", Nordic Hydrology (11), pp. 235-242.
Lacis, A.A. and J.E. Hansen [1974], "A parameterization for the absorption of solar radiation in the earth's atmosphere", Journal of the Atmospheric Sciences (31), pp. 118-133.
Leavesley, G.H. [1989], "Problems of snowmelt runoff modelling for a variety of physiographic and climatic conditions", Hydrological Sciences Journal (34), pp. 617-634.

Leckner, B. [1978], "The spectral distribution of solar radiation at the earth's surface - elements of a model", Solar Energy (20), pp. 143-150.
Liou, K.-N. [1980], "An introduction to atmospheric radiation", International Geophysics Series vol. 26, Academic Press, San Diego, 392 pp.
List, R.J. (editor) [1966], Smithsonian Meteorological Tables, Smithsonian Miscellaneous Collection vol. 114 (6th edition), pp. 417-422, 442-443, 496-505.
Liu, B.Y.H. and R.C. Jordan [1960], "The interrelationship and characteristic distribution of direct, diffuse and total solar radiation", Solar Energy (4), pp. 1-19.
Liu, B.Y.H. and R.C. Jordan [1961], "Daily insolation on surfaces tilted towards the equator", Journal of the American Society of Heating, Refrigerating and Air Conditioning Engineers (3), pp. 53-59.
Lo, C.P. [1986], "Applied remote sensing", Longman Inc., New York, pp. 1-7.
Ma, C.C.Y. and M. Iqbal [1983], "Statistical comparisons of models for estimating solar radiation on inclined surfaces", Solar Energy (31), pp. 313-317.
Male, D.H. and D.M. Gray [1981], "Snowcover ablation and runoff", in D.M. Gray and D.H. Male (editors), "Handbook of snow", Pergamon Press, Toronto, pp. 360-436.
Marks, D. [1988], "Climate, energy exchange, and snowmelt in Emerald Lake watershed, Sierra Nevada", Doctoral Dissertation, University of California, Santa Barbara, 149 pp.
Marks, D. and J. Dozier [1979], "A clear-sky longwave radiation model for remote alpine areas", Archiv für Meteorologie, Geophysik und Bioklimatologie B(27), pp. 159-187.
Marks, D., R. Kattelmann, J. Dozier and R. Davis [1986], "Monitoring snowcover properties and processes in a small alpine watershed", in H.S. Santeford (editor), "Field measurements under winter conditions", Proceedings of the 6th International Northern Research Basins Symposium/Workshop, Michigan Technological University, Houghton, Michigan, January 1986, pp. 259-275.
Martinec, J. [1960], "The degree-day factor for snowmelt-runoff forecasting", in "Surface waters", Proceedings of the General Assembly of Helsinki, IASH, pp. 468-477.
Martinec, J. [1989], "Hour-to-hour snowmelt rates and lysimeter outflow during an entire ablation period", in A. Rango (editor), "Snow cover and glacier variations", Proceedings of the Baltimore symposium, Maryland, May 1989, IAHS Publication no. 183, pp. 19-28.
Martinec, J. and M.R. de Quervain [1975], "The effect of snow displacement by avalanches on snow melt and runoff", in "Snow and ice symposium", Proceedings of the Moscow symposium, August 1971, IAHS Publication no. 104, pp. 364-377.
Martinec, J. and A. Rango [1986], "Parameter values for snowmelt runoff modelling", Journal of Hydrology (84), pp. 197-219.
Martinec, J., A. Rango and E. Major [1983], "The Snowmelt-Runoff Model (SRM) user's manual", NASA Reference Publication no. 1100, 110 pp.
McCullough, E.C. [1968][1], "Total daily radiant energy available extraterrestrially as a harmonic series in the day of the year", Archiv für Meteorologie, Geophysik und Bioklimatologie B(16), pp. 129-143.
McGuffie, K. and A. Henderson-Sellers [1989], "Almost a century of "imaging" clouds over the whole-sky dome", Bulletin of the American Meteorological Society (70), pp. 1243-1253.
Monteith, J.L. [1961][1], "An empirical method for estimating long-wave radiation exchanges in the British Isles", Quarterly Journal of the Royal Meteorological Society (87), pp. 171-179.
Moon, P. and D.E Spencer [1942][1], "Illumination from a non-uniform sky", Transactions of the illumination Engineering Society (37), pp. 707-726.
Morris, E.M. [1989], "Turbulent transfer over snow and ice", Journal of Hydrology (105), pp. 205-223.
Moussavi, M., G. Wyseure and J. Feyen [1989], "Estimation of melt rate in seasonally snow-covered mountainous areas", Hydrological Sciences Journal (34), pp. 249-263.
Müller, H. [1985], "On the radiation budget in the Alps", Journal of Climatology (5), pp. 445-462.
Munro, D.S. and G.J. Young [1982], "An operational net shortwave radiation model for glacier basins", Water Resources Research (18), pp. 220-230.

Nash, J.E. and J.V. Sutcliffe [1970][1], "River flow forecasting through conceptual models, Part I - A discussion of principles", Journal of Hydrology (10), pp. 282-290.
Olyphant, G.A. [1984], "Insolation topoclimates and potential ablation in alpine snow accumulation basins: Front Range, Colorado", Water Resources Research (20), pp. 491-498.
Olyphant, G.A. [1986a], "Longwave radiation in mountainous areas and its influence on the energy balance of alpine snowfields", Water Resources Research (22), pp. 62-66.
Olyphant, G.A. [1986b], "The components of incoming radiation within a mid-latitude alpine watershed during the snowmelt season", Arctic and Alpine Research (18), pp. 163-169.
Olyphant, G.A. and S.A. Isard [1988], "The role of advection in the energy balance of late-lying snowfields: Niwot Ridge, Front Range, Colorado", Water Resources Research (24), pp. 1962-1968.
Petzold, D.E. [1977], "An estimation technique for snow surface albedo", McGill University Climatological Bulletin (21), pp.1-11.
Proy, C., D. Tanré and P.Y. Deschamps [1989], "Evaluation of topographic effects in remotely sensed data", Remote Sensing of the Environment (30), pp. 21-32.
Pysklywec, D.W., K.S. Davar and D.I. Bray [1968], "Snowmelt at an index plot", Water Resources Research (4), pp. 937-946.
Ramanathan, V., B.R. Barkstrom and E.F. Harrison [1989], "Climate and the earth's radiation budget", Physics Today, May 1989, pp. 22-32.
Rango, A. and V.F. van Katwijk [1990], "Development and testing of a snowmelt-runoff forecasting technique", Water Resources Bulletin (26), pp. 135-143.
Reicosky, D.C., L.J. Winkelman, J.M. Baker and D.G. Baker [1989], "Accuracy of hourly air temperatures calculated from daily minima and maxima", Agricultural and Forest Meteorology (46), pp. 193-209.
Robinson, N. (editor) [1966][1], "Solar radiation", Elsevier, New York, pp. 29-160.
Rodgers, C.D. [1967][1], "The radiative heat budget of the troposphere and lower stratosphere", Report no. A2, Planetary Circulations Project, Department of Meteorology, MIT, 99 pp.
Running, S.W., R.R. Nemani and R.D. Hungerford [1987], "Extrapolation of synoptic meteorological data in mountainous terrain and its use for simulating forest evapotranspiration and photosynthesis", Canadian Journal of Forestry Research (17), pp. 472-483.
Satterlund, D.R. [1979], "An improved equation for estimating long-wave radiation from the atmosphere", Water Resources Research (15), pp. 1649-1650.
Sellers, W.D. [1965][1], "Physical climatology", University of Chicago Press, Chicago, Illinois, 272 pp.
Shoshany, M. [1989], "Secondary reflection effect on sensor response for a V-shaped valley", International Journal of Remote Sensing (10), pp. 1197-1206.
Sinott, R.W. [1984], "Taming our chaotic calendar", Sky and Telescope, May 1984, pp. 454-455.
Smietana, Jr., P.J., R.G. Flocchini, R.L. Kennedy and J.L. Hatfield [1984], "A new look at the correlation of K_d and K_t ratios and at global solar radiation tilt models using one-minute measurements", Solar Energy (32), pp. 99-107.
Spencer, J.W. [1971], "Fourier representations of the position of the sun", Search (2), p. 172.
Steven, M.D. and M.H. Unsworth [1979], "The diffuse solar irradiance of slopes under cloudless skies", Quarterly Journal of the Royal Meteorological Society (105), pp. 593-602.
Steven, M.D. and M.H. Unsworth [1980], "The angular distribution and interception of diffuse solar radiation below overcast skies", Quarterly Journal of the Royal Meteorological Society (106), pp. 57-61.
Stuhlmann, R., M. Rieland and E. Raschke [1990], "An improvement of the IGMK model to derive total and diffuse solar radiation at the surface from satellite data", Journal of Applied Meteorology (29), pp. 586-603.
Swinbank, W.C. [1963], "Long-wave radiation from clear skies", Quarterly Journal of the Royal Meteorological Society (89), pp. 339-348.

Swiss Federal Institute for Snow and Avalanche Research [1989], Unpublished data of 1985 ablation season at Weissfluhjoch/Davos, 9 pp.
Temps, R.C. and K.L. Coulson [1977], "Solar radiation incident upon slopes of different orientations", Solar Energy (19), pp. 179-184.
The University of Arizona [1989], Cooperative Extension Service, Unpublished data for April 10, 1989 at Maricopa Agricultural Research Center, 2 pp. plus diskette.
Unsworth, M.H. and J.L. Monteith [1975], "Long-wave radiation at the ground. I. Angular distribution of incoming radiation", Quarterly Journal of the Royal Meteorological Society (101), pp. 13-24.
U.S. Army Corps of Engineers [1956], "Snow hydrology. Final report of the snow investigations", North Pacific Division, USACE, Portland, Oregon, 437 pp.
Van Heuklon, T.K. [1979], "Estimating atmospheric ozone for solar radiation models", Solar Energy (22), pp. 63-68.
Vliet, J.C. van [1988], "Software engineering" (in Dutch), H.E. Stenfert Kroese B.V., Leiden, 391 pp.
Wang, W.-C. [1976], "A parameterization for the absorption of solar radiation by water vapor in the earth's atmosphere", Journal of Applied Meteorology (15), pp. 21-27.
Whiteman, C.D. and K.J. Allwine [1986], "Extraterrestrial solar radiation on inclined surfaces", Environmental Software (1), pp. 164-169.
Whiteman, C.D., K.J. Allwine, L.J. Fritschen, M.M. Orgill and J.R. Simpson [1989], "Deep valley radiation and surface energy budget microclimates. Part I: Radiation", Journal of Applied Meteorology (28), pp. 414-426.
Willet, H.C. and F. Sanders [1959], "Descriptive meteorology", Academic Press, New York, 355 pp.
Williams, L.D. [1988], "Estimation of frequency of occurence of dry snowcover in Germany", Royal Signals and Radar Establishment, Malvern, 41 pp. plus appendix.
Zuzel, J.F. and L.M. Cox [1975], "Relative importance of meteorological variables in snowmelt", Water Resources Research (11), pp. 174-176.

[1] References cited by other investigators.